ČESKÉ VYSOKÉ
UČENÍ TECHNICKÉ
V PRAZE

FAKULTA
STROJNÍ

DIPLOMOVÁ PRÁCE

2017

VÁCLAV
FUČÍK

ČESKÉ VYSOKÉ UČENÍ TECHNICKÉ V PRAZE

ZADÁNÍ DIPLOMOVÉ PRÁCE

I. OSOBNÍ A STUDIJNÍ ÚDAJE

Příjmení: **Fučík** Jméno: **Václav** Osobní číslo: **408554**

Fakulta/ústav: **Fakulta strojní**

Zadávající katedra/ústav: **Ústav energetiky**

Studijní program: **Strojní inženýrství**

Studijní obor: **Energetika**

II. ÚDAJE K DIPLOMOVÉ PRÁCI

Název diplomové práce:

Výměník tepla pro kaskádní cyklus

Název diplomové práce anglicky:

Heat exchanger for cascade cycle

Pokyny pro vypracování:

In the thesis will be calculated a brazed plate heat exchanger for refrigeration cascade cycle using refrigerant R452A on upper circuit and refrigerant R744 on lower circuit for specified conditions. The working parameters on both heat source and heat sink side will be calculated and used for system performance prediction. The general outputs of the thesis will be:
- literature review of cascade cycle types and applications
- description of all circuit components with specification of key parameters of each component
- basic calculation of cascade system for specified conditions
- calculation of brazed plate heat exchanger for calculated cascade cycle
- comparison of calculated and measured data

Seznam doporučené literatury:

José M. Corberán, Pedro Fernández D, Semiexplicit Method For Wall Temperature Linked Equations (SEWTLE): A General Finite-Volume Technique For The Calculation Of Complex Heat Exchangers. Numerical Heat Transfer, Part B: Fundamentals [online]. 2001, 40(1): 37-59. J.R. García-Cascales, F. Vera-García, J.M. Corberán-Salvador, J. González-Macía, Assessment of boiling and condensation heat transfer correlations in the modelling of plate heat exchangers, International Journal of Refrigeration, Volume 30, Issue 6, September 2007, Pages 1029-1041, ISSN 0140-7007; T.L. Bergman, Frank P. Incropera. Fundamentals of heat and mass transfer. 7th ed. /. Hoboken, NJ: Wiley, c2011. ISBN 978-0470-5019/-9.

Jméno a pracoviště vedoucí(ho) diplomové práce:

doc. Ing. Pavel Novák CSc., ústav energetiky FS

Jméno a pracoviště druhé(ho) vedoucí(ho) nebo konzultanta(ky) diplomové práce:

Ing. Jan Sedlář, ústav energetiky FS

Datum zadání diplomové práce: **11.04.2017** Termín odevzdání diplomové práce: **02.06.2017**

Platnost zadání diplomové práce: **31.12.2018**

Podpis vedoucí(ho) práce | Podpis vedoucí(ho) ústavu/katedry | Podpis děkana(ky)

III. PŘEVZETÍ ZADÁNÍ

Diplomant bere na vědomí, že je povinen vypracovat diplomovou práci samostatně, bez cizí pomoci, s výjimkou poskytnutých konzultací. Seznam použité literatury, jiných pramenů a jmen konzultantů je třeba uvést v diplomové práci.

25.4.2017
Datum převzetí zadání

Podpis studenta

Declaration

I thereby declare that the thesis “Heat exchanger for cascade cycle” is a result of my own work. I have faithfully and accurately cited all my sources.

In Prague, 29th May 2017

…….
Václav FUČÍK

Anotační list

Jméno autora:	Václav Fučík
Název DP:	Výměník tepla pro kaskádní cyklus
Anglický název:	Heat exchanger for cascade cycle
Akademický rok:	2016/2017
Ústav/Odbor:	Ústav energetiky
Vedoucí DP:	doc. Ing. Pavel Novák, CSc. a Ing. Jan Sedlář
Konzultant:	
Bibliografické údaje:	Počet stran: 79 Počet obrázků: 32 Počet tabulek: 12 Počet příloh: 0
Klíčová slova:	Kaskádní výměník tepla, SEWTLE, Parní kompresorové chlazení
Keywords:	Cascade heat exchanger, SEWTLE, Vapor-compression refrigeration

Anotace: Práce se zabývá termodynamickým výpočtem výměníku pro kaskádní chladicí zařízení pomocí výpočetního postupu SEWTLE. Zvláštností tohoto typu kaskádního výměníku je, že v něm dochází k fázové změně na obou jeho stranách. Metoda SEWTLE byla úspěšně ověřena na příkladu daného výměníku.

Abstract: The thesis deals with the thermodynamic calculation of a heat exchanger for cascade refrigeration cycle using the SEWTLE calculation procedure. For this type of heat exchanger is characteristic the phase change occurrence at both its sides. The SEWTLE procedure was successfully verified on the given heat exchanger.

Acknowledgement

I would like to express my sincere gratitude to my supervisors doc. Ing. Pavel Novák, CSc. and Ing. Jan Sedlář for the countless time and help provided in course of creation of this thesis.

Table of contents

List of figures

List of tables

List of abbreviations

ASHRAE	American Society of Heating, Refrigerating and Air-Conditioning Engineers
BPHE	Brazed Plate Heat Exchanger
CC	Low Temperature Cycle
CFD	Computational Fluid Dynamics
CHE	Cascade Heat Exchanger
COP	Coefficient of Performance
EEV	Electronic Expansion Valve
EV	Expansion Valve
EVI	Enhanced Vapor Injection
FDM	Finite Difference Method
FEM	Finite Element Method
FVM	Finite Volume Method
GWP	Global Warming Potential
IHE	Internal Heat Exchange/Exchanger
HC	Hydrocarbon
HC	High Temperature Cycle
HE	Heat Exchanger
HFC	Hydrofluorocarbon
HFO	Hydrofluoroolefin
HTC	Heat Transfer Coefficient
LMTD	Logarithmic Mean Temperature Difference
MAC	Mobile Air-Conditioning System
NTU	Number of Transfer Units
ODP	Ozone Depletion Potential
PDE	Partial Differential Equation
PFC	Fully Fluorinated Hydrocarbon
PHE	Plate Heat Exchanger
SEWTLE	Semi Explicit Method for Wall Temperature Linked Equations
RPM	Revolutions per Minute

Nomenclature

A	heat transfer area [m^2]
b	channel spacing [m]
Bo	boiling number [-]
C	heat capacity rate [J. s^{-1}. K^{-1}]
c_p	specific heat capacity [J. kg^{-1}. K^{-1}]
D_h	hydraulic diameter [m]
dt/dx	temperature gradient [K. m^{-1}]
e	emissivity [-]
f	friction factor [-]
g	gravitational acceleration [m. s^{-2}]
G	mass flux / mass velocity [kg. s^{-1}. m^{-2}]
Ge	geometric coefficient [-]
i	enthalpy [J. kg^{-1}]
h	plate height [m]
L	thickness [m]
m	mass flow rate [kg. s^{-1}]
n	number of channels [-]
Nu	Nusselt number [-]
O	wetted perimeter [m]
p	pressure [Pa]
P	perimeter [m]
P	power input [W]
p_{co}	corrugation pitch [m]
Pr	Prandtl number [-]
q	heat flux [$W.m^{-2}$]
Q	heat flow rate [W]
Re	Reynolds number [-]
S	area [m^2]
t	temperature [°C]
T	absolute temperature [K]
ΔT_{cooler}	gas cooler temperature difference [K]
ΔT_s	suction superheat [K]
u	velocity [m. s^{-1}]
U	overall HTC [W. m^{-2}. K^{-1}]
UA	= U.A [W. K^{-1}]
V	volume flow rate [m^3. s^{-1}]
x	vapor quality [-]
w	plate width [m]
z	spatial coordinate [m]

Greek symbols

α	heat transfer coefficient [W. m^{-2}. K^{-1}]
α_A	shear dominated HTC [W. m^{-2}. K^{-1}]
α_{Nu}	gravity dominated HTC [W. m^{-2}. K^{-1}]
$\alpha_{r,l}$	all-liquid nonboiling HTC [W. m^{-2}. K^{-1}]
β	chevron angle [rad]
δ	void fraction [-]
ε	effectiveness [-]
η	efficiency [-]
θ	angle with horizontal [rad]
λ	thermal conductivity [W. m^{-1}. K^{-1}]
λ	volumetric efficiency [-]
μ	dynamic viscosity [Pa. s]
ρ	density [kg. m^{-3}]
σ	surface tension [mN. m^{-1}]
σ	pressure ratio [-]
σ_{SB}	Stefan-Boltzmann constant = 5.67 x 10^{-8} W. m^{-2}. K^{-4}
φ	surface enlargement factor [-]
Φ	two-phase friction multiplier [-]

Subscripts

air	properties of air
0	in a certain distance from the wall
c	cold fluid side
c	condensation
calc	calculated
CC	low temperature cycle
cell	for one cell
ch	channel
CHE	cascade heat exchanger
cnd	conduction
cnv	convection
cold	cold fluid side
cond	condensation
cs	cross-sectional
d	discharge
e	evaporation
est	estimate
evap	evaporation
eq	equivalent
g	saturated vapor
gc	gas cooler
h	hot fluid side
HC	high temperature cycle
hot	hot fluid side
i	inlet
ie	isentropic
input	input value
j	cell index
l	saturated liquid
lg	difference between saturated vapor and saturated liquid state
LO	liquid state with the total flow rate
m	middle of the fluid
n	normal to direction of heat flow
n	nominal
o	outlet
p	pipe or duct
rad	radiation
s	suction
sat	saturation
sur	surface
th	theoretical
theor	theoretical
w	wall

1. Introduction

The rising environmental awareness and legislative measures to promote eco-friendly solutions have a significant impact on development in different fields of technology. The refrigeration problematic is one of the major fields of concern. There are several reasons for this - it represents a considerable potential for energy consumption savings. In addition to this, there is a negative impact of numerous refrigerants on the environment, especially in topics like ozone layer depletion or the greenhouse effect.

Because of this, the most harmful refrigerants are banned or being phased out. Therefore, it is necessary to develop new alternative refrigerants to substitute the undesirable ones. This can include developing new mixtures, testing non-traditional substances or simply using the natural substances, which are generally less harmful to the environment than the artificial ones.

As for the electricity consumption savings, the ways to increase the energy efficiency of refrigeration systems are of main interest. This can include innovative refrigeration engineering approaches as well as the use of more efficient components, which is enforced by the EU legislative measures (e.g., Ecodesign).

This thesis deals with a refrigeration system that could lead the future way in certain fields of refrigeration – a cascade refrigeration system. It is an interconnection of two separate refrigeration cycles operating at different temperature and pressure levels. By choosing suitable refrigerants for a given application, considerable energy efficiency boost can be achieved. On the top of that, such system is characterized with solid operation stability under different conditions.

The described advantages can be further increased if the refrigeration cycle components are selected appropriately. For purposes of this thesis, progressive refrigerants have been selected – carbon dioxide for the low temperature cycle and R452A (widely considered as a substitute for R404A) as one of the newest refrigerant mixtures for the high temperature cycle.

The main objective of this thesis is to formulate a complex calculation procedure of the cascade refrigeration cycle with special emphasis on the cascade heat exchanger for purpose of verifying the cycle working parameters and functionality under specified ambient/refrigerated space conditions.

The thesis is constructed from several basic elements. The first, theoretical part provides an overview of vapor-compression refrigeration cycle principle and its elementary components, including the hardware elements as well as description of selected refrigerants. As the main focus of the thesis is the cascade heat exchanger, the second part is dedicated to the heat exchanger problematic. The work offers an overview of heat exchanger types with biggest emphasis on the plate-type as well as extensive study on heat exchanger design including the description of the SEWTLE procedure – a calculation method used for the purposes of this thesis. Another notable part of this paper is the analysis of applicable heat transfer correlations, which is important for the success of the whole calculation. The final part elaborates on the refrigeration cycle calculation structure with specific results provided at the very end of the thesis.

2. Vapor compression refrigeration system

The most common method of refrigeration in current applications is a vapor compression system. However, there are also other less ordinary possibilities such as [1]:

- absorption system,
- gas cycle,
- steam jet cycle,
- dry ice refrigeration,
- thermoelectric system,
- and many others.

Refrigeration and air-conditioning systems absorb heat from the cooled space (a heat source). In case of vapor compression systems, this heat is absorbed in an evaporator (refrigerant undergoes a phase change) and it is to be released later if the system is intended to work continuously as a cycle. Most commonly, the heat absorbed in evaporator is rejected in a condenser (or a gas cooler in case of supercritical applications) to ambient air. To achieve this, the refrigerant pressure levels are set accordingly – to ensure that the temperature inside a refrigerated space is within required range and that the pressure on the condenser side is high enough to make the heat transfer from inside the cycle out into the ambient air (heat sink) possible.

The system basically operates between two pressure levels – evaporation and condensation pressure. To simplify basic thermodynamic calculations, the vapor compression cycle is considered as a Reverse Rankine Cycle where secondary pressure losses and heat losses throughout the system are neglected [2].

A standard basic refrigeration system consists of four essential elements [3]:

- a **compressor**, where the compression part of a cycle takes place,
- a **condenser**, where desuperheating, condensation and subcooling generally occur,
- a **throttling device**, which maintains the pressure difference between condensing and evaporating part of the cycle and sprays the coolant into the evaporator,
- an **evaporator**, where evaporation and superheating take place.

The pressure-enthalpy diagram with relevant thermodynamic changes is shown in Figure 1. In real applications, there are many more additional devices for regulation purposes - to improve the operation characteristics, to ensure safe operation under all working conditions, to increase the overall system efficiency, additional evaporators for multipurpose refrigeration etc.

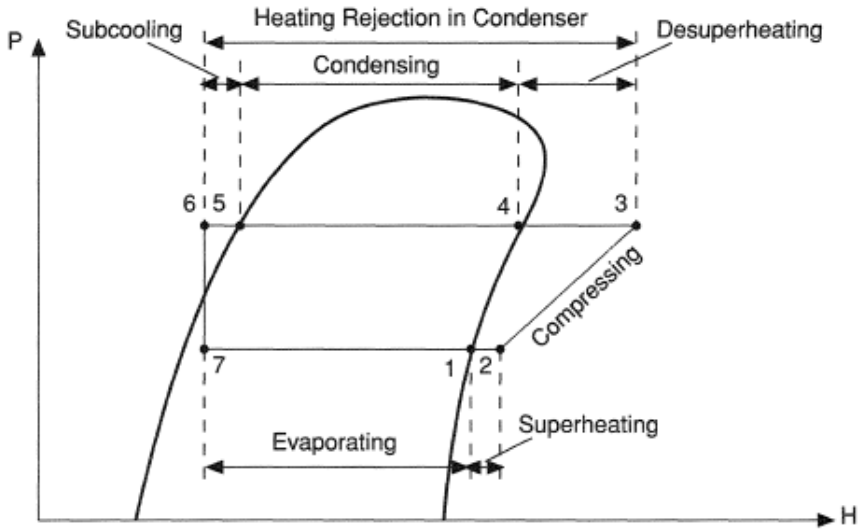

Figure 1: Vapor compression refrigeration cycle [100]

Vapor compression systems cover a wide spectrum of applications ranging from as low as few Watts of refrigeration capacity up to Megawatts [4]. It is used for a broad variety of cooling/freezing purposes [5]:

- household and commercial freezers and refrigerators,
- industrial, commercial, home as well as transportation air conditioning,
- food processing and cold storage,
- industrial cooling.

In certain cases, the temperature difference between heat source and heat sink is too large to be handled by a common single-stage compressor. Either, the pressure ratio is out of compressor technical capabilities, or the discharge temperature is higher than the safety limits for the materials used in compressors [6]. This issue is generally solved by dividing the compression process into smaller steps (two or more), which leads to lower discharge temperatures, lower compressor work needed for desired compression and subsequently higher coefficient of performance (COP), which means that the refrigeration cycle works more efficiently. Another possible solution is a cascade refrigeration system.

2.1. Cascade refrigeration system

A cascade refrigeration system consists of two (or more) refrigeration cycles (a low and a high temperature) linked together by an intermediate heat exchanger. This heat exchanger serves as a condenser for the low temperature cycle and the other side as an evaporator for the high temperature cycle simultaneously. A basic process schematic of individual devices in a cascade refrigeration system is in following Figure 2.

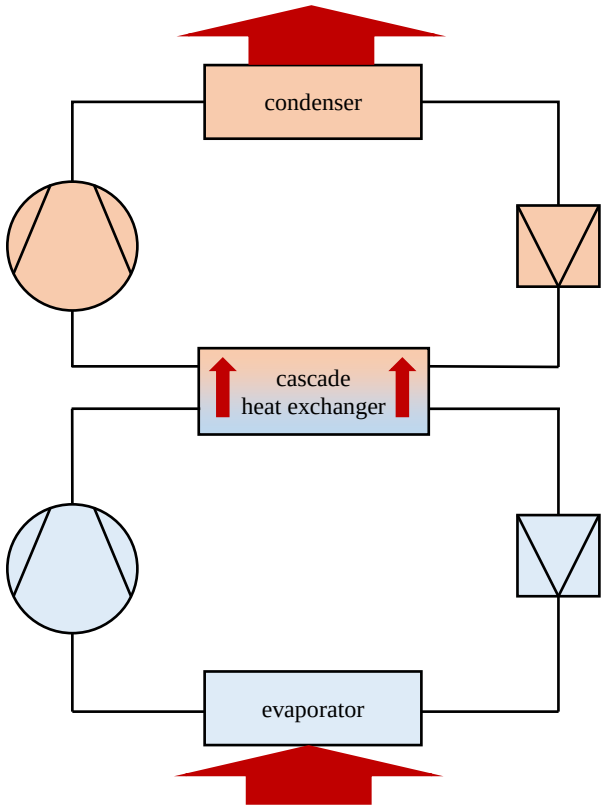

Figure 2: Cascade refrigeration system

However, it is often necessary to equip a cascade cycle with a gas desuperheater after the low-temperature compressor. The reason for this is to minimize the risk of thermal fatigue of a cascade heat exchanger – the low-temperature compressor discharge temperatures can often be around 80°C whereas the evaporator side of a cascade unit can be as low as - 20°C [7]. Cascade heat exchangers are most often plate-type for their compactness or more robust shell-and-tube type (example of such heat exchanger working with CO_2 (low) and NH_3 (high) is in Figure 3). In majority of cascade systems there are two different refrigerants in each sub-cycle. However, applications where the same fluid is in both loops can also be found [8].

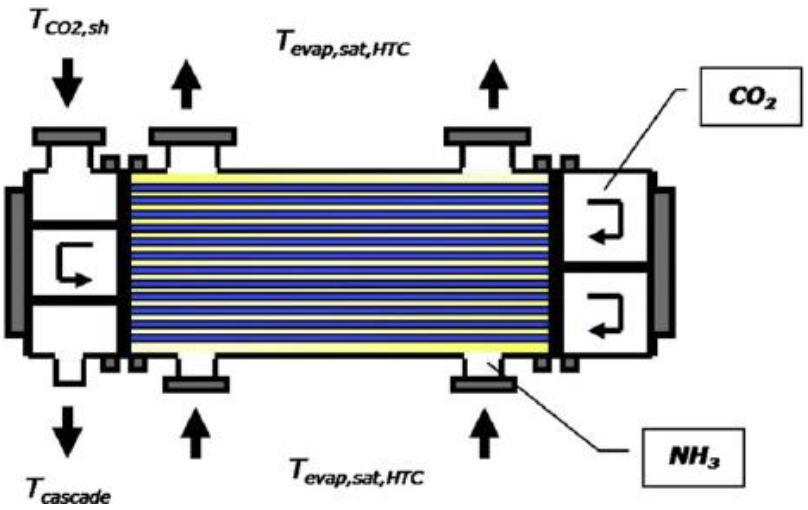

Figure 3: Shell and tube cascade heat exchanger [101]

As mentioned above, a cascade system is employed when the pressure ratio or discharge temperature would be too high from compressor perspective or simply too inefficient. However, it also helps to overcome a situation when the pressure range (i.e., temperature range) is too wide to manage with only one refrigerant with a regard to its thermodynamic properties. A common application for cascade refrigeration is therefore moderately low-temperature freezing (appr. from - 25°C to - 75°C) [9], [10].

The main advantages are [11]:

- maximum possible energy efficiency is achieved by selecting the refrigerants with the most suitable temperature characteristics for both cycles,
- the system operation is stable even for ultra-low-temperature conditions,
- reasonable operating and service costs.

2.2. Compressors used in refrigeration systems

The essential part of every vapor-compression refrigeration system is the compressor itself. In basic arrangement, the compressor draws in the superheated gas from the evaporator (the low-pressure part of the refrigeration loop), compresses and delivers it to the condenser at higher pressure.

Numerous types of compressors have been developed for many specific applications. Based on the required working parameters, refrigerants, available power supply and other features it is generally possible to determine the suitable kind of compressor. The following types have proven themselves as the most suitable for refrigeration applications [12]:

- reciprocating compressors,
- rotary compressors,
    - scroll,
    - screw,

    - rotary vane,
- centrifugal compressors.

2.2.1. Hermetic / Semi-hermetic / Open

Commonly used refrigerants (e.g., F-gases or ammonia) have negative impact on the environment and/or in some cases even present a threat to human health. Therefore, the highest possible tightness of a refrigeration circuit is required.

The best protection from undesirable leakage presents a hermetic compressor - the entire device is welded in a casing, which is not intended to be opened under any circumstances. When a part of such compressor fails, it generally cannot be repaired and the whole appliance is replaced. On the other hand, semi-hermetic compressors offer a fine balance of good tightness properties and a possibility of opening the shell (in case of servicing, repair etc.) without damage.

However, hermetic and semi-hermetic compressors are limited to only one possible drive source – the electricity. The open-type compressor overcomes this limitation – it can be driven by an internal combustion engine or a turbine [13]. Nevertheless, the long-term tightness of such arrangement can be problematic.

2.2.2. Reciprocating compressors

Thanks to its massive use in major appliances (home refrigerators), reciprocating compressor is currently the most common type. Many different designs and operation variants have been developed – the individual models can be lubricated or oil-free, be single- or double-acting or have specific number of cylinders in different geometrical arrangements. The working elements are pistons driven by a crankshaft.

Majority of piston compressors work with self-acting valves that ensure the intake of refrigerant and its exhaust after compression. The use of lubricated compressors brings additional issues that require special attention. The oil for refrigeration compressors needs to have specific properties to ensure the proper functionality of the system [14]:

- compatibility of the refrigerant-oil couple – good miscibility and solubility of the oil in the refrigerant,
- favorable thermodynamic properties at low temperatures,
- chemical and thermal stability,
- resistance against ageing.

Oil in a refrigeration compressor has several important roles [15]:

- protection against corrosion,
- reduction of friction between moving parts (pistons, piston rings, valves etc.),
- better sealing,
- compressor cooling.

One of the advantages of this compressor type is flexibility when working under other than nominal conditions. Unlike other types with built-in volume ratio (e.g., scroll or screw compressors), the reciprocating compressors by nature of their operation adjust to the actual evaporating/condensing pressure [16]. This generally leads to smoother operation or lower energy consumption. On the other hand, they are generally less "compact" than more sophisticated types. Example of such compressor is in Figure 4.

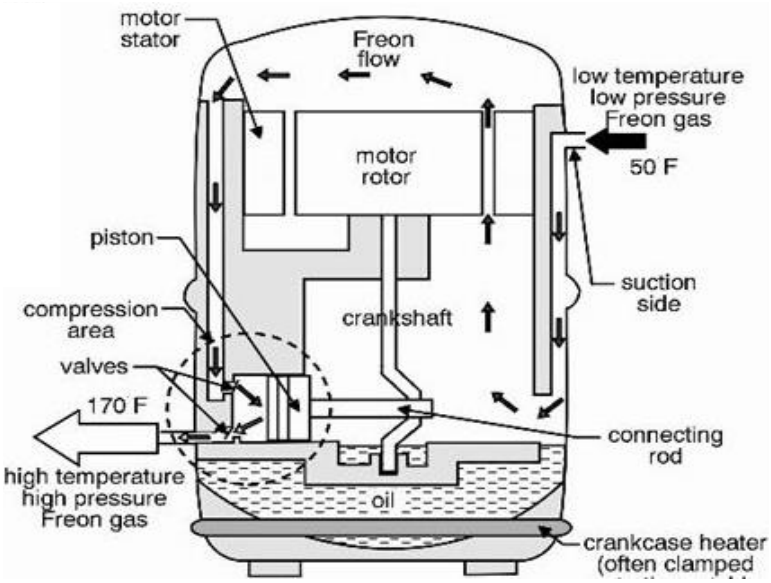

Figure 4: Reciprocating hermetic compressor [102]

2.2.3. Scroll compressors

One of the world's first scroll compressor specimens was built in 1979 [17]. Since then, it spread across many fields of technology. Significant is their success among the heat pump industry where they have sidelined the originally dominant reciprocating compressors [18].

There are several reasons for this [19], [20]:

- smooth, silent operation without great pressure or volume pulsations on the discharge,
- very low or none clearance volume compared to reciprocating compressors,
- low level of vibrations,
- most commonly non-lubricated design, which leads to low oil concentrations in discharge gas (e.g., suitable for compressed air applications),
- high durability and reliability thanks to simple design (lack of moving parts).

The compressor itself comprises of two main elements – the fixed (stationary) spiral and the eccentrically mounted orbiting spiral. The two parts are coupled in a manner, which ensures that the gas is periodically captured and drawn in at the outside diameter and is then gradually compressed and moved towards the center where the discharge is situated.

2.2.3.1. Enhanced vapor injection

To achieve reduction in total operation costs or increase in the efficiency of a refrigeration system, several measures can be taken. One of them is equipping the system with the so called EVI (Enhanced Vapor Injection) compressor instead of a regular one. In chilling systems with evaporating temperatures below - 25°C (in combination with subcooling of saturated liquid-phase refrigerant) the savings on electricity can be as high as 30 % with an EVI compressor [21]. For refrigeration applications, the increase in COP and cooling capacity is of importance. This increase in capacity can lead to lower requirements on compressor size – thereby saving space and costs.

The fundamental principle of its operation is combining of two refrigerant streams at different pressure levels during the compression process. After the refrigerant was condensed in the condenser, a portion of the flow is separated and throttled by an expansion valve to the intermediate pressure. After this, it flows into the economizer (generally a counterflow plate heat exchanger), where it is evaporated, while subcooling of the condensate takes place on the other side of the economizer (Figure 5). During the first stage of the compression the refrigerant exiting the evaporator is compressed to the intermediate pressure. Now, the vapor from the economizer is injected into the scroll compressor by two symmetrically positioned ports to ensure the induced forces are balanced [22]. The two refrigerant streams are then mixed and compressed to the condensation pressure.

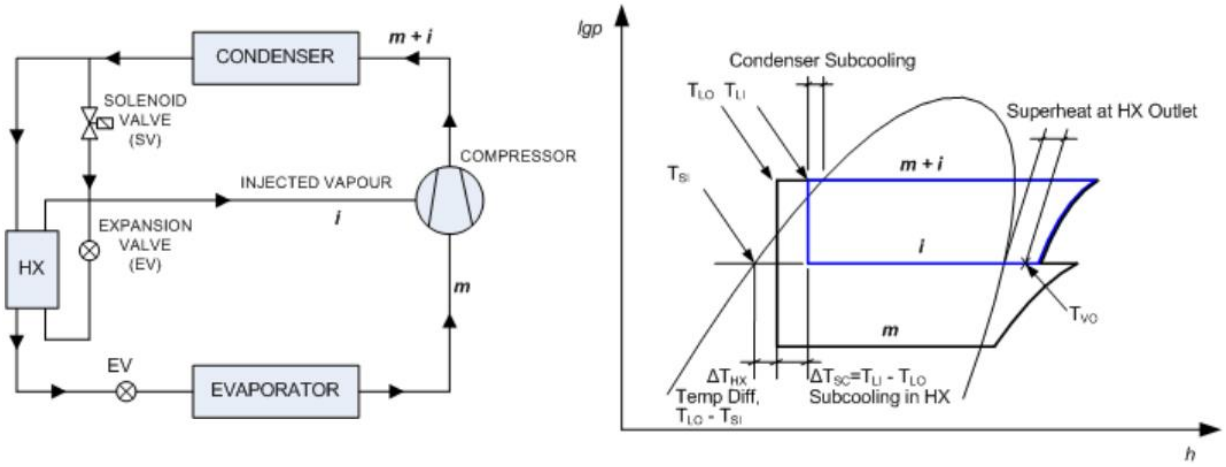

Figure 5: Circuit diagrams - the main circuit (mass flow rate m) and the economizer circuit (mass flow rate i) [22]

Although EVI compressors are suitable particularly for air source heat pumps [22], their many advantages can be used in refrigeration applications as well. By mixing the partially compressed refrigerant from evaporator and the minor quantity of refrigerant evaporated in economizer, temperature of the resulting mixture is significantly lower than for ordinary single-stage compression. Thanks to this, the discharge area materials are not so heavily exposed to high temperatures. Another advantage is a larger operating envelope and therefore larger range of compressor usability.

2.2.4. Screw compressors

Screw compressors are mostly used for commercial refrigeration. Their design combines the advantages of reciprocating, rotary and even dynamic compressors. Although special configurations with a single rotor or three rotors exist, they generally contain two screw-profile rotors (Figure 6) with the opposite sense of rotation. The intake gas is compressed in gradually dwindling chambers formed by the outside of the rotors (a male and a female) and the casing. This arrangement has a built-in volume ratio, which can be viewed as a slight disadvantage [23].

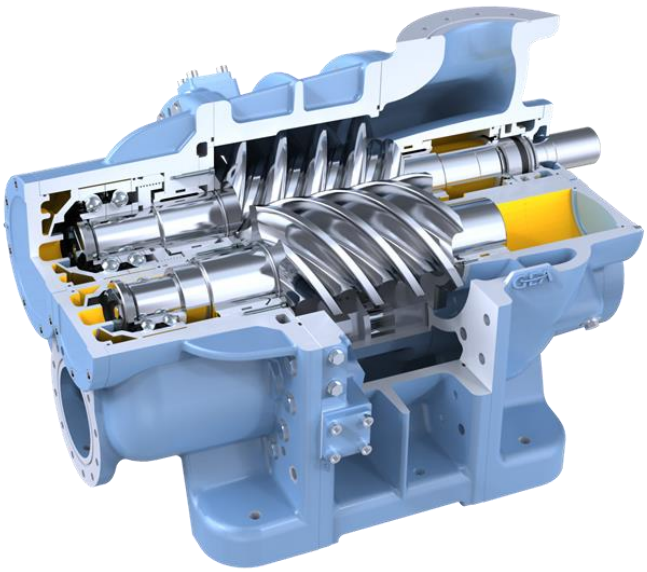

Figure 6: Two-rotor screw compressor [103]

However, a screw compressor has only a minimum of moving parts and no significant sources of rotor imbalance. Thanks to this, it can work at very high speeds (1,450 – 30,000 RPM [3]), thus making the compressor compact even for higher performance levels [24]. The maintenance requirements are relatively low. Moreover, the volumetric efficiency is very high - similarly to above mentioned scroll compressors - due to the absence of clearance volume. The oil-related problematic is extensive with screw-type compressors.

Cooling capacities of the systems with screw compressors for refrigeration purposes can range from tens to thousands kW [3]. They are suitable for majority of currently used refrigerants.

2.4. Internal heat exchange

Internal heat exchange is a measure that involves inserting an extra heat exchanger into the existing vapor compression cycle (Figure 7). The hot side of this heat exchanger contains the condensed refrigerant. Heat is transferred into the refrigerant vapor at the other side of the HE. The resulting effect of this on the whole refrigeration cycle can vary depending on the refrigerant used. Coefficient of performance (COP) can be increased (e.g., R134a) as well as decreased (R717 - ammonia) [6]. Generally, the outcome is highly dependable on vapor heat capacity – the higher the value, the higher potential efficiency of the cycle [25].

Nevertheless, the internal heat exchange is frequently used to stabilize the system operation, to protect the integrity of its components as well as to increase the amount of heat contained in vapor after compression. It can also result in increased specific compressor suction volume and discharge temperature, lower mass flow rate and the internal HE itself is a source of a pressure drop [26].

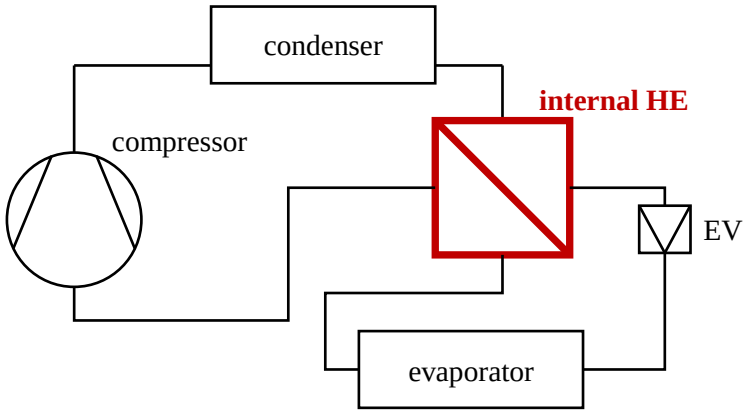

Figure 7: Internal heat exchange

According to [27], compressor manufacturers often recommend the superheating of 20 K for commercial refrigeration systems using CO_2. The reason for this is to prevent the problems with compressor lubrication, which can occur at temperatures well below 0°C. The superheat can be achieved by setting the expansion device correspondingly so that the entire superheating process takes place in evaporator.

Another option is to use an internal liquid-line/suction-line heat exchanger, which is very common in commercial refrigeration [25]. In case of a simple subcritical CO_2 cycle, this device is not thermodynamically favorable as it tends to slightly reduce the cycle overall COP [28]. However, when used inside a cascade cycle, the internal heat exchange can have a positive effect on the COP under certain conditions [27].

2.5. Expansion valves

Expansion valves play an important role in any vapor compression refrigeration system. They help to facilitate the pressure difference between the condenser and the evaporator side of a cycle. An expansion valve is also one of its elementary regulation elements – it has a direct effect on refrigerant vapor superheating at the evaporator outlet [29].

Expansion valves inject a certain amount of refrigerant into the evaporator in order to achieve the proper level of superheating. A sufficient level of superheating is necessary for a smooth and reliable operation of the compressor which intakes this superheated vapor. This should ensure that pure vapor without any residual liquid drops enters the compressor. If the undesirable liquid drops enter the compression chamber, a severe damage to the compressor due to a sudden pressure surge (liquid hammer) can occur [30].

A thorough analysis is necessary to choose the most appropriate type of expansion element for given refrigeration system. There is currently a lot of types of expansion elements (Figure 8) and the research in this field continues [31].

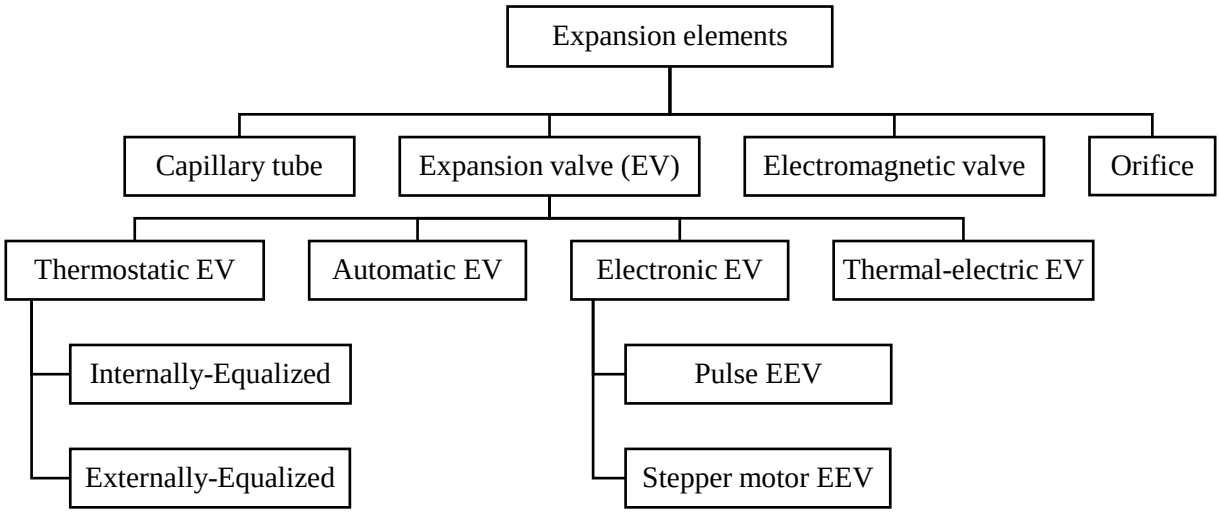

Figure 8: Expansion elements for vapor compression systems [104], [3]

2.6. Refrigerants

Refrigerants lie at the heart of refrigeration cycles operation. Basically, any fluid can be used as a refrigerant in vapor compression cycles. However, certain important properties are required for a refrigerant to be used conveniently and reliably in a larger scale. The most relevant properties are [3]:

- range of working pressures and temperatures,
- easy production or wide availability,
- safe handling, low level of toxicity and flammability,
- other properties related to energy efficiency or environmental friendliness.

2.6.1. Classification

Refrigerants can be divided by various characteristics. The most common is their classification by origin:

- natural – e.g., ammonia, carbon dioxide, water, air, hydrocarbons (HCs) or sulfur dioxide,
- synthetic – e.g., hydrofluorocarbons (HFCs) or hydrofluoroolefins (HFOs).

Refrigerants can either be pure or mixtures. There are azeotropic and zeotropic (i.e., non-azeotropic) mixtures. The difference between these two types of mixtures is their behavior during a phase change – azeotropic refrigerants (as well as pure substances) evaporate/condense at a constant temperature, whereas zeotropic mixture temperature at the beginning and the end of a phase change differs. This temperature difference is called as a temperature glide [32].

2.6.2. Ozone depletion potential

ODP quantifies the refrigerant potential to damage the ozone layer. It is a relative value, the basis represents R11 (trichlorofluoromethane) - a fully halogenated chlorofluorocarbon with ODP equal to one. The use of refrigerants with ODP greater than zero is regulated [33].

2.6.3. Global warming potential

GWP quantifies the impact of a refrigerant on the global warming process. Again, GWP is a relative value. The basis represents carbon dioxide – its GWP is equal to one. The refrigerant GWP indicates, how much does it contribute to the greenhouse effect in comparison with CO_2. The value is determined by refrigerant radiation properties as well as by time of its dissolvement in the atmosphere [33].

2.6.4. Montreal Protocol

The first attempt to suppress the negative impact of various substances on the environment was discussed at the Vienna Convention for the Protection of the Ozone Layer in 1985 [34]. On the successive conference in 1987, The Montreal Protocol on Substances that Deplete the Ozone Layer was signed and entered to force from the start of 1989. Majority of the world's countries, including Czech Republic, USA or China, have committed themselves to comply with these treaties [35]. The aim of these efforts is to reduce the production of ozone depleting refrigerants and subsequently reduce their presence in the atmosphere [36].

The Montreal Protocol undergoes continuous adjustments in accordance with evolving scientific knowledge and more demanding environmental requirements. The last adjustment was adopted in 2008 [36]. It is one of the best functioning environmental treaties due to the elaborate financial mechanisms for consumption reduction support and for the phase-out of the most harmful substances [35].

2.6.5. F-gases legislation

The group of fluorinated greenhouse gases, often abbreviated as the F-gases, contains substances such as partially fluorinated hydrocarbons (HFCs), fully fluorinated hydrocarbons (PFCs), sulfur hexafluoride SF_6 and many others [37]. They have only negligible ODP. However, their GWP can amount to as high as tens of thousands in some cases [38].

Because of this negative impact, the EU attempts to regulate their use by issuing legislative acts. Most recently, there are two documents [39]:

- MAC Directive – deals with air conditioning systems of personal vehicles. The Directive prohibits the use of F-gases with GWP greater than 150.
- F-gas Regulation – covers all other key applications where F-gases are of importance. The original Directive was adopted in 2006, the update one applies from the beginning of 2015. The three fundamental principles are [39]:
    1. Limiting the total quantity of the most relevant F-gases,
    2. Banning the use of F-gases in numerous new types of equipment,
    3. Preventing emissions of F-gases from already existing equipment.

2.6.6. Refrigerant R744 (carbon dioxide)

Carbon dioxide as one of the most common natural refrigerants has a long tradition of use in the field of mechanical cooling. Highly valued was its inertness to construction materials and non-flammability. The use of CO_2 systems reached its peak during the 1920s and the early 1930s [40]. After wide expansion of halogenated hydrocarbon-based refrigerants the R744 importance diminished [6]. However, with increasing environmental protection tendencies in the last few decades it became clear, that carbon dioxide could be a reasonable solution. It has zero ODP and only a GWP equal to unity.

R744 has convenient thermodynamic properties and together with low energy usage it could possibly be a suitable refrigerant for applications such transport and commercial refrigeration, mobile air conditioning, cascade refrigeration systems, industrial heat extraction or shipping vessels [41]. As for now, it is mostly used in stationary refrigeration (e.g., supermarkets). The effectiveness of R744 systems is enabled by its low moisture content, which also contributes to low corrosive effects on refrigeration installation [42]. The above mentioned convenient thermodynamic properties also lead to lesser requirements on refrigerant charge, thus leading to saving on piping.

One of the most significant attributes of carbon dioxide as a refrigerant are its relatively high operating pressures in comparison to other commonly used refrigerants. The new rise of R744 was also made possible by the development of brazed plate heat exchangers (BPHE), which can withstand these high pressures [43]. In combination with low critical temperature (approximately 88°F / 31°C) it is not a suitable solution for retrofitting of existing, e.g., fluorocarbon systems [41]. Because of that low critical temperature, carbon dioxide installations working with ambient air condensers would often get into the supercritical region.

On the top of that, there are numerous potential hazards that are to be taken into account. Carbon dioxide is a natural component of the Earth's atmosphere. However, it can become toxic when its concentration is high enough - as low as 2 % concentration in the air can cause breathing problems, 20 % concentration is generally fatal [44]. Moreover, contact of liquid or solid R744 with human skin can cause freeze burns [45].

Table 1: Selected R744 properties [41]

ASHRAE Number	R-744
Critical Pressure	72.8 bar_g
Critical Temperature	31°C
Ozone Depletion Potential	0
Global Warming Potential	1
ASHRAE Safety Classification	A1
Temperature Glide	0 K

2.6.7. Refrigerant R452A

R452A, known also under its commercial name Opteon XP44, is a relatively new mixture that was in a larger scale introduced in 2014 [46]. Right from this beginning, it was intended as a possible future substitute for R404A in new devices or retrofits in low/medium temperature transport and commercial refrigeration applications [47]. R452A is a non-flammable hydrofluoro-olefin (HFO) based refrigerant mixture consisting of R32 (11 %), R125 (59 %) and R1234yf (30 %). It offers a 45 % reduction in GWP in comparison to R404A [47] and has a zero ODP.

Apart from lower environmental impact, it also exhibits lower temperatures at compressor discharge, which has a positive effect on compressor service life [48]. The ASHRAE Standard for Designation and Safety Classification of Refrigerants recognizes the R452A as a low toxic compound with no flame propagation – therefore putting it into the Safety class A1. R452A is a quasi-azeotrope refrigerant mixture, which means that it exhibits a temperature glide during phase changes. Overview of the main R452A properties is in Table 2.

Table 2: Selected R452A properties [49]

ASHRAE Number	R-452A
Composition (weight %)	R-32 (11) / R-125 (59) / R-1234yf (30)
Boiling point at 1 atm	- 47°C
Critical Pressure	39.0 bar_g
Ozone Depletion Potential	0
Global Warming Potential	1945
ASHRAE Safety Classification	A1
Temperature Glide	≈ 3 K

3. Heat exchangers

Heat exchangers are devices used for transfer of heat between two (or more in special cases) substances at different temperature levels. As a result of validity of the fundamental laws of thermodynamics, heat leaves the warmer substance and is absorbed by the colder substance.

The following types of HEs are among the most commonly used in refrigeration engineering [58]:

- plate heat exchangers,
- microchannel heat exchangers,
- tubular heat exchangers (e.g., internal heat exchange),
- coaxial coil heat exchangers (e.g., water-cooled condenser, liquid cooling evaporator),
- fin-and-tube heat exchangers (e.g., air-cooled condenser, air cooling evaporator).

Due to the extensive use of PHEs in refrigeration applications, biggest emphasis will be put on this HE type in the following text.

3.1. Plate heat exchangers

Thanks to their specific advantages and unique characteristics, PHEs are nowadays employed as substitutes for less compact shell-and-tube heat exchangers and are used for numerous applications in refrigeration – as condensers, evaporators and coolers of gases or liquids [59].

Most of the available literature focus mainly on traditional gasketed plate and frame HEs, which consist of either smooth or corrugated thin plates held together by compression bolts in a frame (Figure 9).

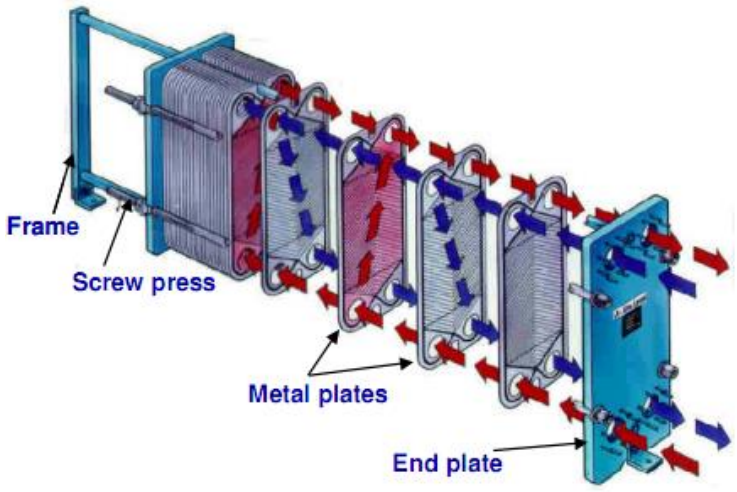

Figure 9: Plate heat exchanger [105]

The channels can be arranged in numerous ways – two basic configurations are depicted in Figure 10. Different combinations of these two approaches are possible.

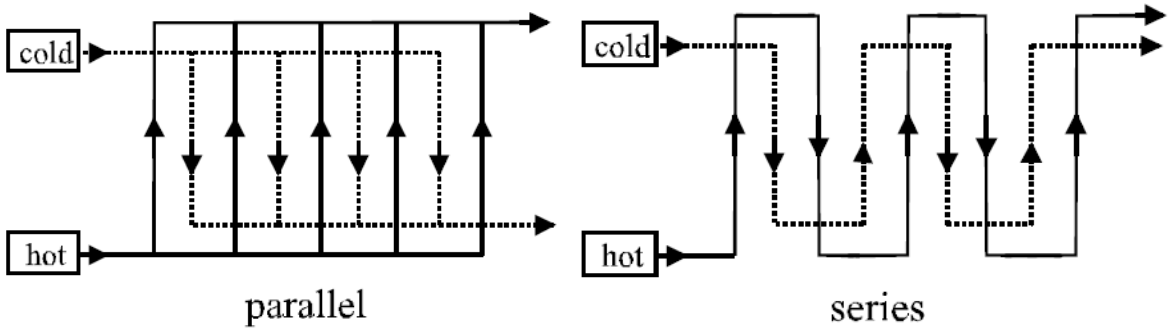

Figure 10: Parallel and series PHE channel arrangement [65]

3.1.1. PHE advantages

The main advantage is high compactness – large heat transfer area per unit volume. This feature makes it particularly suitable for applications where dimensions and weight reduction are of special importance – e.g., transport refrigeration and other mobile applications. Their convenient construction enables to achieve nearly ideal countercurrent flow. This fact, in combination with intense turbulent flow (high Reynolds numbers induced by the plate corrugation) inside PHE channels provides excellent heat transfer characteristics [60].

A great advantage of basic gasketed PHEs (not brazed nor welded) is their operational flexibility. They can be disassembled rather easily, which enables the operator to remove (resp. add) plates from the package if needed. Additionally, the inspection and cleaning activities are also simplified [61]. Mechanical fouling is relatively low due to high turbulences of the flow, however [62]. Another advantage is of economical nature – cost of PHEs is relatively low [63].

3.1.2. Brazed PHEs

Gasketed PHEs are limited to a certain pressure and temperature level – high pressures can cause undesirable leakages; high temperatures generally have a negative impact on the gasket material etc. To extend the PHE usability to higher operating conditions and to ensure safe handling of environmentally hazardous substances (e.g., chemicals or HFC refrigerants), welded and brazed PHEs were introduced.

BPHEs are generally manufactured in a vacuum furnace – corrugated stainless steel plates are brazed together using copper or nickel, which makes the channels perfectly tight and ready to use under high pressures [64].

3.1.3. Plates

The plates have generally one hole (port) in every corner and are sealed around in a way that the fluids flow alternately in the channels formed by successive plates while the heat is being exchanged between the fluids through these plates [65]. There are basically two options how the fluid can be forced to flow along a plate - it can either flow diagonally or parallel (Figure 11).

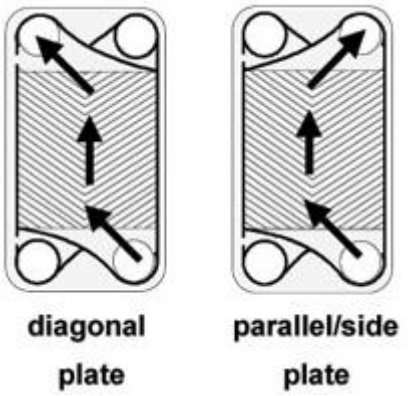

Figure 11: Fluid flow along a PHE plate [106]

Most of BPHEs have their plates corrugated, but even corrugation patterns and characteristics can vary. Probably the most important herringbone parameter is its corrugation angle (referred to most often as beta or theta in literature). The chevrons can either be acute (i.e., high-beta plate or L-channel type) or obtuse (i.e., low-beta plate or H-channel type) or multiple corrugation angles can be used inside one BPHE (i.e., mixed plate or M-channel type) [66]. The most characteristic dimensions of PHE plates and corrugation are depicted in Figure 107.

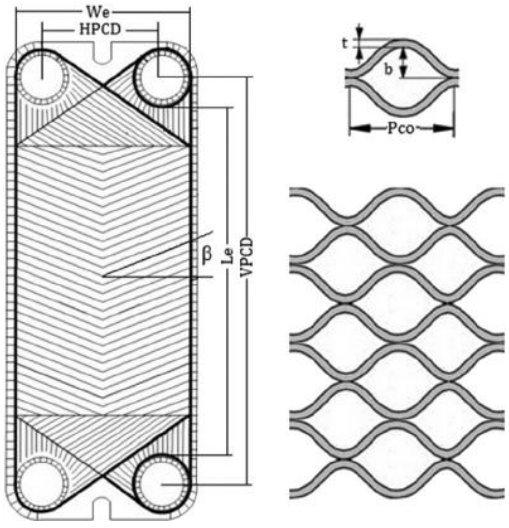

Figure 12: PHE plate geometry [107]

3.2. Heat transfer modes

There are three main physical heat transfer modes [50]:

- conduction,
- convection,
- radiation.

3.2.1. Conduction

Conduction is a transfer of heat energy from the more energetic (warmer) to the less energetic (colder) particles of one substance due to interactions between these particles. Through conduction, the temperature field across one substance tends to even out, as the heat energy is transferred from the more energetic (warmer) to the less energetic (colder) particles of this substance due to the interactions between its particles. Mostly, this heat transfer mode occurs in solid substances; to a lesser extent also in liquids and gases [51]. Conduction is generally quantified with the Fourier's law, which states that "the time rate of heat transfer through a material is proportional to the negative gradient in the temperature and to the area." [52] :

$$Q_{cnd} = -\lambda . S_{cs,n} . \left(\frac{dt}{dx}\right) \qquad (3.1)$$

3.2.2. Convection

Convection, on the other hand, is the major heat transfer mode concerning fluids and their interaction with solid objects. There are two basic types. Natural convection is induced by spontaneous motion of fluid based on local differences in its densities (according with Archimedes' principle). However, due to fact that fluid velocities are low with natural convection, the heat transfer coefficients also remain relatively low [53].

Much higher heat transfer coefficients can be achieved with forced convection, which occurs when intervention from outside (e.g., pump, ventilator or pressure difference) initiates the fluid flow. The rate of convection heat transfer is expressed in the Newton's Law of Cooling [54]. It states that "rate of change of the temperature of an object is proportional to the difference between its own temperature and the temperature of its surroundings" [55]. This idea can be transformed into a formula valid for both convection regimes [50] (for $t_w > t_o$):

$$q_{cnv} = \alpha . (t_w - t_o) \qquad (3.2)$$

The heat transfer coefficient is a complex empirical figure which depends on numerous variables related to flowing fluid properties, flow regime, geometric characteristics of the wall etc. More detailed analysis on heat transfer coefficients is provided later in the thesis.

3.2.3. Radiation

In most of commonly used industrial heat exchangers, the radiation plays an insignificant role. A matter – solid as well as liquid or gas - that has a temperature above absolute zero (0 K) emits a certain amount of energy in the form of electromagnetic radiation. This process is quantified by the Stefan-Boltzmann Law, which states that „the thermal energy radiated by a blackbody radiator per second per unit area is proportional to the fourth power of the absolute temperature“ [56]. For other objects than blackbody radiators the formula can be written as [57]:

$$Q_{rad} = e.\sigma_{SB}.T^4.S_{sur} \qquad (3.3)$$

In a real heat exchanger, all three heat transfer modes are present to a certain extent. To make calculations as accurate as possible, the overall heat transfer coefficient incorporating various thermal resistances that occur in the way of a heat flow is to be used.

3.3. Heat exchanger design

Selection of an adequate heat exchanger for given application is a complex problem. It comprises of quite a lot of different tasks - such as design specification, thermal, hydraulic and mechanical design as well as cost calculations or optimization aspects [67]. Most of above mentioned tasks are interconnected - therefore it is necessary to solve them in as complex and simultaneous manner as possible (an example of such process in Figure 13). The result of such analysis can be ambiguous - more different solutions can prove themselves suitable.

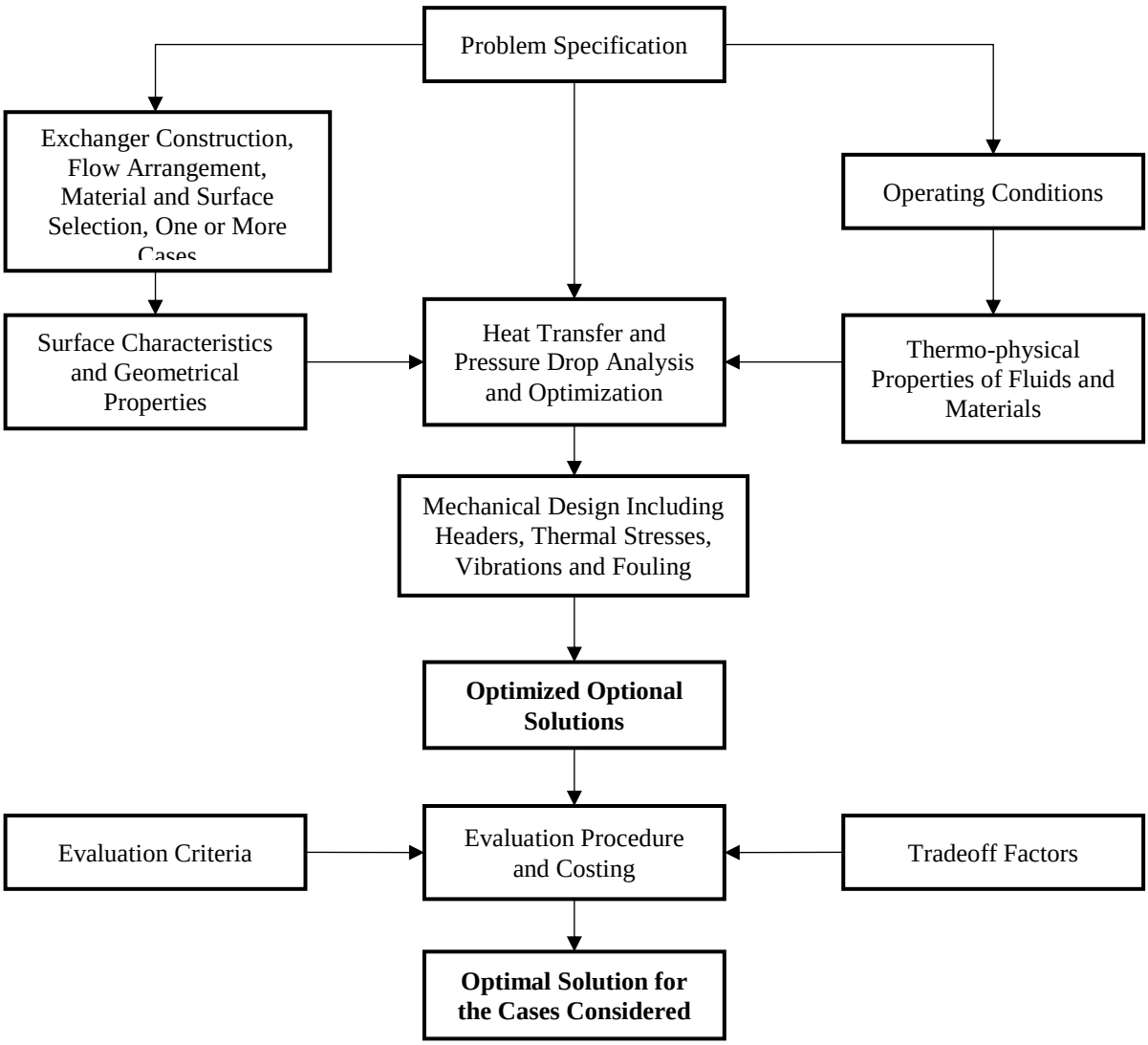

Figure 13: Heat exchanger design methodology [108]

3.3.1. Rating and sizing

Among the heat exchanger design problematic, two areas are of special significance – rating and sizing of a heat exchanger. A rating task is generally performed for an existing equipment (i.e., geometry and arrangement of the heat exchanger is given) and includes most commonly heat transfer and pressure drop performance evaluation, temperature distribution [68] etc. The objective can be testing the heat exchanger under other than nominal conditions or verifying specifications given by a vendor [67].

Sizing requires an actual design procedure – choosing the appropriate heat exchanger construction type, selecting the materials to use and determining the necessary physical dimensions (including heat transfer areas, plate geometry in case of PHE etc.) [69].

Although both rating and sizing procedures are fundamentally universal, slight differences need to be taken into consideration when dealing with different types of heat exchangers. In case of PHE, the sizing process gets "easier" as there is only a limited range of available plate types. This applies particularly for gasketed PHE as it is quite simple to add or remove plates if the heat exchanger performance differs from expected values.

3.3.2. HE design methods

Numerous heat exchanger design methods have been developed and are described in available literature. The most widely used are the Logarithmic Mean Temperature Difference (LMTD) Method and the Effectiveness-Number of Transfer Units (ε-NTU) method. Although each of these methods uses a different approach to analyze given heat exchanger, the results concerning exchanger thermal capacity should be identical [70].

However, these basic methods generally adopt several simplifications (such as single-phase flows, constant thermo-physical properties along the heat exchanger, negligible longitudinal heat conduction throughout the wall etc.), which make them not accurate enough for solving more complex cases (e.g., phase changes) and due to great local differences in fluid properties, as well as friction factor and heat transfer coefficient, the discretization of the HE becomes inevitable [71]. Because of the need to develop a reliable approach for these less common cases, a group of specialists from Universitat Politècnica de València developed a method called SEWTLE.

3.3.3. SEWTLE

The authors themselves describe their HE analysis tool as a cell-by-cell type general finite volume technique for the calculation of complex heat exchangers and decided to call it Semi Explicit Method for Wall Temperature Linked Equations (SEWTLE) [72]. This method is based on an iterative procedure consisting of several steps. It requires the knowledge of inlet fluid conditions on both sides (cold and hot) of the heat exchanger as well as their mass flow rates. Outputs of this method are thermodynamic properties of both fluids at HE outlets, including pressure drop. The authors claim that convergence of the presented technique is rapid and that it generally takes no more than ten iterations to reach it.

3.3.3.1. General solution procedure

After the heat exchanger is discretized into elementary cells (there are generally two types – fluid cells and wall cells), an initial estimation of temperature distribution across the wall cells is to be performed. After this, thermodynamic calculations for all fluid cells are to be carried out. As soon as this is achieved and thermodynamic properties at every fluid cell are known, the wall temperature distribution is recalculated based on fluid properties in the surrounding fluid cells and with the regard to the balance of heat transferred across the given wall cell.

This sequence of steps is repeated until the convergence is achieved, i.e., the heat removed from the hot side fluid stream equals the heat absorbed by the cold side fluid stream [73]. Thanks to its flexibility, the SEWTLE can be applied on various heat exchanger types and configurations. However, this thesis will mainly focus on plate heat exchanger specifics of this approach in the following text.

3.3.3.2. Finite Volume Method (FVM)

As mentioned above, the SEWTLE procedure represents a finite-volume-type approach. The FVM is a discretization technique designed for partial differential equations (PDE), conveniently used for those that can be derived from physical conservation laws [74]. In comparison with older Finite Element Methods (FEM) or the Finite Difference Methods (FDM), the FVM is particularly suitable and popular in Computational Fluid Dynamics (CFD) [75]. Reasons for this are [76]:

- faithful to the general physics (especially conservation),
- ability to capture shocks,
- ability to produce relatively simple stencils,
- possibility of applying a wide range of fluid flow equations, or
- facilitation of multigrid solutions.

The FVM discretization procedure involves two basic steps [75]:

1. The PDEs are integrated and transformed into balance equations over an element, which results in a set of semi-discretized equations.
2. Interpolation profiles are chosen to approximate the variation of the variable members within the element, relate the surface and the cell values of the variable members and thus transform the relations into algebraic equations.

3.3.3.3. Discretization scheme

To carry out the numerical calculation, it is necessary to divide the heat exchanger into a certain number of elementary pieces called cells. This procedure must be done for both fluid streams and the walls separating them. For a purpose of keeping the computational time in acceptable boundaries, a simplifying assumption is made – the fluid flows are considered as one-dimensional along a fluid cell [72], which corresponds fairly to the actual flow properties inside a PHE inter-plate channel.

In Figure 14 there are two different discretization approaches of a simple plate geometry with a parallel countercurrent flow of the refrigerants. Figure 14a shows us the so called **centered** arrangement, where the wall cell (plate is treated as a two-dimensional body for this purpose) area is identical to a "wall side" of both three-dimensional fluid cells at each side of the wall. Due to this, the wall temperature is defined at the center point of the wall cell – halfway between the inlet and the outlet point of a fluid cell.

On the contrary, the **staggered** discretization arrangement (Figure 14b) defines the fluid inlet and outlet properties in the same place as the wall temperatures – the wall cells are shifted relatively to the "wall sides" of the fluid cells. The SEWTLE authors strongly recommend the former arrangement as the latter approach is problematic in terms of satisfying the boundary conditions at the edge of the heat exchanger plates and therefore is not suitable for the FVM used here [72].

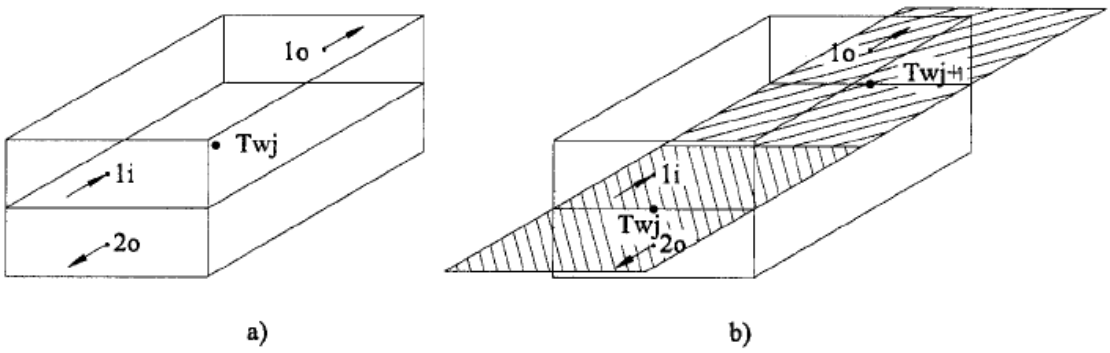

Figure 14: Discretization of a wall: (a) centered, (b) staggered arrangement [72]

3.3.3.4. PHE governing equations

Depending on whether the heat transfer process includes phase changes of refrigerants or not, the form of applied governing equations may differ. However, the first one is common for both cases – the conservation of the mass flow rate (or mass velocity) along a fluid path is represented in the continuity equation [77]. The mass velocity G can be calculated upon the knowledge of the refrigerant inlet conditions and remains constant:

$$G = \rho.u = \frac{m}{S_{cs,ch}} = const. \qquad (3.4)$$

Apart from the continuity equation, there are two more fundamental governing equations in the field of computational thermodynamics – the energy equation (based on the principle that energy is conserved) and the momentum equation (based on the Newton's Second Law of Motion) [78]. For the purposes of PHE calculations using SEWTLE, their following forms are used [71]:

- the energy equation for a steady single-phase one-dimensional flow:

$$S_{cs,ch} G \frac{d\left(i + \frac{u^2}{2}\right)}{dz} = \sum_{j=1}^{2} P_j \alpha_j \left(t_{wj} - t\right) \qquad (3.5)$$

- the momentum equation for a steady single-phase one-dimensional flow:

$$\frac{dp}{dz} = -\frac{d(\rho u^2)}{dz} - \frac{1}{2} f \rho \frac{u^2}{D_h} - \frac{d(zg\rho)}{dz} \qquad (3.6)$$

- the energy equation for a steady two-phase one-dimensional flow:

$$S_{cs,ch} G \frac{\partial}{\partial z}\left[x\left(i_g + \frac{G^2 x^2}{2\rho_g^2 \delta^2}\right) + (1-x)\left(i_l + \frac{G^2(1-x)^2}{2\rho_l^2(1-\delta)^2}\right)\right] +$$

$$+ S_{cs,ch} G \frac{\partial}{\partial z}(zgsin\theta) = P\alpha(T_w - T) \qquad (3.7)$$

- the momentum equation for a steady two-phase one-dimensional flow:

$$-\frac{dp}{dz} = \frac{2fG^2(1-x)^2}{D_h \rho_l} \Phi^2 + G^2 \frac{d}{dz}\left(\frac{x^2}{\rho_g \delta} + \frac{(1-x)^2}{\rho_l(1-\delta)}\right) + \left(\delta\rho_g + (1-\delta)\rho_l\right) gsin\theta \qquad (3.8)$$

3.3.3.5. Discretized governing equations

Due to the nature of processes inside a cascade heat exchanger, the two-phase governing equations are of the greatest importance. After their discretization, we get an explicit equation for the pressure drop along a cell (or more precisely - cell outlet pressure) [71]:

$$p_o = p_i - \left[\frac{2fG^2(1-x)^2}{D_h\rho_l}\Phi^2\right]'' \Delta z + G[CV_o - CV_o]^* + \left(\overline{\delta\rho_g + (1-\delta)\rho_l}\right)'' g\, sin\theta\, \Delta z \quad (3.9)$$

where superscript * indicates “evaluated at previous iteration”. Term CV can be determined as:

$$CV = G\left[\frac{x^2}{\rho_g\delta} + \frac{(1-x)^2}{\rho_l(1-\delta)}\right] \quad (3.10)$$

Determining the cell outlet pressure is the first step towards the calculation of all other outlet thermodynamic properties of the fluid. Most importantly the temperature - in case of zero temperature glide of the refrigerant (e.g., carbon dioxide), the pressure itself is sufficient for temperature determination. However, when the temperature glide is present (e.g., R452A), the outlet temperature is to be determined upon the knowledge of outlet pressure and outlet enthalpy [71]:

$$i_o = i_i + \sum_j \frac{\alpha_j}{m}\left(t_{wj} - \frac{t_i + t_o}{2}\right) P\, \Delta z - g\, sin\theta\, \Delta z \quad (3.11)$$

or

$$i_o = x_o\left(i_{g,o} + \frac{G^2x_o^2}{2\rho_o^2\delta_o^2}\right) + (1-x_o)\left(i_{l,o} + \frac{G^2(1-x_o)^2}{2\rho_o^2(1-\delta)^2}\right) \quad (3.12)$$

For the purposes of this thesis, the first equation has been chosen as the second one requires the estimation of the fluid outlet quality (the equation can be found in [71]), which further increases the difficulty and computational requirements of the whole calculation.

3.3.3.6. Wall temperature distribution

As soon as the thermodynamic calculations for all fluid cells are completed, it is time to recalculate the initial guess about the wall temperature distribution (i.e., wall temperature at the center of every wall cell). To find the desired wall temperature (in case that the wall thickness is neglected), an equilibrium must be found between the heat leaving the hot fluid and the heat absorbed by the cold fluid:

$$Q_{hot} = Q_{cold} \qquad (3.13)$$

$$\alpha_{hot}\, P_{hot}\, \Delta z_{hot}(t_{hot} - t_w) = \alpha_{cold}\, P_{cold}\, \Delta z_{cold}(t_w - t_{cold}) \qquad (3.14)$$

For most PHE, the perimeter and Δz (elementary cell height) are for both fluids the same, therefore the equation (3.14) is reduced to:

$$\alpha_{hot}\, (t_{hot} - t_w) = \alpha_{cold}\, (t_w - t_{cold}) \qquad (3.15)$$

and the expression for the wall temperature (under the assumption of negligible longitudinal heat conduction) is then:

$$t_w = \frac{\alpha_{hot} t_{hot} + \alpha_{cold} t_{cold}}{\alpha_{hot} + \alpha_{cold}} \qquad (3.16)$$

The equation (3.16) as well as (3.11) and (3.9) contains friction factors or heat transfer coefficients. These parameters depend on numerous variables and their calculation is often carried out using experimentally determined correlations.

3.4. Heat transfer coefficient determination

Convection is the dominant heat transfer mode in the channels of a BPHE. When describing the attributes or intensity of such heat transfer and carrying out the necessary calculations, one of the fundamental issues is to determine the convection heat transfer coefficient α and subsequently also the overall heat transfer coefficient U (of a wall separating two fluids, for instance), which considers convection heat transfer on both sides of the wall as well as heat conduction through it (Figure 15).

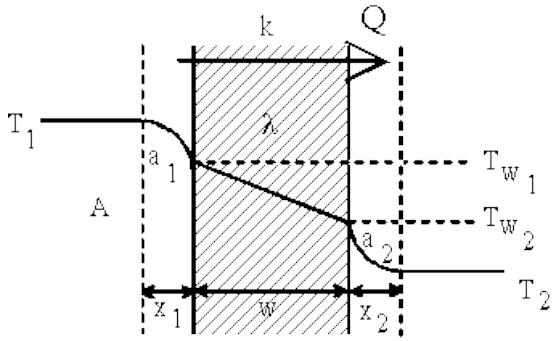

Figure 15: Heat transfer through a wall [109]

In this case, the overall HTC can be determined as [79]:

$$U = \left[\frac{1}{\alpha_c} + \frac{L_w}{\lambda_w} + \frac{1}{\alpha_h}\right]^{-1} \qquad (3.17)$$

The local HTC α describes the convection process in one specific point of the fluid-wall interface. However, this parameter is of little use when investigating the heat exchanger as whole. For this purpose, the average heat transfer coefficient $\bar{\alpha}$ along the entire fluid path is more appropriate [50]:

$$\bar{\alpha} = \frac{1}{A}\int_A \alpha \, dA \qquad (3.18)$$

3.4.1. Dimensionless parameters

The general approach contains the use of dimensionless parameters to obtain the desired HTC – most commonly the Reynolds, the Nusselt, the Prandtl, the Grashof or the Péclet number. HTC is most closely connected to the Nusselt number, which is commonly described as a basic dimensionless convective HTC and represents the ratio of convection heat transfer to conduction with a hydraulic diameter D_h [80]:

$$Nu = \frac{\alpha . D_h}{\lambda} \qquad (3.19)$$

The Reynolds number is a ratio of inertia and viscous forces inside a fluid. Apart from its use in HTC-related correlations, it is an important figure for a purpose of determining of whether the flow is turbulent or not.

$$Re = \frac{\rho . c . D_h}{\mu} = \frac{G . D_h}{\mu} \qquad (3.20)$$

Another parameter commonly used in investigated HTC correlations is the Prandtl number, which represents the ratio of the molecular momentum and the thermal diffusivities [83]:

$$Pr = \frac{\mu . c_p}{\lambda} \qquad (3.21)$$

3.4.2. Heat transfer correlations

HTC as well as pressure drop correlations have been studied extensively in the last decades and the results of these investigations were published in numerous articles. However, a general theory able to cover the whole variety of PHE geometries and arrangements still does not exist and is most likely impossible to create [82]. Therefore, each investigation for these correlations should be carried out bearing in mind that presented methodology is only applicable to a limited range of cases.

There are correlations suitable for quick informative calculations as well as more complex relations which take more variables into account and should generally provide better accuracy. Moreover, when applying a correlation for a certain case, one must keep in mind that most of these relations have their specific range of validity, e.g., given by the Reynolds numbers, heat fluxes etc.

3.4.2.1. Hydraulic diameter

Every heat transfer correlation needs to determine the characteristic dimension to calculate with. In case of tubular or other form of somehow channeled flow, the hydraulic diameter D_h is generally considered to be the characteristic dimension. The generic equation to determine this value is [83]:

$$D_h = \frac{4 S_{cs,p}}{O_p} \qquad (3.22)$$

The examples of hydraulic diameter values for basic channel or duct geometries are in Figure 16.

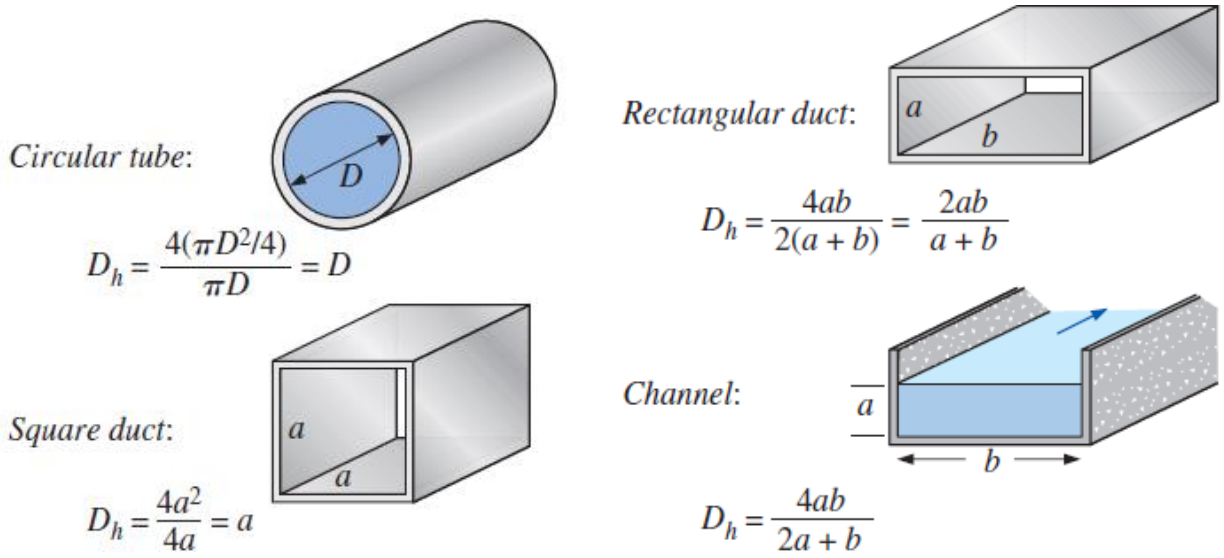

Figure 16: Hydraulic diameter calculation examples [110]

In case of plate heat exchangers, the channel cross sections are not as simple as the depicted cases. Therefore, the hydraulic diameter calculation needs to be somewhat simplified to obtain satisfactory results without the need to deploy advanced calculations. Two relations were extracted from the available literature. Mori et al. define D_h followingly [84]:

$$D_h = \frac{2b}{\varphi} \qquad (3.23)$$

where φ is the surface enlargement factor. It is a function of the corrugation pitch and depth. The authors recommend to $\varphi_{average} = 1.17$.

More complex relation including also the plate width w is provided by Abu-Khader in [60]:

$$D_h = \frac{4bw}{2(b + w\varphi)} \qquad (3.24)$$

The author approves to use the simplified version if b << w, however. These two relations were tested as a part of the investigation – the calculated differences were quite negligible.

3.4.2.2. Single-phase correlations

In case of forced convection, which generally occurs in BPHE channels, heat transfer coefficients are commonly correlated using the following relation [81]:

$$Nu = C_1 Re^{C_2} Pr^{C_3} \left(\frac{\mu_m}{\mu_w}\right)^{C_4} \qquad (3.25)$$

where the Nusselt number is a function of the Reynolds and the Prandtl number, the ratio of dynamic viscosity in the middle of the fluid flow and on the wall. The correction factors C_1, C_2, C_3 and C_4 are experimentally determined parameters, which generally can depend on heat exchanger geometric characteristics, plate pattern or even type of working fluid. However, in the studied literature are presented also different forms of correlations.

3.4.2.2.1. Correlations by Focke, Thonon and Muley&Manglik

Hayes and Jokar provide in their text [85], which studies carbon dioxide condensation in BPHEs and applicable correlations, a comprehensible comparison of well-established single-phase correlations used for this type of heat exchangers for heat transfer (Table 3) as well as friction factor analysis.

Table 3: Single-phase correlations coefficients (Focke, Thonon, Muley&Manglik) [85]

	β	Re	C1	C2	C3	C4
Focke	30	20 – 150	1.89	0.46	0.50	0.00
	30	150 – 600	0.57	0.7	0.50	0.00
	30	600 – 16,000	1.11	0.6	0.50	0.00
	45	45 – 300	1.67	0.44	0.50	0.00
	45	300 – 2,000	0.41	0.7	0.50	0.00
	45	2,000 – 20,000	0.84	0.6	0.50	0.00
	60	120 – 1,000	0.77	0.54	0.50	0.00
	60	1,000 – 42,000	0.44	0.64	0.50	0.00
Thonon	30	50 – 15,000	0.29	0.7	0.33	0.00
	45	50 – 15,000	0.3	0.65	0.33	0.00
	60	50 – 15,000	0.23	0.63	0.33	0.00
Muley&Manglik	30	over 1,000	0.09	0.7	0.33	0.14
	45	over 1,000	0.08	0.76	0.33	0.14
	60	over 1,000	0.08	0.78	0.33	0.14

3.4.2.2.2. Correlation by Khan&Khan

Study [86] presented in 2010 contains even larger comparison of different correlations for corrugated PHE. Based on performed experiments, it also presents correlations of its own for two different chevron angles – for symmetric (30° and 60°) as well as mixed plate arrangement (30°/60° plates alternately in one PHE). The study highlights significant effect of corrugation angle and the Reynolds number on the HTC [86]. The correlation form is again

$$Nu = c_1 Re^{c_2} Pr^{c_3} \left(\frac{\mu_m}{\mu_w}\right)^{c_4} \qquad (3.26)$$

where the correction factors c_i differ depending on the chevron angle (Table 4). The Prandtl number exponent remains the same as well the coefficient C_4.

Table 4: Khan&Khan single-phase correlation coefficients [86]

β	C1	C2	C3	C4
60/60	0.1449	0.8414	0.35	0.14
30/60	0.1437	0.7810	0.35	0.14
30/30	0.1368	0.7424	0.35	0.14

The paper also presents a universal correlation that can be used for PHE regardless of the plate chevron angle. It is valid for Reynolds numbers ranging from 500 to 2,500, in case of the Prandtl numbers the range is from 3.5 to 6.

$$Nu = \left(0.0161 \frac{\beta}{\beta_{max}} + 0.1298\right) Re^{\left(0.198 \frac{\beta}{\beta_{max}} + 0.6398\right)} Pr^{0.35} \left(\frac{\mu}{\mu_w}\right)^{0.14} \qquad (3.27)$$

where β_{max} is the maximal value of chevron angles used in given PHE.

3.4.2.3. Condensation correlations

For the case of condensation inside a PHE, the range of available literature is considerably more limited. However, some of the PHE correlations were obtained directly for the carbon dioxide condensation, e.g. [87]. In the end, several potentially appropriate correlations were chosen and tested.

3.4.2.3.1. Correlation by Hayes

As stated previously, the study [87] presents HTC correlations developed primarily for CO_2 condensation inside a BPHE for three different chevron angles. The authors created a complex relation, where the Nusselt number is a function of not only the Reynolds and the Prandtl numbers, but also of four more dimensionless terms. The three observed chevron angles were:

- low profile (L) – 60° chevron angle,
- medium profile (M) – consists of 60° and 27° alternating plates,
- high profile (H) – 27° chevron angle.

Each of these angles goes with different correlation coefficients as well as range of validity.

$$Nu = C_1 Re_l^{c_2} Pr_l^{c_3} \left(\frac{G^2}{\rho_l^2 c_{p,l} \Delta T}\right)^{c_4} \left(\frac{\rho_l^2 i_{lg}}{G^2}\right)^{c_5} \left(\frac{\rho_l \sigma_l}{\mu_l G}\right)^{c_6} \left(\frac{\rho_l}{\rho_l - \rho_g}\right)^{c_7} \qquad (3.28)$$

The coefficients valid for different chevron angles are in Table 5. As in the Khan&Khan single-phase correlation, the Prandtl number exponent is constant and equal to 0.35 in all three cases.

Table 5: Hayes condensation correlation coefficients [87]

Plate	C1	C2	C3	C4	C5	C6	C7	Re range
L	0.37	0.706	0.35	1.07	0.91	0.0320	1.18	67 – 1,276
M	0.16	0.727	0.35	1.07	0.90	0.1470	1.00	164 – 1,233
H	0.11	0.771	0.35	1.04	0.92	0.0105	2.00	129 – 1,156

3.4.2.3.2. Correlation by Mancin

Although the paper [88] studies the condensation of hydrofluorocarbon refrigerants R410A and R407C, the developed correlation has been selected for our purposes to be tested. The reason for this was besides other favorable features the fact that the correlation provides direct calculation of the HTC. Moreover, it incorporates the influence of vapor quality to the calculation, which was perceived as an important fact.

This approach determines the total HTC as a form of average between the gravity dominated HTC α_{Nu} and the shear dominated HTC α_A:

$$\alpha_{total} = \sqrt{\alpha_A^2 + \alpha_{Nu}^2} \qquad (3.29)$$

The shear dominated heat transfer coefficient:

$$\alpha_A = \alpha_{LO}.\left[1 + 1.128\, x^{0.817}\left(\frac{\rho_l}{\rho_g}\right)^{0.3685}\left(\frac{\mu_l}{\mu_g}\right)^{0.2363}\left(1 - \frac{\mu_g}{\mu_l}\right)^{2.144} Pr^{-0.1}\right] \qquad (3.30)$$

where α_{LO} is according to [89]:

$$\alpha_{LO} = 0.023\frac{\lambda_l}{D_h} Re_{LO}^{0.8} Pr_l^{0.4} = 0.023\frac{\lambda_l}{D_h}\left(\frac{G D_h}{\mu_l}\right)^{0.8} Pr_l^{0.4} \qquad (3.31)$$

where the "LO" subscript stands for the liquid state with the total flow rate.

The gravity dominated heat transfer coefficient:

$$\alpha_{Nu} = 0.943.\left[\frac{\rho_l\left(\rho_l - \rho_g\right) g\, i_{lg}\, \lambda_l^3}{\mu_l\, L\, (T_{sat} - T_w)}\right]^{0.25} \qquad (3.32)$$

3.4.2.3.3. Correlation by Han

The authors of the paper [96] have studied the condensation of refrigerants R410A and R22 and the BPHE chevron angles of 20°, 35° and 45°. They came up with the conclusion, that the HTC (as well as the pressure drop) increases with the increasing mass flux and the vapor quality. On the hand, it decreases with the increasing condensation temperature and the chevron angle. They have proposed the HTC correlation in the following form:

$$Nu = Ge_1 Re_{Eq}^{Ge_2} Pr^{1/3} \qquad (3.33)$$

The coefficients Ge_1 and Ge_2 depend on the HE geometry (including the corrugation pitch p_{co}):

$$Ge_1 = 11.22\left(\frac{p_{co}}{D_h}\right)^{-2.83}\left(\frac{\pi}{2} - \beta\right)^{-4.5} \qquad (3.34)$$

$$Ge_2 = 0.35\left(\frac{p_{co}}{D_h}\right)^{0.23}\left(\frac{\pi}{2} - \beta\right)^{-1.48} \qquad (3.35)$$

This correlation can be used for the range of the equivalent Reynolds numbers Re_{eq} from 300 to 4,000. It can be determined as:

$$Re_{eq} = \frac{G_{eq} D_h}{\mu_l} \qquad (3.36)$$

where the equivalent mass flux is:

$$G_{eq} = G\left[1 - x + x\left(\frac{\rho_l}{\rho_g}\right)^{1/2}\right] \qquad (3.37)$$

3.4.2.4. Evaporation correlations

In contrast to the carbon dioxide condensation, there is a temperature glide present when a mixture of two or more refrigerants with different evaporation temperature is used. Therefore, it is necessary to use appropriate correlations, which take the temperature glide-related phenomena into consideration.

3.4.2.4.1. Correlation by Han

The group of authors led by Dong-Hyouck Han have developed not only condensation correlations for BPHEs, but also relations for evaporation using R410A and R22 again [97]. The approach is similar with the condensation case – using geometrical coefficients which make the HTCs significantly dependent on corrugation properties.

The equivalent Boiling number Bo_{eq} is introduced in this correlation:

$$Bo_{eq} = \frac{q_w}{G_{eq} i_{lg}} \qquad (3.38)$$

where q_w is the heat flux through the wall and G_{eq} is the equivalent mass flux, which is vapor quality-dependent. The HTC increases with the increasing mass flux and the vapor quality and it decreases with the increasing evaporation temperature and the chevron angle.

The Nusselt number correlation and the geometrical coefficient are defined as follows:

$$Nu = Ge_1 Re_{Eq}^{Ge_2} Bo_{Eq}^{0.3} \mathrm{Pr}^{0.4} \qquad (3.39)$$

$$Ge_1 = 2.81 \left(\frac{p_{co}}{D_h}\right)^{-0.041} \left(\frac{\pi}{2} - \beta\right)^{-2.83} \qquad (3.40)$$

$$Ge_2 = 0.746 \left(\frac{p_{co}}{D_h}\right)^{-0.082} \left(\frac{\pi}{2} - \beta\right)^{0.61} \qquad (3.41)$$

3.4.2.4.2. Correlation by Hsieh

As well as in previous Han's correlation, also in this case have been the results developed upon experiments with R410A [98]. However, only one chevron angle value (60°) has been investigated. The authors came to conclusion that the HTC is affected almost negligibly by the mass flow rate, but it increases linearly with the increasing heat flux [81]. The changes of saturation pressure have only limited effect on the HTC.

Based on the experimental measurements, the authors correlate the boiling HTC as:

$$\alpha_{r,sat} = \alpha_{r,l}(88Bo^{0,5}) \qquad (3.42)$$

where $\alpha_{r,l}$ is the all-liquid nonboiling HTC and is determined as:

$$\alpha_{r,l} = 0.2092\left(\frac{\lambda_l}{D_h}\right)Re^{0.78}Pr^{1/3}\left(\frac{\mu_m}{\mu_w}\right)^{0.14} \qquad (3.43)$$

and the boiling number is calculated as [99]:

$$Bo = \frac{q}{Gi_{lg}} \qquad (3.44)$$

3.4.2.4.3. Correlation by Yan

The group of authors Yan, Lin and Yang derived a heat transfer and a pressure drop correlation based upon experiments with the refrigerant R134a. As in the previous case, only one chevron angle (60°) has been investigated. This correlation puts emphasis on the vapor quality – it is explicitly present in the HTC correlation through the equivalent mass flux.

Some of the interesting conclusions of this study [90]:

- the mass flux has a significant effect on the HTC only in the region of high vapor qualities,
- the heat flux, on the other hand, shows bigger influence in the region of low vapor qualities,
- an increase in the evaporation pressure results in a lower HTC at higher vapor qualities.

The heat transfer correlation for the refrigerant Nusselt number can be expressed as [81]:

$$Nu = 1.926Pr_l^{1/3}Bo_{eq}^{-0.3}Re_{eq}^{0.5}\left[(1-x)+\left(\frac{\rho_l}{\rho_g}\right)^{0.5}\right] \qquad (3.44)$$

and is valid for equivalent Reynolds number Re_{eq} ranging from 2,000 to 10,000.

3.4.2.5. Correlations comparison

Although it is a very important task to choose the suitable heat transfer correlation for the heat exchanger calculations, it is often not completely unambiguous, which one is the “correct” one. The results can differ significantly when applying different correlations on the same flow conditions.

The group of authors around J. R. García-Cascales has published a comparison of several heat transfer multi-phase correlations commonly used in PHE design. As can be seen from the Figure 17 comparing the HTC values obtained for the boiling case for defined mass flow rate, different correlations provide very variable results depending on vapor quality. In case of lower qualities, the correlation conformity is relatively satisfactory. On the other hand, in the high vapor quality region the resulting HTC can vary by as much as hundred per cent.

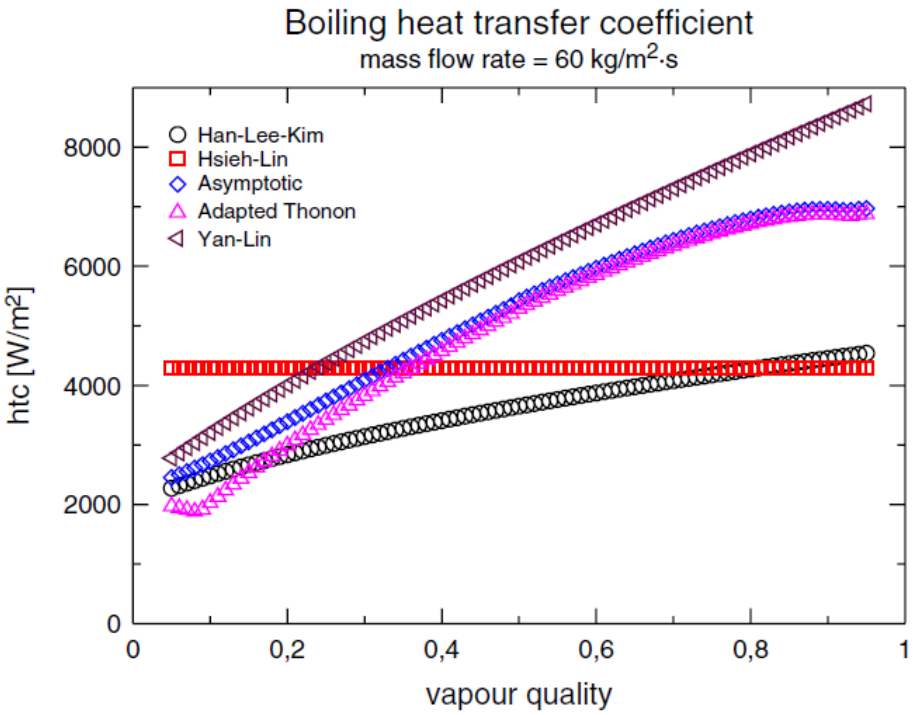

Figure 17: Boiling heat transfer coefficient variation [81]

Even greater differences can be observed among the condensation correlations (see Figure 18). Most of these correlations consider the HTC to increase with increasing vapor quality – except for the Thonon correlation. This is in contrast with the boiling correlations where the agreement of all the authors on this HTC-quality dependency is universal.

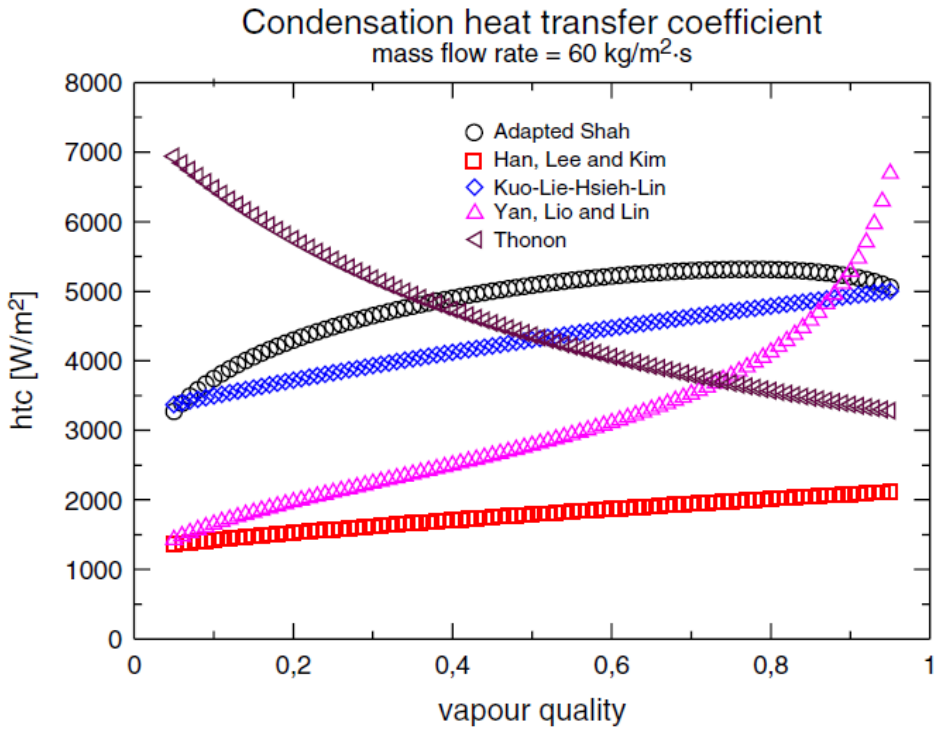

Figure 18: Condensation heat transfer coefficient variation [81]

A slight discrepancy can be also observed in the approach of different authors to the influence of the chevron angle on the HTC. In some of the correlations the HTC increases with the decreasing chevron angle (e.g., Han, Focke or Thonon), others show the opposite dependency (e.g., Muley and Manglik). Generally, the inclination angle between the plate corrugations is considered as one of the most vital parameters in the thermohydraulic performance calculations of PHEs.[1] However, the PHE manufacturers generally do not disclose this kind of data as it is an important part of their know-how.

[1] The effect of the corrugation inclination angle on the thermohydraulic performance of plate heat exchangers

4. Cascade heat exchanger – calculation theory

The goal of this thesis is the calculation of thermal processes taking place inside a given cascade brazed plate heat exchanger. The basic task is given like this: to calculate the outlet conditions of both refrigerants for the given inlet conditions and the heat exchanger geometry and characteristics. After an extensive research, it was decided to use the SEWTLE procedure for this purpose as it proved itself to be an interesting and non-traditional method.

However, to perform a calculation like this, it is necessary to incorporate the heat exchanger into the closed refrigeration cycle to prove its usefulness for practical purposes. Therefore, the heat exchanger numerical analysis is only one of the calculations performed within the whole refrigeration system calculation process. Nevertheless, it is by far the most complex calculation of all the refrigeration cycle components.

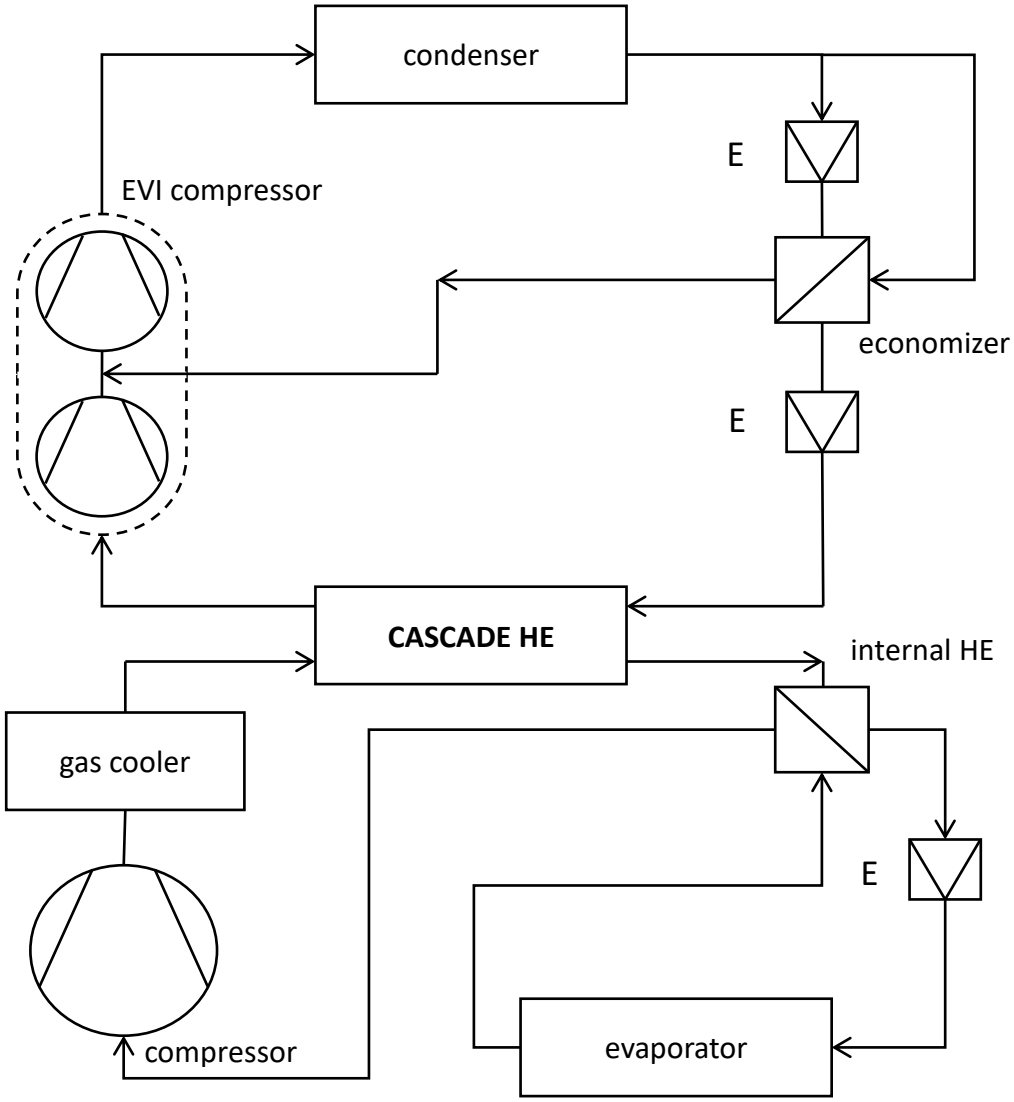

Figure 19: Advanced cascade refrigeration cycle

4.1. Refrigeration cycle – calculation theory

To perform thermodynamic calculations of the whole refrigeration cycle, it is necessary to define its main components first. To have an opportunity to compare the calculated figures with available empirical results, the refrigeration cycle had to be chosen accordingly. The cycle with its most significant components is in Figure 19.

In order to keep the whole calculation process at an acceptable complexity level, certain simplifying assumptions were adopted. This applies for instance to internal heat exchange, EVI compressor or gas cooler as will be described in the following paragraphs.

4.1.1. Calculation methodology

The general idea of this calculation method is to find the equilibrium between the heat absorbed by the low temperature cycle (abbr. CC – cold cycle) refrigerant inside the evaporator and the heat released by the high temperature cycle (abbr. HC – hot cycle) refrigerant inside the condenser while meeting all the specified conditions (input values). Of course, also the heat balance between the two sides of the cascade heat exchanger is to be met to ensure the equilibrium of the cascade cycle.

The entire cycle calculation can be therefore divided into several sub-calculations, such as:

- CC calculation,
- HC calculation,
- CC evaporator balance,
- HC condenser balance,
- heat flows balance,
- cascade heat exchanger balance.

These sub-calculations are combined and repeated to create an iterative procedure that should provide the desired solution – the state of equilibrium of the whole cascade refrigeration cycle. This means that the refrigerant properties at any point of the cycle are known.

The vital task is the determination of all four pressure levels (i.e., the phase change temperatures) inside the system. The system operates only at these pressures as the pressure losses are neglected in our calculation:

- CC evaporation pressure $p_{evap,CC}$ => CC evaporation temperature $t_{evap,CC}$
- CC condensation pressure $p_{cond,CC}$ => CC condensation temperature $t_{cond,CC}$
- HC evaporation pressure $p_{evap,HC}$ => HC evaporation temperature $t_{evap,HC}$
- HC condensation pressure $p_{cond,HC}$ => HC condensation temperature $t_{cond,HC}$

First, these pressures (i.e., corresponding saturation temperatures) are given by the initial estimate. In the course of the calculation, they are changed until the system convergence is reached. The iterative procedure is based on the bisection method, which is described in the previous part of the thesis.

The saturation temperatures were selected over the pressure levels in the calculations as it proved to be advantageous for the iteration procedure and related calculations. There is no difficulty with this approach

with pure refrigerants and azeotropic mixtures. However, zeotropic refrigerant mixtures exhibit temperature glide during a phase change. In this case, the condensation/evaporation temperature is considered the one on the saturated vapor line. Throughout the calculation, critical temperature is tested at several points to ensure the cycle stays within the sub-critical boundaries.

4.1.2. Bisection method

Throughout the global calculation procedure, there are several points where desired result cannot be explicitly calculated. In these cases, an iterative process is necessary to obtain such values. Therefore, a variant of the bisection method is employed inside the SEWTLE procedure. Its authors recommend the Newton-Raphson algorithm, which is based on the similar foundations. Even though it generally offers a faster convergence than the bisection method, it can become quite unreliable at certain conditions [91].

It is a numerical method generally used to find a root of a given function [92]. In our modification of the bisection method when calculated values x_{calc} are compared with the input ones x_{input}, the sequence of steps is defined followingly:

1. Calculation is performed using the initial estimate input $v_{initial}$ to obtain $x_{calc,1}$
2. Both values are compared: $x_{calc,1} - x_{input} = y_1$
3. Depending on the y_1 value, three possible scenarios are to be selected from:
    a. $|x_{calc,1} - x_{input}| < z$, where z is the desired calculation accuracy. If this condition is met, the root has been found and the calculation cycle is terminated.
    b. $|x_{calc,1} - x_{input}| > z$ and y_1 is a positive value: the initial estimate $v_{initial}$ is adjusted by adding (resp. subtracting)[2] initial step $s_{initial}$.
    c. $|x_{calc,1} - x_{input}| > z$ and y_1 is a negative value: the initial estimate $v_{initial}$ is adjusted by subtracting (resp. adding) initial step $s_{initial}$.
4. Calculation is performed using the adjust value $v_{adjusted,1} = v_{initial} +/- s_{initial}$ to obtain $x_{calc,2}$
5. Values are compared again: $x_{calc,2} - x_{input} = y_2$
6. Depending on the y_2 value, several possible scenarios are to be selected from:
    a. $|x_{calc,2} - x_{input}| < z$, where z is the desired calculation accuracy. If this condition is met, the root has been found and the calculation cycle is terminated.
    b. $|x_{calc,2} - x_{input}| > z$: now, the sign of the y_2 value is to be analyzed – if it is the same as for the previous value (y_1 in this case), the adjusting step $s_2 = s_{initial}$
    c. $|x_{calc,2} - x_{input}| > z$: if the sign of y_2 value is different from the previous value (y_1 in this case), the adjusting step is halved: $s_2 = s_{initial} / 2$. Additionally, if $s_{initial}$ was added previously, s_2 is now subtracted and vice versa.
7. The iteration cycle continues as described until $|x_{calc,i} - x_{input}| < z$.

[2] the choice between adding and subtracting has to be made according to the impact that this will have on the final value

4.1.3. Input values

4.1.3.1. Compressors

Due to the fact, that every compressor is designed for different operating conditions or substances, it becomes necessary to choose the optimal compressor for given requirements. Generally, the possible range of application is defined by the compressor operating envelope. It defines the limitations to the use of a given compressor. In other words, the manufacturer cannot ensure its reliable operation when running outside these boundaries [93]. These are mostly given in terms of allowed evaporation-condensation temperature pairs for a certain refrigerant (see Figure 20).

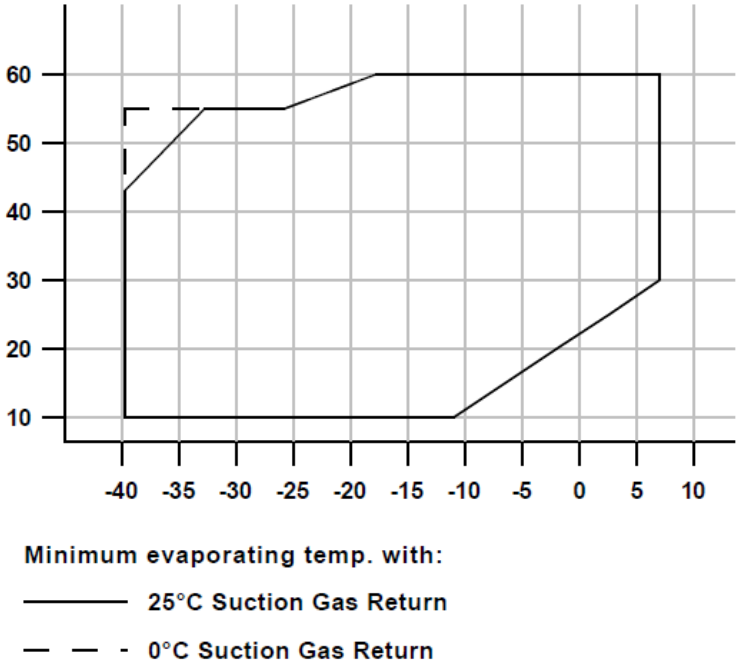

Figure 20: Operating envelope – compressor ZFD18KVE-TFD [94]

For this approved range of temperatures pairs, certain measured data (e.g., cooling capacity, power input P, mass flow rate m or electric current) are provided by the manufacturer, as well as nominal value of displacement V_n, level of suction superheat, sound pressure levels [94] etc.

First, it is necessary to consolidate these data to make the following calculations possible. The aim is to obtain a pressure-ratio-dependent relation for both isentropic efficiency and volumetric efficiency. From given temperature pairs, the respective refrigerant pressures (and the pressure ratio σ, subsequently) are determined using the CoolProp (a refrigerant library extension for MS Excel).

The compressor suction temperature t_s is calculated as a sum of the evaporation temperature and the suction superheat ΔT_s:

$$t_s = t_e + \Delta T_s \qquad (4.1)$$

Thanks to the knowledge of the suction temperature and the evaporation pressure, the refrigerant suction state is determined completely - it is now possible to identify the enthalpy i_s, entropy s_s and density ρ_s at this point of the cycle.

In the case of an isentropic compression of the refrigerant, also the refrigerant properties at the compressor discharge (e.g., enthalpy $i_{d,ie}$) can be determined as functions of condensation pressure and entropy. The isentropic power input P_{ie} is calculated as:

$$P_{ie} = m\left(i_{d,ie} - i_s\right) \qquad (4.2)$$

This value is then compared with the power input P given by the manufacturer – thus the isentropic efficiency η_{ie} is determined:

$$\eta_{ie} = \frac{P_{ie}}{P} \qquad (4.3)$$

The theoretical mass flow rate m_{th} can be determined at the compressor suction as:

$$m_{th} = V_n\,\rho_s \qquad (4.4)$$

This value is then compared with the mass flow rate m given by the manufacturer – thus the volumetric efficiency λ is determined:

$$\lambda = \frac{m}{m_{th}} \qquad (4.5)$$

These calculations are carried out for all the temperature pairs and the resulting isentropic and volumetric efficiencies are transferred into the chart as functions of the pressure ratio. Finally, the appropriate trendlines (generally polynomial) are selected (e.g., Figure 21 for ZFD18KVE-TFD EVI). The resulting coefficients of these equations are then used as input parameters, along with the compressor displacement, for the whole refrigerant system calculation.

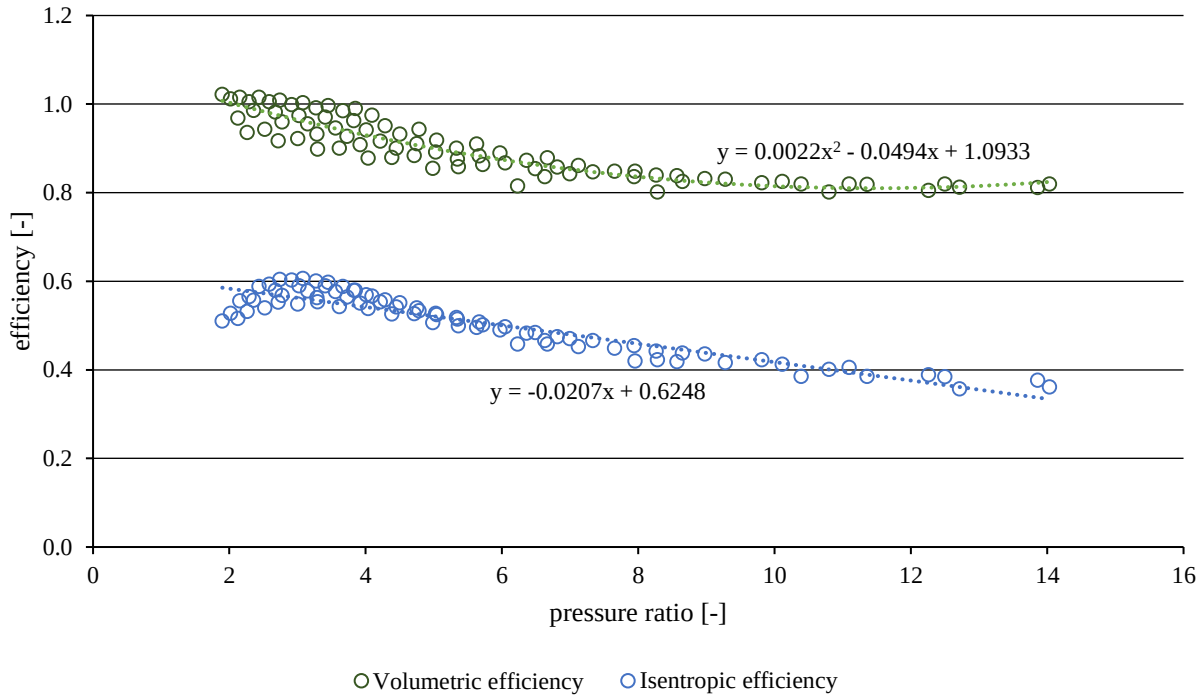

Figure 21: Volumetric and isentropic efficiency

4.1.3.2. Internal heat exchange

Inside an internal heat exchanger, the subcooling of the condensed vapors take place on one side, while on the other side the evaporated refrigerant is further superheated. To keep the calculation at relatively simple level, the decision has been made to withdraw from the intention to define the internal heat exchanger in detail. Instead, the IHE effectiveness is introduced.

First, the heat capacity rates of the two fluids (hot and cold) are to be compared [95]:

$$C_h = \left(m\, c_p\right)_h \qquad (4.6)$$

$$C_c = \left(m\, c_p\right)_c \qquad (4.7)$$

where m is the mass flow rate and c_p is the specific heat. In elementary case when the mass flow rate is on both sides equal, the vapor side (i.e., the cold side) heat capacity rate will always be lower due to fact that the specific heat of a gas is generally lower than of a liquid. Therefore, the inlet liquid temperature presents the upper limit for vapor outlet temperature. However, this potential is never fully utilized – the vapor outlet temperature will always be lower, which is reflected by the IHE efficiency. Therefore, it is another cycle calculation input.

4.1.3.3. Gas cooler

In case of an ambient-air-cooled gas cooler, which is used in our low temperature part of the cycle, we assume that its heat transfer area and the air flow rate are large enough to always ensure the same cold side temperature difference ΔT_{cooler}, which is also one of the input parameters for the cycle calculation.

For instance, if ΔT_{cooler} is set to 2 K and the ambient air temperature $t_{air,c}$ is 40°C, the resulting outlet temperature of the cooled carbon dioxide will be:

$$t_3 = t_{air,c} + \Delta T_{cooler} = 40 + 2 = 42°C$$

4.1.3.4. Economizer (EVI)

The theoretical analysis of a system containing an EVI compressor (i.e., the refrigerant mass flow is divided after the condenser and reunited in the compressor again) is a complex difficult process and exceeds the options and the scope of this thesis. Therefore, we omit this feature in our calculations – the compressor is for purpose of our calculations considered to be an "ordinary" one. The economizer is also left out.

4.1.3.5. Expansion valves

Expansion valves control the amount of gas-liquid mixture entering the evaporator, thus directly affecting the resulting vapor superheating. This level of superheating is necessary to be determined as one of the input parameters for the cycle calculation – for the CC evaporator as well as HC evaporator (i.e., cascade heat exchanger in this case).

Apart from the superheating, also the level of refrigerant subcooling after the condensation is a necessary input variable for both high and low temperature parts of the cycle.

The throttling process is considered as adiabatic, which is valid for expansion valves placed close to the evaporator.

4.1.3.6. Heat exchangers

In order to be able to carry out the evaporator and the condenser heat balance calculation, several input values are necessary. In case of the evaporator, the heat is transferred from the freezer air to the refrigerant. In the condenser, the heat is released from the refrigerant into the ambient air. The required properties of the freezer air and the ambient air are:

- mass flow rate,
- inlet temperature,
- specific heat.

Another important heat exchanger characteristic is to be added – the "size" of both the evaporator and the condenser. In this calculation, the size of a heat exchanger is specified if the overall heat transfer coefficient U and the heat transfer area A are known.

In case of the cascade heat exchanger, there are refrigerants on both hot and cold side. Therefore, there are no inputs regarding ambient or freezer air necessary. However, its size is still to specified using the same approach as for the previous HEs – using the overall HTC U and the heat transfer area A. These two parameters are later used together as $UA_{input.}$

4.1.4. Sub-calculations

As mentioned earlier, the whole calculation consists of several sub-calculations that provide results for the designated part of the system. Some of them contain an iterative calculation.

4.1.4.1. High Temperature Cycle Calculation

The aim of this sub-calculation is the determination of refrigerant properties at all relevant points of the HC, which are (with their respective numbers, Figure 22):

1. end of evaporation
2. evaporator (i.e., cascade HE) outlet
3. compressor intake
4. compressor discharge = condenser inlet
5. start of condensation
6. end of condensation
7. condenser outlet
8. evaporator (i.e., cascade HE) inlet

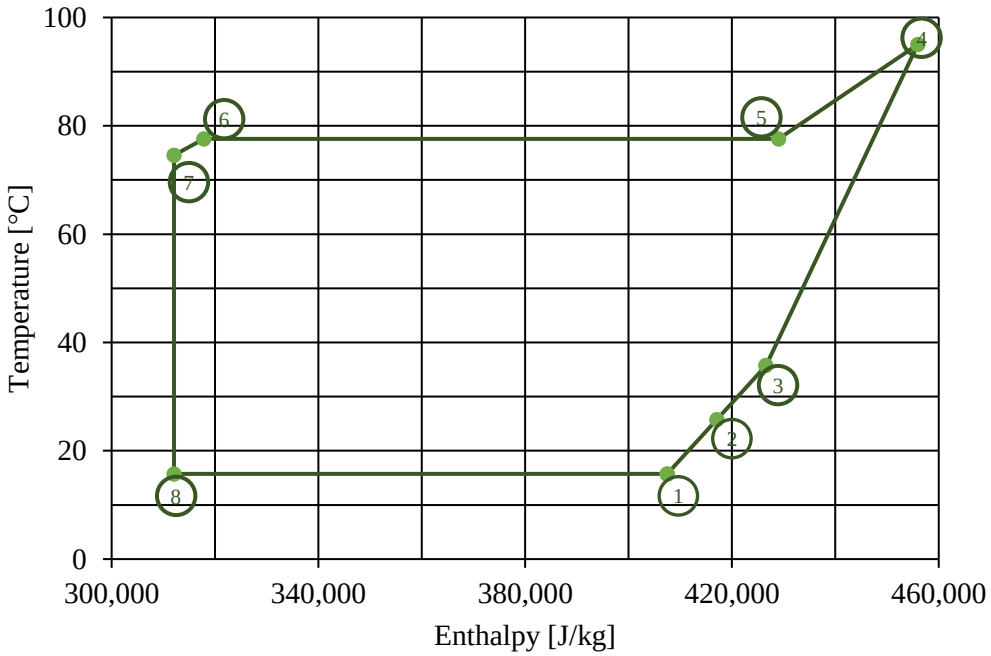

Figure 22: High temperature cycle, theoretical T-i diagram

As stated earlier, the condensation and evaporation temperature levels are known (either from initial estimate or some of the following iterations). This enables us to calculate the refrigerant properties:

- point 1 – end of evaporation
  - t_1 = known
  - $p_1 = f(t_1, x = 1)$
  - $i_1 = f(p_1, x = 1)$

- point 2 – evaporator (cascade HE) outlet
  - $t_2 = t_1 + \Delta T_{evap}$ (ΔT_{evap} … superheating in the evaporator)
  - $p_2 = p_1$
  - $i_2 = f(t_2, p_2)$
- point 3 – compressor intake
  - $t_3 = t_2 + \Delta T_s$ (ΔT_s … suction superheat)
  - $p_3 = p_2$
  - $i_3 = f(t_3, p_3)$
  - entropy $s_3 = f(t_3, p_3)$
  - density $\rho_3 = f(t_3, p_3)$
- point 4 – compressor discharge / condenser inlet
  - $p_4 = f(t_5, x = 1)$
  - pressure ratio $\sigma = p_4 / p_1$
  - isentropic efficiency η_{ie} can be calculated upon the knowledge of the pressure ratio
  - volumetric efficiency λ can be calculated upon the knowledge of the pressure ratio
  - enthalpy in case of isentropic refrigerant vapor compression $i_{4\_ie} = f(p_4, s_3)$
  - $i_4 = i_3 + [(i_{4\_ie} - i_3) / \eta_{ie}]$ (4.83)
  - $t_4 = f(p_4, i_4)$
- point 5 – start of condensation
  - t_5 = known
  - $p_5 = p_4$
  - $i_5 = f(p_5, x = 1)$
- point 6 – end of condensation
  - $t_6 = f(p_6, x = 0)$
  - $p_6 = p_5$
  - $i_6 = f(p_6, x = 0)$
- point 7 – condenser outlet
  - $t_7 = t_6 - \Delta T_{cond}$ (ΔT_{cond} … subcooling in the condenser)
  - $p_7 = p_6$
  - $i_7 = f(t_7, p_7)$
- point 8 – evaporator (cascade HE) inlet
  - $p_8 = p_1$
  - $i_8 = i_7$ (throttling is considered as adiabatic)
  - $t_8 = f(p_8, i_8)$

The refrigerant mass flow rate in the HC is calculated as: $m_{HC} = V_n \rho_3 \lambda$ (4.84)

4.1.4.2. Low Temperature Cycle Calculation

The aim of this sub-calculation is the determination of refrigerant properties at all relevant points of the CC, which are (with their respective numbers, Figure 23):

1. end of evaporation
2. evaporator outlet
3. IHE outlet (vapor)
4. compressor intake
5. compressor discharge
6. gas cooler outlet
7. after first stage of vapor cooling (CHE)
8. start of condensation
9. end of condensation
10. condenser (CHE) outlet
11. IHE outlet (liquid)
12. evaporator inlet

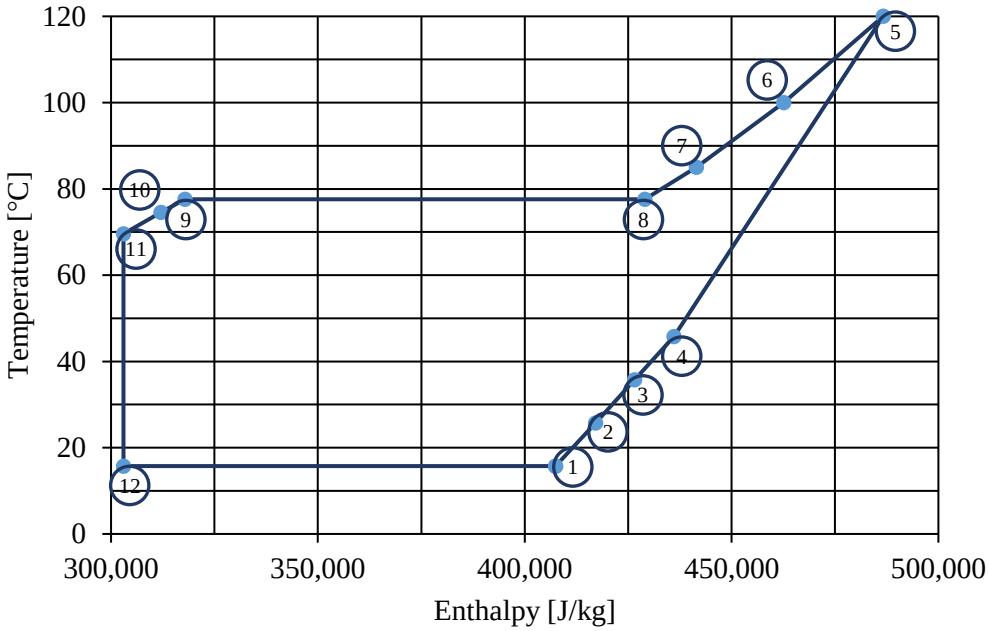

Figure 23: Low temperature cycle, theoretical T-i diagram

As stated earlier, the condensation and evaporation temperature levels are known (either from initial estimate or some of the following iterations). This enables us to calculate the refrigerant properties:

- point 1 – end of evaporation
  - t_1 = known
  - $p_1 = f(t_1, x = 1)$
  - $i_1 = f(p_1, x = 1)$
- point 2 – evaporator outlet
  - $t_2 = t_1 + \Delta T_{evap}$ (ΔT_{evap} … superheating in the evaporator)
  - $p_2 = p_1$
  - $i_2 = f(t_2, p_2)$
- point 3 – internal heat exchange outlet (vapor)
  - $p_3 = p_2$

- temperature t_{3_theor} for theoretical case of 100 % IHE efficiency is equal to the temperature of the subcooled condensed vapor t_9
- $i_{3\_theor} = f(p_3, t_{3\_theor})$
- the IHE enthalpy change Δi_{IHE} considering the actual IHE efficiency η_{IHE}:
  $\Delta i_{IHE} = \eta_{IHE} (i_{3\_theor} - i_2)$ (4.85)
- $i_3 = i_2 + \Delta i_{IHE}$
- $t_3 = f(p_3, i_3)$

- point 4 – compressor intake
  - $t_4 = t_3 + \Delta T_s$ (ΔT_s … suction superheat)
  - $p_4 = p_3$
  - $i_4 = f(t_4, p_4)$
  - entropy $s_4 = f(t_4, p_4)$
  - density $\rho_4 = f(t_4, p_4)$
- point 5 – compressor discharge / gas cooler inlet
  - $p_5 = f(t_7, x = 1)$
  - pressure ratio $\sigma = p_5 / p_1$
  - isentropic η_{ie} and volumetric efficiency λ are calculated from the pressure ratio
  - enthalpy in case of isentropic refrigerant vapor compression $i_{5\_ie} = f(p_5, s_4)$
  - $i_5 = i_4 + [(i_{5\_ie} - i_4) / \eta_{ie}]$ (4.86)
  - $t_5 = f(p_5, i_5)$
- The refrigerant mass flow rate in the CC is calculated as: $m_{CC} = V_n \rho_4 \lambda$ (4.87)
- point 6 – gas cooler outlet / condenser (cascade HE) inlet
  - $p_6 = p_5$
  - $t_6 = t_{air,c} + \Delta T_{cooler}$
  - $i_6 = f(t_6, p_6)$
- point 7 – after first stage of vapor cooling
  - the energy released between points 6 and 7 $Q_{6\text{-}7}$ equals the energy needed to superheat the refrigerant on the HC side of cascade HE
  - $Q_{6\text{-}7} = m_{HC} (i_{2,HC} - i_{1,HC})$ (4.88)
  - $i_7 = i_6 - (Q_{6\text{-}7} / m_{CC})$ (4.89)
  - $p_7 = p_6$
  - $t_7 = f(p_7, i_7)$
- point 8 – start of condensation
  - t_8 = known
  - $p_8 = p_7$
  - $i_8 = f(p_8, x = 1)$

- point 9 – end of condensation
  - $t_9 = f(p_9, x = 0)$
  - $p_9 = p_8$
  - $i_9 = f(p_9, x = 0)$
- point 10 – condenser outlet
  - $t_{10} = t_9 - \Delta T_{cond}$ (ΔT_{cond} … subcooling in the condenser)
  - $p_{10} = p_9$
  - $i_{10} = f(T_{10}, p_{10})$
- point 11 – internal heat exchange outlet (liquid)
  - $p_{11} = p_{10}$
  - $i_{11} = i_{10} - (i_3 - i_2)$ (4.90)
  - $t_{11} = f(p_{11}, i_{11})$
- point 12 – evaporator inlet
  - $p_{12} = p_1$
  - $i_{12} = i_{11}$ (throttling is considered as adiabatic)
  - $t_{12} = f(p_{12}, i_{12})$

4.1.4.3. High Temperature Cycle Condenser Balance

The first two sub-calculations (HC and CC Calculation) do not have any effect on the value of the four main temperatures. They only use their value to calculate the thermodynamic properties of refrigerants throughout the cycles. HC condenser balance, on the other hand, has direct impact on one of the four main temperatures – the HC condensation temperature $t_{cond,HC}$.

The main part of this sub-calculation is the cycle, which loops the calculation until the convergence is reached and the actual condenser UA_{calc} is equal to the one prescribed as an input value. In each step of the calculation cycle the $t_{cond,HC}$ is adjusted in accordance with the bisection method.

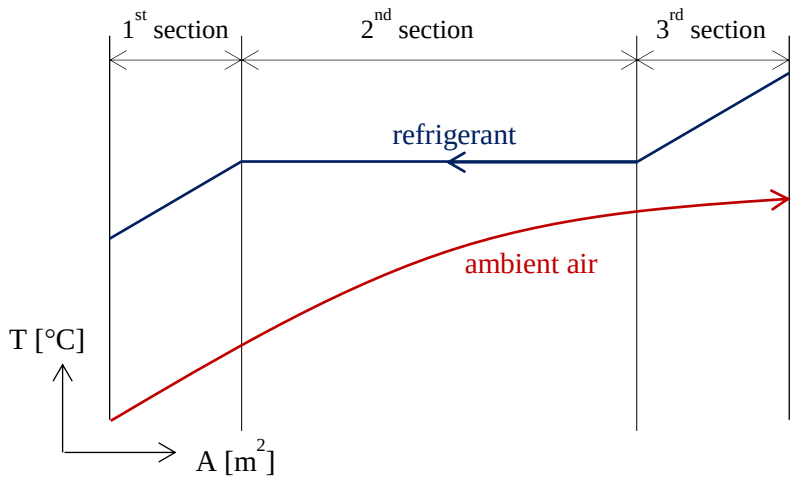

Figure 24: High temperature cycle condenser sections

The calculation cycle is constructed as follows:

1. The previously defined sub-calculations HC and CC calculation are performed to recalculate both hot and cold cycles with the new $t_{cond,HC}$.

2. The $UA_{cond,i}$ for all three respective sections of the condenser are calculated:

   a. Liquid refrigerant subcooling section (first section)

   heat transferred in the 1st section: $Q_{cond,1} = m_{HC} (i_{6,HC} - i_{7,HC})$ (4.8)

   air temperature at the 1st section outlet: $t_{air,2,c} = t_{air,1,c} + [Q_{cond,1} / (m_{air,c} c_{p,air,c})]$ (4.9)

   temp. difference at the 1st section cold side: $\Delta T_{c,cs,1} = t_{7,HC} - t_{air,1,c}$ (4.10)

   temp. difference at the 1st section hot side: $\Delta T_{c,hs,1} = t_{6,HC} - t_{air,2,c}$ (4.11)

   LMTD in the 1st section:[3] $LMTD_{cond,1} = (\Delta T_{c,cs,1} - \Delta T_{c,hs,1}) / [\ln (\Delta T_{c,cs,1} / \Delta T_{c,hs,1})]$ (4.12)

   UA of the 1st section: $UA_{cond,1} = Q_{cond,1} / LMTD_{cond,1}$ (4.13)

   b. Vapor condensation section (second section)

   heat transferred in the 2nd section: $Q_{cond,2} = m_{HC} (i_{5,HC} - i_{6,HC})$ (4.14)

   air temperature at the 2nd section outlet: $t_{air,3,c} = t_{air,2,c} + [Q_{cond,2} / (m_{air,c} c_{p,air,c})]$ (4.15)

   temp. difference at the 2nd section cold side: $\Delta T_{c,cs,2} = t_{5,HC} - t_{c,air,2}$ (4.16)

   temp. difference at the 2nd section hot side: $\Delta T_{c,hs,2} = t_{6,HC} - t_{c,air,3}$ (4.17)

   LMTD in the 2nd section: $LMTD_{cond,2} = (\Delta T_{c,cs,2} - \Delta T_{c,hs,2}) / [\ln (\Delta T_{c,cs,2} / \Delta T_{c,hs,2})]$ (4.18)

   UA of the 2nd section: $UA_{cond,2} = Q_{cond,2} / LMTD_{cond,2}$ (4.19)

   c. Vapor desuperheating section (third section)

   heat transferred in the 3rd section: $Q_{cond,3} = m_{HC} (i_{4,HC} - i_{5,HC})$ (4.20)

   air temperature at the 3rd section outlet: $t_{air,4,c} = t_{air,3,c} + [Q_{cond,3} / (m_{air,c} c_{p,air,c})]$ (4.21)

   temp. difference at the 3rd section cold side: $\Delta T_{c,cs,3} = t_{4,HC} - t_{air,3,c}$ (4.22)

   temp. difference at the 3rd section hot side: $\Delta T_{c,hs,3} = t_{5,HC} - t_{air,4,c}$ (4.23)

   LMTD in the 3rd section:[4] $LMTD_{cond,3} = (\Delta T_{c,cs,3} - \Delta T_{c,hs,3}) / [\ln (\Delta T_{c,cs,3} / \Delta T_{c,hs,3})]$ (4.24)

   UA of the 3rd section: $UA_{cond,3} = Q_{cond,3} / LMTD_{cond,3}$ (4.25)

[3] for $\Delta T_{c,cs,1} > \Delta T_{c,hs,1}$
[4] for $\Delta T_{c,cs,1} > \Delta T_{c,hs,1}$

3. The partial UA_i are then summed up to obtain the total condenser $UA_{calc,c}$:

$$UA_{calc,c} = UA_{cond,1} + UA_{cond,2} + UA_{cond,3} \quad (4.26)$$

4. The total $UA_{calc,c}$ is compared with the $UA_{input,c}$ and the difference $|UA_{calc,c} - UA_{input,c}|$ is calculated

   a. If $|UA_{calc,c} - UA_{input,c}| > 10$, the $t_{cond,HC}$ is adjusted in accordance with the bisection method and the calculation cycle is performed again.

   b. If $|UA_{calc,c} - UA_{input,c}| < 10$, the desired accuracy has been achieved and the calculation loop is terminated.

4.1.4.4. Low Temperature Cycle Evaporator Balance

The sub-calculation called HC condenser balance is relatively similar with the previous one. It has direct impact on one of the four main temperatures – the CC evaporation temperature $t_{evap,CC}$.

The main part of this sub-calculation is the cycle, which loops the calculation until the convergence is reached and the actual evaporator UA_{calc} is equal to the one prescribed as an input value. In each step of the calculation cycle the $t_{evap,CC}$ is adjusted in accordance with the bisection method.

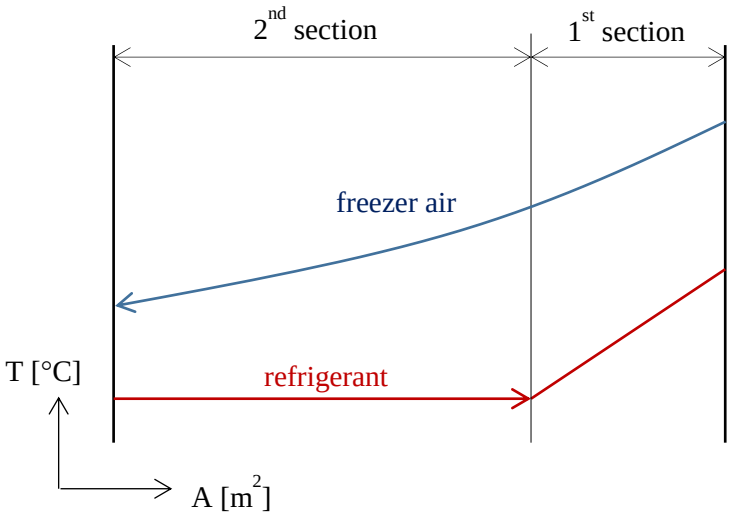

Figure 25: Low temperature cycle evaporator sections

The calculation cycle is constructed as follows:

1. The previously defined sub-calculations HC and CC Calculation are called to recalculate both hot and cold cycles with the new $t_{evap,CC}$.

2. The $UA_{evap,i}$ for both sections of the evaporator are calculated:

   a. <u>Refrigerant vapor superheating section (first section)</u>

   heat transferred in the 1st section: $Q_{evap,1} = m_{CC} (i_{2,CC} - i_{1,CC})$ (4.27)

   air temperature at the 1st section outlet: $t_{e,air,2} = t_{e,air,1} - [Q_{evap,1} / (m_{e,air} c_{p,e,air})]$ (4.28)

   temp. difference at the 1st section cold side: $\Delta T_{e,cs,1} = t_{e,air,2} - t_{1,CC}$ (4.29)

   temp. difference at the 1st section hot side: $\Delta T_{e,hs,1} = t_{e,air,1} - t_{2,CC}$ (4.30)

   LMTD in the 1st section:[5] $LMTD_{evap,1} = (\Delta T_{e,cs,1} - \Delta T_{e,hs,1}) / [\ln (\Delta T_{e,cs,1} / \Delta T_{e,hs,1})]$ (4.31)

   UA of the 1st section: $UA_{evap,1} = Q_{evap,1} / LMTD_{evap,1}$ (4.32)

   b. <u>Refrigerant evaporation section (second section)</u>

   heat transferred in the 2nd section: $Q_{evap,2} = m_{CC} (i_{1,CC} - i_{12,CC})$ (4.33)

   air temperature at the 2nd section outlet: $t_{e,air,3} = t_{e,air,2} - [Q_{evap,2} / (m_{e,air} c_{p,e,air})]$ (4.34)

   temp. difference at the 2nd section cold side: $\Delta T_{e,cs,2} = t_{e,air,3} - t_{12,CC}$ (4.35)

   temp. difference at the 2nd section hot side: $\Delta T_{e,hs,2} = t_{e,air,2} - t_{1,CC}$ (4.36)

   LMTD in the 2nd section: $LMTD_{evap,2} = (\Delta T_{e,hs,2} - \Delta T_{e,cs,2}) / [\ln (\Delta T_{e,hs,2} / \Delta T_{e,cs,2})]$ (4.37)

   UA of the 2nd section: $UA_{evap,2} = Q_{evap,2} / LMTD_{evap,2}$ (4.38)

3. The partial UA_i are then summed up to obtain the total evaporator $UA_{calc,e}$:

$$UA_{calc,e} = UA_{evap,1} + UA_{evap,2} \quad (4.39)$$

4. The total $UA_{calc,e}$ is compared with the $UA_{input,e}$ and the difference $|UA_{calc,e} - UA_{input,e}|$ is calculated
   a. If $|UA_{calc,e} - UA_{input,e}| > 10$, the $t_{evap,CC}$ is adjusted in accordance with the bisection method and the calculation cycle is performed again.
   b. If $|UA_{calc,e} - UA_{input,e}| < 10$, the desired accuracy has been achieved and the calculation loop is terminated.

[5] for $\Delta T_{e,cs,1} > \Delta T_{e,hs,1}$

4.1.4.5. Heat Flows Balance

The former two sub-calculations have impact on the "non-cascade-HE" temperatures. In this case, saturation temperatures for both the cold side and the hot side of the cascade HE are involved.

The core of this sub-calculation is again an iterative cycle that aims to achieve the balance of the heat flows on both sides of the cascade HE by adjusting both $t_{evap,HC}$ and $t_{cond,CC}$. These two temperatures are coupled through the ΔT_{CHE} variable:

$$\Delta T_{CHE} = t_{cond,CC} - t_{evap,HC} \qquad (4.40)$$

This value remains constant throughout this sub-calculation and is also a subject to iteration in the further calculations.

The sequence of steps in this sub-calculation is:

1. The previously defined sub-calculations CC Evaporator Balance and HC Condenser Balance are performed with the most actual values.
2. Heat transfer rates on both sides of the cascade HE are calculated:

$$Q_{CHE,CC} = m_{CC}\left(i_{6,CC} - i_{10,CC}\right) \qquad (4.41)$$

$$Q_{CHE,HC} = m_{HC}\left(i_{2,HC} - i_{8,HC}\right) \qquad (4.42)$$

3. The two calculated values $Q_{CHE,CC}$ and $Q_{CHE,HC}$ are then compared:
    a. If $\left| Q_{CHE,CC} - Q_{CHE,HC} \right| > 10$, the $t_{cond,CC}$ is adjusted in accordance with the bisection method and the calculation cycle is performed again. At the same time, the value of $t_{evap,HC}$ is also adjusted as ΔT_{CHE} remains unchanged.
    b. If $\left| Q_{CHE,CC} - Q_{CHE,HC} \right| < 10$, the desired accuracy has been achieved and the calculation loop is terminated.

4.1.4.6. Cascade Heat Exchanger UA

This sub-calculation serves the only purpose – to determine the total UA of the cascade heat exchanger. Therefore, it is to be carried out after the CHE balance has been found. The CHE is the most complex in terms of individual sections count – there is four of them, depending on heat transfer modes combination on both sides.

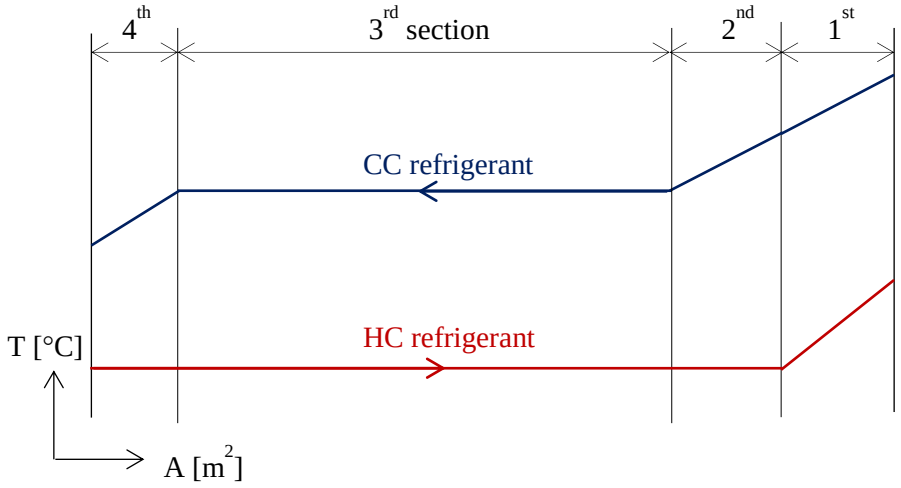

Figure 26: Cascade heat exchanger sections

Thanks to the fact that both heat flow rates are equal (convergence has been reached in previous sub-calculation), the result does not depend on which side (hot or cold) is chosen for the calculation:

1. CC refrigerant vapor cooling + HC refrigerant vapor superheating section (first section)

   heat transferred in the 1st section: $Q_{CHE,1} = m_{HC} (i_{2,HC} - i_{1,HC})$ (4.43)

   temp. difference at the 1st section cold side: $\Delta T_{CHE,cs,1} = t_{7,CC} - t_{1,HC}$ (4.44)

   temp. difference at the 1st section hot side: $\Delta T_{CHE,hs,1} = t_{6,CC} - t_{2,HC}$ (4.45)

   LMTD 1st section:[6] $LMTD_{CHE,1} = (\Delta T_{CHE,hs,1} - \Delta T_{CHE,cs,1}) / [\ln(\Delta T_{CHE,hs,1} / \Delta T_{CHE,cs,1})]$ (4.46)

   UA of the 1st section: $UA_{CHE,1} = Q_{CHE,1} / LMTD_{CHE,1}$ (4.47)

2. CC refrigerant vapor cooling + HC refrigerant evaporation (second section)

   heat transferred in the 2nd section: $Q_{CHE,2} = m_{CC} (i_{7,CC} - i_{8,CC})$ (4.48)

   enthalpy at point 1' of the HC: $i_{1',HC} = i_{1,HC} - (Q_{CHE,2} / m_{HC})$ (4.49)

   pressure at point 1' of the HC: $p_{1',HC} = p_{1,HC}$ (4.50)

[6] for $\Delta T_{CHE,hs,1} > \Delta T_{CHE,cs,1}$

temperature at point 1' of the HC: $t_{1',HC} = f(p_{1',HC}, i_{1',HC})$ (4.51)

temp. difference at the 2nd section cold side: $\Delta T_{CHE,cs,2} = t_{8,CC} - t_{1',HC}$ (4.52)

temp. difference at the 2nd section hot side: $\Delta T_{CHE,hs,2} = t_{7,CC} - t_{1,HC}$ (4.53)

LMTD 2nd section: $LMTD_{CHE,2} = (\Delta T_{CHE,hs,2} - \Delta T_{CHE,cs,2}) / [\ln(\Delta T_{CHE,hs,2} / \Delta T_{CHE,cs,2})]$ (4.54)

UA of the 2nd section: $UA_{CHE,2} = Q_{CHE,2} / LMTD_{CHE,2}$ (4.55)

3. <u>CC refrigerant condensation + HC refrigerant evaporation (third section)</u>

heat transferred in the 3rd section: $Q_{CHE,3} = m_{CC} (i_{8,CC} - i_{9,CC})$ (4.56)

enthalpy at point 8' of the HC: $i_{8',HC} = i_{1',HC} - (Q_{CHE,3} / m_{HC})$ (4.57)

pressure at point 8' of the HC: $p_{8',HC} = p_{1',HC}$ (4.58)

temperature at point 8' of the HC: $t_{8',HC} = f(p_{8',HC}, i_{8',HC})$ (4.59)

temp. difference at the 3rd section cold side: $\Delta T_{CHE,cs,3} = t_{9,CC} - t_{8',HC}$ (4.60)

temp. difference at the 3rd section hot side: $\Delta T_{CHE,hs,3} = t_{8,CC} - t_{1',HC}$ (4.61)

LMTD 3rd section: [7] $LMTD_{CHE,3} = (\Delta T_{CHE,hs,3} - \Delta T_{CHE,cs,3}) / [\ln(\Delta T_{CHE,hs,3} / \Delta T_{CHE,cs,3})]$ (4.62)

UA of the 3rd section: $UA_{CHE,3} = Q_{CHE,3} / LMTD_{CHE,3}$ (4.63)

4. <u>CC refrigerant subcooling + HC refrigerant evaporation (fourth section)</u>

heat transferred in the 4th section: $Q_{CHE,4} = m_{CC} (i_{9,CC} - i_{10,CC})$ (4.64)

temp. difference at the 4th section cold side: $\Delta T_{CHE,cs,4} = t_{10,CC} - t_{8,HC}$ (4.65)

temp. difference at the 4th section hot side: $\Delta T_{CHE,hs,4} = t_{9,CC} - t_{8',HC}$ (4.66)

LMTD 4th section: [8] $LMTD_{CHE,4} = (\Delta T_{CHE,hs,4} - \Delta T_{CHE,cs,4}) / [\ln(\Delta T_{CHE,hs,4} / \Delta T_{CHE,cs,4})]$ (4.67)

UA of the 4th section: $UA_{CHE,4} = Q_{CHE,4} / LMTD_{CHE,4}$ (4.68)

The partial $UA_{CHE,i}$ are then summed up to obtain the total cascade heat exchanger UA:

$$UA_{CHE,calc} = UA_{CHE,1} + UA_{CHE,2} + UA_{CHE,3} + UA_{CHE,4} \quad (4.69)$$

[7] In case of no temperature glide on either side of the CHE, $LMTD_{CHE,3} = \Delta T_{CHE,cs,3} = \Delta T_{CHE,hs,3}$
[8] In case of no temperature glide on either side of the CHE, $LMTD_{CHE,3} = \Delta T_{CHE,cs,3} = \Delta T_{CHE,hs,3}$

4.1.4.7. Cascade HE Balance

As with the condenser or the evaporator, also the size of the CHE is to be given in terms of overall heat transfer coefficient U and heat transfer area A. Also in this case, the calculated UA is to be compared with the input value to ensure that they are equal.

The Cascade HE Balance sub-calculation is divided into two parts:

1. Initial estimate of all four saturation temperatures:
   a. $\mathbf{t_{evap,CC}} = t_{air,e} - \Delta T_{evap,CC} - 5$ (4.70)
   b. $\mathbf{t_{cond,HC}} = t_{air,C} + \Delta T_{cond,HC} + 5$ (4.71)
   c. $\mathbf{t_{cond,CC}} = ((t_{cond,HC} + t_{evap,CC}) / 2) + 2$ (4.72)
   d. $\Delta T_{CHE} = 10\ K \Rightarrow \mathbf{t_{evap,HC}} = t_{cond,CC} - \Delta T_{CHE}$ (4.73)

2. Calculation cycle consisting of several steps:
   a. The previously defined sub-calculations Heat Flows Balance and Cascade Heat Exchanger UA are performed to obtain all four saturation temperatures
   b. The total $UA_{CHE,calc}$ is compared with the $UA_{CHE,input}$
   c. If $\left| UA_{CHE,calc} - UA_{CHE,input} \right| > 10$, the ΔT_{CHE} is adjusted in accordance with the bisection method and the calculation cycle is performed again.
   d. If $\left| UA_{CHE,calc} - UA_{CHE,input} \right| < 10$, the desired accuracy has been achieved and the calculation loop is terminated.

4.2. Cascade heat exchanger

When all the calculations described in the previous chapter are performed, it is time to analyze the CHE in more detail. Some of the refrigeration cycle calculation outputs are taken as input values for the SEWTLE procedure applied on the CHE.

4.2.1. Input values

The vital input values are:

1. Low temperature cycle refrigerant properties at the CHE inlet
   - pressure $p_{6,CC}$
   - temperature $t_{6,CC}$
   - enthalpy $i_{6,CC}$
2. High temperature cycle refrigerant properties at the CHE inlet
   - pressure $p_{8,HC}$
   - temperature $t_{8,HC}$
   - enthalpy $i_{8,CC}$
3. Mass flow rates m_{HC} and m_{CC}

Apart from these parameters, more of them are needed to successfully carry out the SEWTLE calculations as well as heat transfer correlations. The desired values for both refrigerants/HE sides are:

- density ρ_l and ρ_g at both saturated liquid and saturated vapor lines for given pressure
- enthalpy i_l and i_g at both saturated liquid and saturated vapor lines for given pressure
- thermal conductivity λ_l and λ_g at both saturated liquid and sat. vapor lines for given pressure
- dynamic viscosity μ_l and μ_g at both saturated liquid and vapor saturated lines for given pressure
- surface tension σ_l and σ_g at both saturated liquid and saturated vapor lines for given pressure
- PHE channels geometry
    - channel spacing b
    - plate width w
    - plate height h
    - number of channels n
- number of elementary cells along a fluid path n_{cells}

4.2.2. Calculation procedure

The general calculation approach is described in chapter regarding the theory of the SEWTLE procedure. The heat exchanger is no longer considered as a whole – a reduction has been made for simplification purposes. The HE is therefore represented by only one of its plates with one fluid from each side in these calculations. The calculated intensive properties (e.g., temperatures, specific enthalpies) are then the same for the simplified case as well as for the whole HE. Extensive properties (e.g., total heat loads, mass flow rates), on the other hand, are to be adjusted adequately.

4.2.2.1. Preliminary calculations

Before determining the thermodynamic properties evolution along a fluid path, two steps are necessary to be made:

1. Initial wall temperature distribution estimate

   In accordance with the SEWTLE procedure authors' recommendation, the initial wall temperature evolution is chosen to be linear as the initial estimate has only negligible influence on the result [72]. Therefore, two points of the line are to be defined:

   - HC inlet: $t_{w,est,1} = t_{8,HC} + 0.1$ (4.74)
   - HC outlet: $t_{w,est,2} = t_{1,HC} + \Delta T_{evap,HC} + 0.1$ (4.75)

   The linear evolution of the wall temperature goes through these points.

2. Mass flow rate per channel, heat transfer area per one wall cell

$$m_{1ch} = m_{total} / n \quad (4.76)$$

$$A_{1cell} = w\ h / n_{cells} \quad (4.77)$$

4.2.2.2. Properties evolution along a fluid path

Generally, the evolution of three thermodynamic properties is of major interest – pressure, temperature and enthalpy. In addition to this, the heat transfer coefficient and the heat load are necessary to perform the desired calculations. This equals a total of eight variables to be computed for each fluid cell:

1. Inlet pressure p_{inlet}
2. Outlet pressure p_{outlet}
3. Inlet temperature t_{inlet}
4. Outlet temperature t_{outlet}
5. Inlet enthalpy i_{inlet}
6. Outlet enthalpy i_{outlet}
7. Heat flow rate Q_{cell}
8. Heat transfer coefficient α

In our case of negligible pressure losses, the pressure along a fluid path remains constant. The i^{th} cell outlet values are concurrently the $i^{th}+1$ inlet values. For a random HC cell (e.g., evaporation side of a CHE), the calculation sequence can look as follows:

- p_{inlet} and p_{outlet} are known as pressure is constant
- i_{inlet} and t_{inlet} are known from the previous cell calculation
- heat transfer coefficient α is to be determined
- heat load Q_{cell} can be determined now as:

$$Q_{cell} = \alpha\, A_{cell}\, (t_w - t_{inlet}) \qquad (4.78)$$

- outlet enthalpy i_{outlet} can be determined now as:

$$i_{outlet} = i_{inlet} + \frac{Q_{cell}}{m_{1ch}} \qquad (4.79)$$

- outlet temperature t_{outlet} can be determined now as a function of i_{outlet} and p_{outlet}

4.2.2.3. Wall temperature recalculation

The previous calculation sequence is carried out for every cell of both hot and cold fluid path. After this, it is time to recalculate the wall temperature distribution using the previously stated expression:

$$t_w = \frac{\alpha_{hot} t_{hot} + \alpha_{cold} t_{cold}}{\alpha_{hot} + \alpha_{cold}} \qquad (4.80)$$

where t_{hot} and t_{cold} are average temperatures between respective cell inlet and outlet. When temperature at every wall cell is recalculated, the fluid paths calculations can be initiated once again.

4.2.2.4. Heat loads comparison

At the end of every calculation cycle, it is necessary to compare the heat loads released (condensation side) and absorbed (evaporation side). Heat load is calculated from the total mass flow rate on one side and the enthalpy differential between inlet and outlet of a channel:

- heat load released: $Q_{CC} = m_{CC} (i_{CC,CHE,inlet} - i_{CC,CHE,outlet})$ (4.81)
- heat load absorbed: $Q_{HC} = m_{HC} (I_{HC,CHE,outlet} - i_{HC,CHE,inlet})$ (4.82)

The $|Q_{CC} - Q_{HC}|$ value should decrease over the course of wall temperature iterations. Once this difference is low enough (depends on desired calculation accuracy), the iteration cycle is terminated – the cascade heat exchanger balance has been found.

4.3. Calculations interconnection

In course of the calculation process the refrigeration cycle is set to its balanced state and the cascade heat exchanger is thoroughly analyzed. The one final adjustment need to be carried out – one of the inputs is the CHE size (in terms of UA). While the heat transfer area A can be determined quite accurately for given heat exchanger, the input value of the overall heat transfer coefficient U is only an initial estimate. The searched system balance is a state, when HC refrigerant superheating after evaporation ΔT_{evap} is equal in both calculation sub-systems.

To achieve this, a major calculation was created to interconnect the two calculation sub-systems, adjust the input value of cascade heat exchanger UA and ensure the balance of the whole refrigeration system. Again, it is an iteration procedure – the calculation cycle keeps repeating until the convergence is reached.

This major calculation incorporates all previously described sub-calculations. The calculation cycle is constructed followingly:

1. The sub-calculation called Cascade HE Balance is executed.
2. The SEWTLE procedure for the CHE is carried out.
3. The HC refrigerant superheating after evaporation $\Delta T_{evap,CHE}$ is compared with the $\Delta T_{evap,SEWTLE}$.
4. If $\Delta T_{evap,CHE} \neq \Delta T_{evap,SEWTLE}$, the U_{CHE} is adjusted in accordance with the bisection method and the calculation cycle is performed again.
5. If $\Delta T_{evap,CHE} = \Delta T_{evap,SEWTLE}$, the desired accuracy has been achieved and the calculation loop is terminated.

5. Cascade heat exchanger calculation

In this final part of the thesis, an example of the cascade refrigeration system calculation, including the thorough analysis of given cascade heat exchanger, is provided. Before the selection of calculation input values, it is necessary to introduce several simplifying assumptions adopted for the SEWTLE procedure. This was necessary due to the high complexity level of previously described calculation process and related equations.

5.1. Simplifying assumptions

The key SEWTLE-related simplifying assumptions were:

1. Pressure losses inside the entire refrigeration system are neglected (the only pressure differences are caused by compressors and expansion valves).
2. The potential positional energy term in Equation (3.11) is neglected.
3. The Equation (3.11) used for calculation of outlet enthalpy works with outlet temperature. This value, however, is not known beforehand and should be determined using an iterative process. This step was eliminated by discretizing the cascade heat exchanger into large number of cells. Thanks to this, the inlet temperature, instead of average temperature across a cell, can be used while maintaining acceptable calculation accuracy. The accuracy loss does not apply to azeotropic substance phase changes, where the temperature during this process remains constant.
4. The longitudinal conduction inside the heat exchanger plates is neglected.
5. Corberán et al. offer the possibility of dividing the cells where the heat transfer mechanism switch occurs (e.g., end of vapor cooling, start of condensation) into two parts in order to use the correct heat transfer coefficients in respective cell sections. This was omitted with respect to substantial increase in difficulty of thermodynamic calculations conditioning. As well as for point 3 of this list - the number of cells is high enough to sufficiently reduce the impact of this inaccuracy.

5.2. Calculation inputs

The following input values were used for the demonstration purposes of the refrigeration cycle calculation capabilities:

- refrigerants
    - low temperature cycle – R744
    - high temperature cycle – R404A[9]
- compressors
    - low temperature cycle – Frascold S10-10TK
        - displacement – $V_n = 9.64\ m^3.\ h^{-1}$
        - isentropic efficiency coefficients – $C_1 = 0.6857$; $C_2 = C_3 = C_4 = 0$
        - volumetric efficiency coefficients – $C_1 = 0.8847$; $C_2 = C_3 = C_4 = 0$
    - high temperature cycle – Copeland ZFD18KVE-TFD EVI
        - displacement – $V_n = 17.1\ m^3.\ h^{-1}$
        - isentropic efficiency coefficients – $C_1 = 0.6315$; $C_2 = -0.0214$; $C_3 = C_4 = 0$
        - volumetric effic. coefficients – $C_1 = 1.1059$; $C_2 = -0.0509$; $C_3 = 0.0022$; $C_4 = 0$
- high temperature cycle condenser
    - ambient air temperature – $t_{air,c} = 30°C$
    - ambient air mass flow – $m_{air,c} = 3\ kg.\ s^{-1}$
    - ambient air specific heat – $c_{p,air,c} = 1{,}010\ J.\ kg^{-1}.\ K^{-1}$
    - effective heat transfer surface – $A_c = 1\ m^2$
    - overall heat transfer coefficient – $U_c = 1{,}500\ W.\ m^2.\ K$
- low temperature cycle evaporator
    - freezer air temperature – $t_{air,e} = -20°C$
    - freezer air mass flow – $m_{air,e} = 3\ kg.\ s^{-1}$
    - freezer air specific heat – $c_{p,air,e} = 1{,}010\ J.\ kg^{-1}.\ K^{-1}$
    - effective heat transfer surface – $A_e = 1\ m^2$
    - overall heat transfer coefficient – $U_e = 1{,}500\ W.\ m^2.\ K$
- cascade heat exchanger
    - effective heat transfer surface – $A_{CHE} = 0.901\ m^2$
    - initial overall heat transfer coefficient estimate – $U_{CHE,est} = 1{,}000\ W.\ m^2.\ K$
- internal heat exchange effectiveness – $\varepsilon_{IHE} = 0.8$

[9] CoolProp does not contain some of the necessary R452A thermodynamic properties

- gas cooler cold side temperature difference – ΔT_{cooler} = 0.7 K
- refrigeration cycle settings
    - low temperature cycle evaporator superheat – ΔT_{evap} = 5 K
    - high temperature cycle condenser subcooling – ΔT_{cond} = 0.01 K
    - cascade heat exchanger superheat – $\Delta T_{evap,CHE}$ = 10 K
    - cascade heat exchanger subcooling – $\Delta T_{cond,CHE}$ = 1 K

For the SEWTLE procedure calculations, following heat transfer correlations were selected based upon thorough analysis:

- R744 condensation – correlation by Han (see Chapter 3.4.2.3.3.)
- R404A evaporation – correlation by Han (see Chapter 3.4.2.4.1.)
- single-phase heat transfer – correlation by Thonon (see Chapter 3.4.2.2.1.)

Number of cells for heat exchanger discretization – 94

The plate geometry of the heat exchanger used as a cascade HE can be found in Figure 27. A brazed plate heat exchanger SWEP B17 has been chosen for the calculation purposes. It is a compact heat exchanger particularly suitable for cold chain applications, heat pumps and mobile air-conditioning [111]. The plates are made of steel with copper brazing.

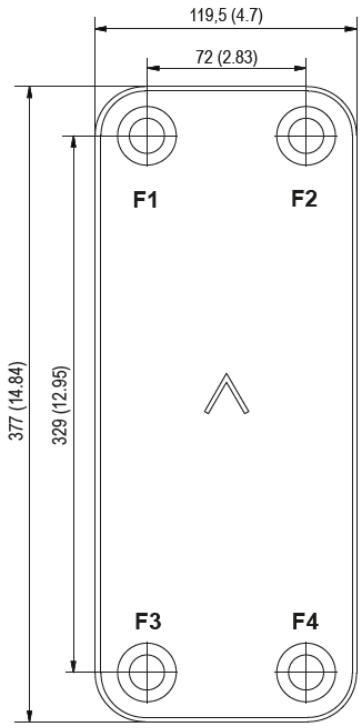

Figure 27: Plate geometry of the cascade heat exchanger [111]

5.3. Low temperature cycle

The carbon dioxide properties in every significant point of the refrigeration cycle are summarized in Table 6. The cycle operates at evaporating temperature -32.56°C and condensing temperature 17.93°C, which makes the pressure ratio 4.169. A fact worth highlighting is the compressor discharge temperature exceeding 150°C, which is partly caused by the low isentropic efficiency of the compressor (see Tab. 7).

Table 6: Low temperature cycle properties

Designation	Point	t [°C]	p [kPa]	i [kJ/kg]
End of evaporation	1	-32.56	1,308.71	436.56
Evaporator outlet	2	-27.56	1,308.71	442.02
Compressor intake (after IHE)	4	7.70	1,308.71	477.44
Compressor discharge	5	151.19	5,456.65	595.70
Gas cooler outlet	6	30.70	5,456.65	444.22
Cascade HE 1st section outlet	7	22.69	5,456.65	426.61
Start of condensation	8	17.93	5,456.65	411.88
End of condensation	9	17.93	5,456.65	249.05
Cascade HE outlet	10	16.93	5,456.65	245.34
IHE outlet (liquid)	11	4.79	5,456.65	209.92
Evaporator inlet	12	-32.56	1,308.71	209.92

Table 7: Low temperature cycle compressor

Power input	7,569	W
R744 mass flow	0.064	kg/s
Pressure ratio	4.169	-
Volumetric efficiency	0.8847	-
Isentropic efficiency	0.6857	-

The CC evaporator working conditions can be seen in Table 8. The freezer air entering the heat exchanger at -20°C is cooled to nearly -25°C, while majority of the heat load is transferred in the evaporating section.

Table 8: Low temperature cycle evaporator

Section		Superheating	Evaporation	Unit
Heat load	Q	348.33	14,464.86	W
Total heat load	Q	14,813.18		W
R744 temperature	outlet	-27.563	-32.563	°C
	inlet	-32.563	-32.563	°C
air temperature	inlet	-20.000	-20.115	°C
	outlet	-20.115	-24.889	°C
LMTD		9.803	9.869	K
UA		35.533	1,465.700	W/K
UA_total		1,501.232		W/K
Difference		-1.232		W/K

The R744 properties evolution along the cycle is depicted in Figure 28. The curve shape is quite non-traditional due to the high compressor discharge temperature. Because of this, heat load of nearly 10 kW of is to be released into the ambient air via the gas cooler. Due to the internal heat exchange, a refrigerant subcooling of nearly 15 K is achieved before throttling.

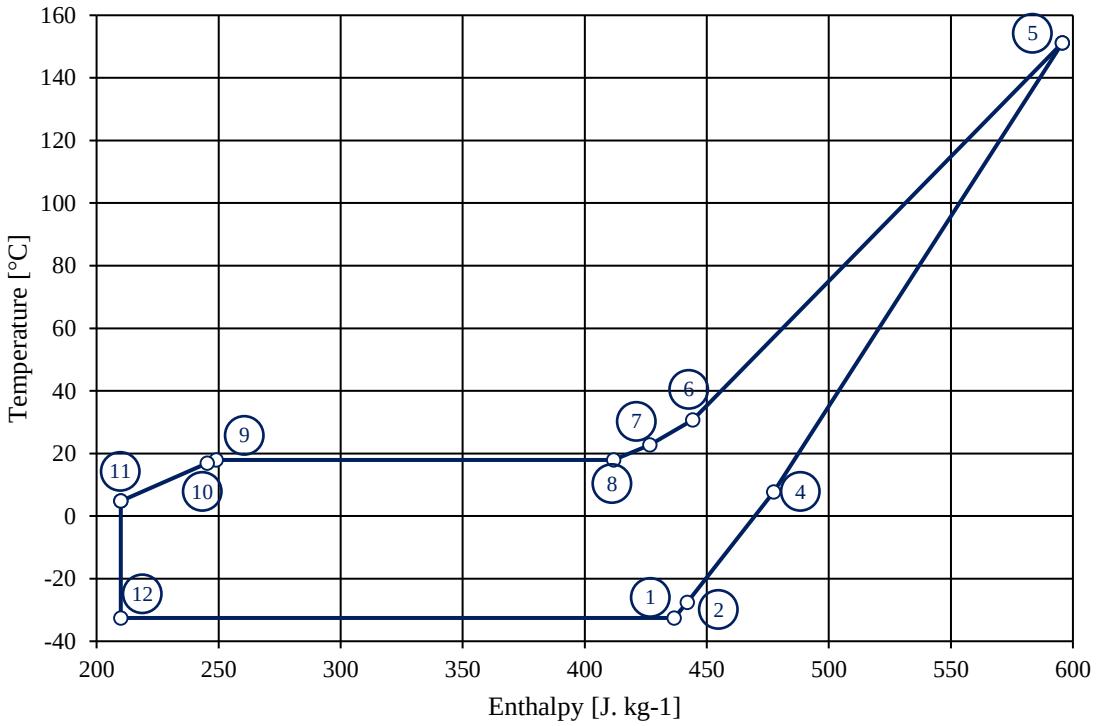

Figure 28: Low temperature cycle, actual T-i diagram

5.4. High temperature cycle

The R404A properties in every significant point of the refrigeration cycle are summarized in Table 10. The cycle operates at evaporating temperature -1.32°C (saturated vapor line) and condensing temperature 42.82°C (saturated vapor line), which makes the pressure ratio 3.375. A temperature glide of approximately 0.3 K can be observed during both phase changes. The mass flow of the refrigerant is almost twice as high as in the low temperature cycle (see Table 9).

Table 9: High temperature cycle compressor

Power input	4,269	W
R404A mass flow	0.115	kg/s
Pressure ratio	3.375	-
Volumetric efficiency	0.8847	-
Isentropic efficiency	0.6857	-

Table 10: High temperature cycle properties

Designation	Point	t [°C]	p [kPa]	i [kJ/kg]
End of evaporation	1	-1.32	575.51	365.16
Compressor intake	3	8.68	575.51	374.95
Compressor discharge	4	66.27	1,942.09	412.14
Start of condensation	5	42.82	1,942.09	380.83
End of condensation	6	42.50	1,942.09	264.37
Condenser outlet	7	42.49	1,942.09	264.35
Cascade HE inlet	8	-1.63	575.51	264.35
Cascade HE section break 3/4	8'	-1.62	575.51	266.42
Cascade HE section break 2/3	1'	-1.34	575.51	356.97

The R404A properties evolution along the cycle is depicted in Figure 29. The refrigerant discharge temperature is not as extreme as in the previous case. A temperature glide can be observed with a closer look on the phase change sections of the cycle curve.

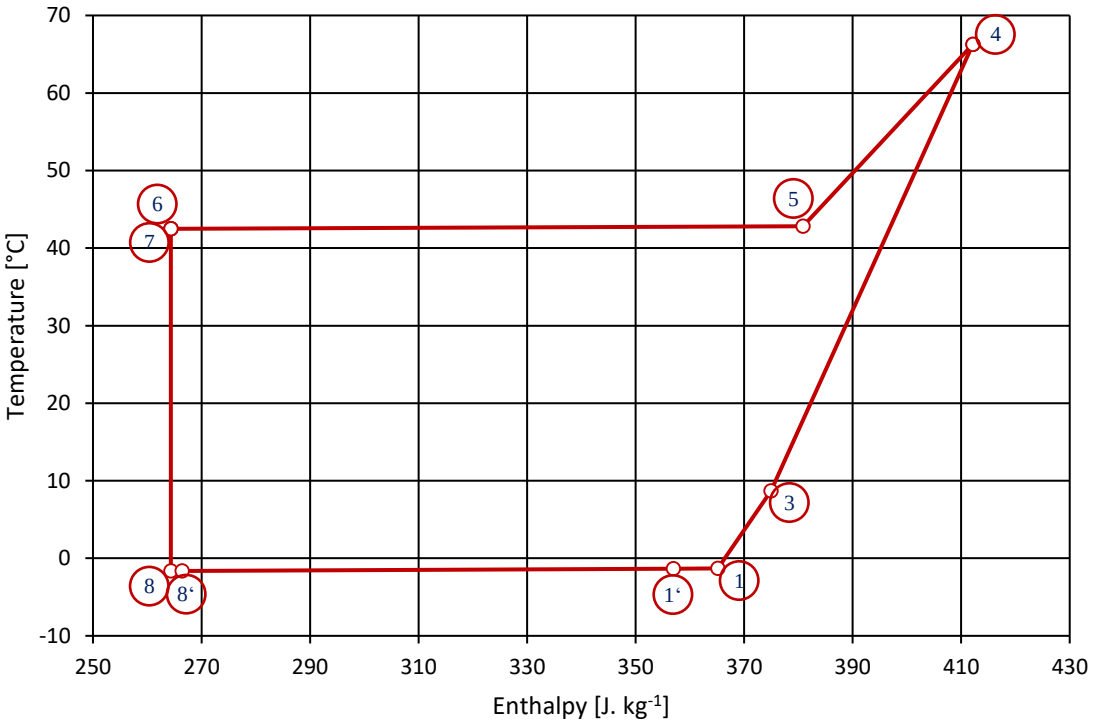

Figure 29: High temperature cycle, actual T-i diagram

The HC condenser working conditions can be seen in Table 11. The ambient air entering the heat exchanger at 30°C is heated to 35.6°C, while majority of the heat load is transferred in the condensing section. The heat load transferred during vapor cooling present around 20 per cent of the total. The difference between the input value of UA and the calculated value is only 4.1 W/K, i.e., 0.3 %. This indicates the successful outcome of the iteration process.

Table 11: High temperature cycle condenser

Section		Vapor cooling	Condensation	Subcooling	Unit
Heat load	Q	3,593.81	13,366.83	2.03	W
Total heat load	Q	16,962.66			W
R404A temperature	inlet	66.266	42.823	42.504	°C
	outlet	42.823	42.504	42.494	°C
air temperature	outlet	35.598	34.412	30.001	°C
	inlet	34.412	30.001	30.000	°C
LMTD		17.204	10.322	12.498	K
UA		208.896	1,295.013	0.162	W/K
UA_total		1,504.071			W/K
Difference		-4.071			W/K

5.5. Cascade heat exchanger

The cascade heat exchanger working conditions can be seen in Table 12. The total heat load transferred in the cascade heat exchanger is approximately 12,693 W. As in the previous heat exchanger cases, majority of the heat is transferred inside the phase-change section (R404A evaporation and R744 condensation simultaneously). R744 is cooled by 13 K before the condensation starts. R404A on the other side of the heat exchanger is superheated by 10 K as stated in the input value.

Table 12: Cascade heat exchanger

Section		1st	2nd	3rd	4th	Unit
Heat load R744	Q	1,123.96	940.03	10,392.20	237.21	W
Total heat load R744	Q	12,693.40				W
Heat load R404A	Q	1,123.96	940.03	10,392.20	237.88	W
Total heat load R404A	Q	12,694.08				W
R744 temperature	inlet	30.700	22.687	17.935	17.935	°C
	outlet	22.687	17.935	17.935	16.935	°C
R404A temperature	outlet	8.685	-1.315	-1.341	-1.623	°C
	inlet	-1.315	-1.341	-1.623	-1.630	°C
LMTD		22.994	21.552	19.416	19.057	K
UA		48.880	43.616	535.229	12.447	W/K
UA_total		640.173				W/K
Difference		-0.410				W/K

The detailed view of the CHE processes presents Fig.30. The temperature evolution offers better understanding of how much heat transfer area is needed for different heat transfer mechanisms. E.g., it takes over one third of the heat transfer surface to cool the R744 to condensing temperature. The R404A superheating requires only 25 % of the surface. The discontinuous wall temperature evolution is caused by its dependency on the heat transfer coefficient evolution, which is also not continuous (see Fig.31).

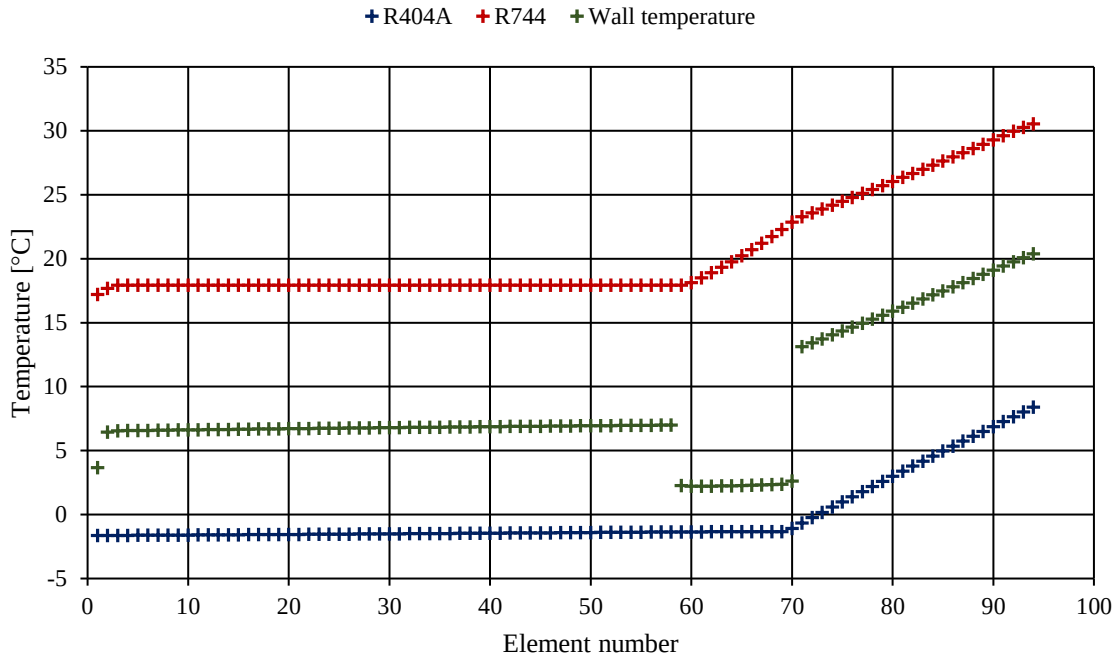

Figure 30: Cascade heat exchanger - temperature evolution

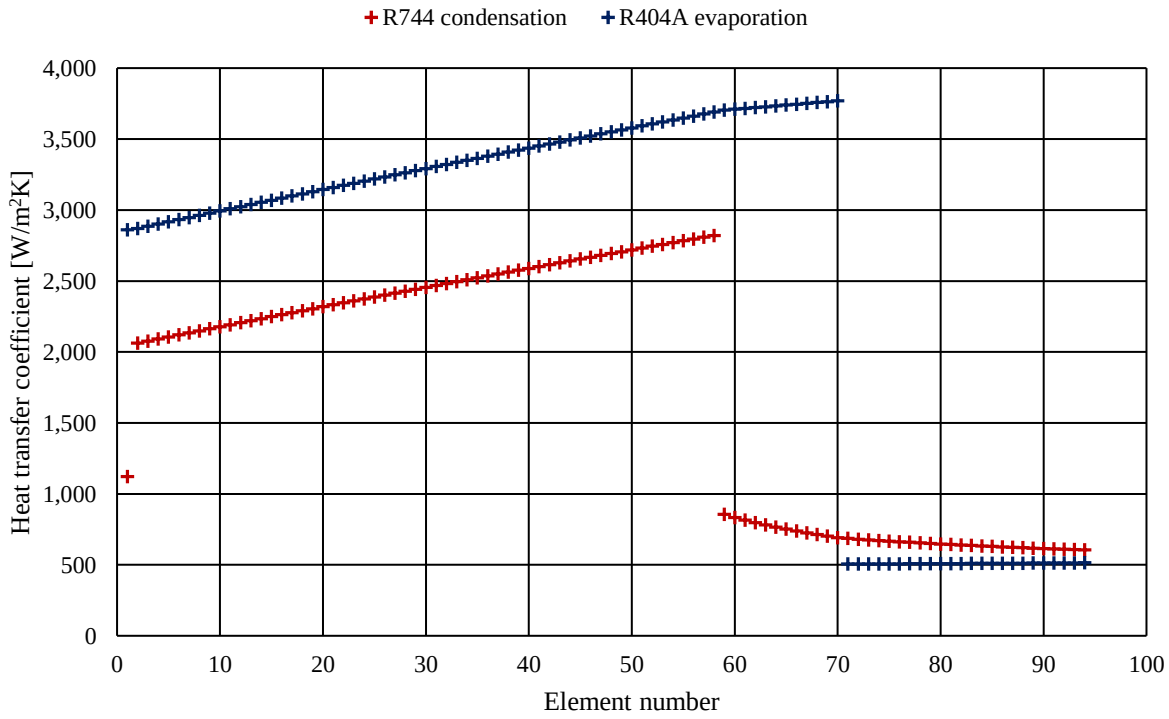

Figure 31: Cascade heat exchanger - heat transfer coefficient evolution

The heat transfer coefficient evolution shows several trends:

- phase-change HTC is much larger than the single-phase HTC,
- single-phase HTC generally increases as the vapor gets closer to the saturated vapor line,
- phase-change HTC increases with increasing vapor quality.

Interesting is the comparison of superheated vapor HTC evolution of both refrigerants. In case of R744 cooling, it follows the previously mentioned trend. On the other hand, the R404A superheating exhibits very slight increase in HTC as it gets farther from the saturated vapor line.

5.6. SEWTLE procedure convergence speed

As the authors claim in their study [72], the SEWTLE procedure offers an excellent convergence speed. This was verified during the cascade heat exchanger calculation. The convergence is observed in terms of total heat load difference on both sides of the CHE. As can be seen in Figure 32, the convergence (determined in this case by the 2% line) for given conditions was reached in the sixth iteration. The tenth iteration exhibited the heat load discrepancy of 0.18 % with ongoing trend of reduction, reaching the zero difference after iteration #15.

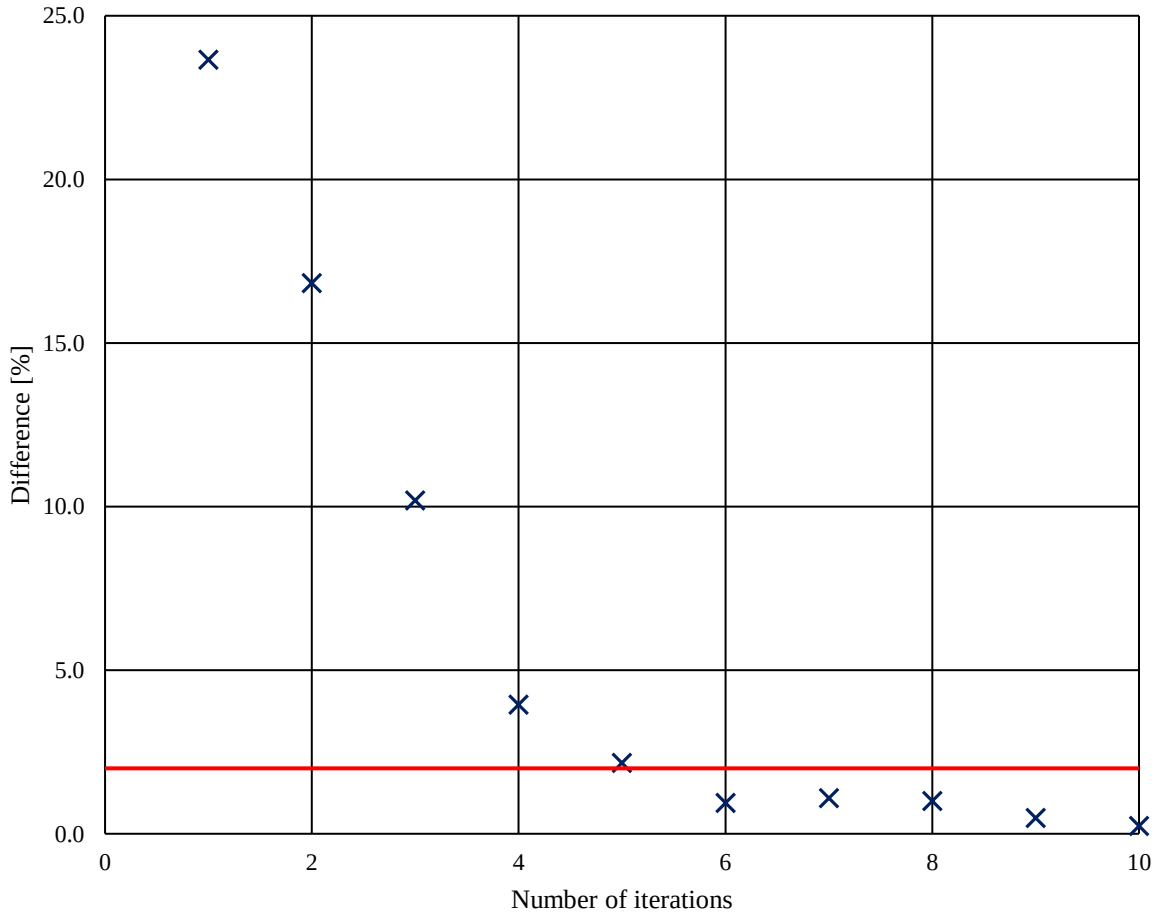

Figure 32: SEWTLE procedure convergence speed

5.6. Heat loads

Heat load comparison can serve as a practical verification if there was any major mistake made during the calculation process. Basically, the energy absorbed by/inserted into the refrigeration cycle must be equal to the heat released from the cycle.

In the low temperature cycle, this balance contains four components:[10]

- heat absorbed in the evaporator (+),
- power input of the compressor (+),
- heat rejected in the gas cooler (-),
- heat rejected in the condenser, i.e., cascade heat exchanger (-).

The internal heat exchange is excluded from this balance calculation as the energy flow stays within the system – therefore not having any impact on the global balance.

In the high temperature cycle, the balance contains three components as there is no gas cooler present:

- heat absorbed in the evaporator, i.e., cascade heat exchanger (+),
- power input of the compressor (+),
- heat rejected in the condenser (-).

Evaporator	Q_e	14 813	W
CC Compressor	P_{CC}	7 569	W
Gas Cooler	Q_{gc}	9 694	W
Cascade HE	Q_{CHE}	12 693	W
HC Compressor	P_{HC}	4 269	W
Condenser	Q_C	16 962	W

The comparison of given values proves the calculation to be correct in terms of heat balances across the whole refrigeration system. For instance, the balance excluding the cascade heat exchanger – the heat absorbed by the cycle must be equal to the heat released by the cycle:

$$Q_e + P_{CC} + P_{HC} = Q_{gc} + Q_C \quad (5.1)$$

$$26\,651 \approx 26\,656$$

As can be seen from the balance equation, the difference between the calculated heat load values differs by less than 0.02 per cent.

[10] + designates absorbed energy, - designates released energy

6. Conclusion

The originally set target of performing a thermodynamic calculation of a cascade refrigeration cycle with special emphasis on the cascade heat exchanger was achieved. It proved itself convenient to split the whole calculation process into a series of smaller steps, when equilibrium of partial elements was found one after another to reach the global equilibrium of the entire refrigeration system.

The calculation process was carried out using MS Excel, which was chosen for its user-friendliness and particularly for its suitability for given circumstances – the need to perform a large series of iteration calculations of beforehand unknown extent. This was achieved using the integrated programming language Visual Basic, which makes the calculation cycling quite accessible.

To better understand the processes taking place inside a cascade heat exchanger, a special computational procedure called SEWTLE was employed to provide the detailed calculation of thermodynamic properties evolution of the fluids inside the brazed plate heat exchanger channels. Thanks to the discretization of the wall and fluid paths, it was possible to observe the development of numerous characteristics along the fluid paths, e.g., the evolution of a heat transfer coefficient in course of a phase change as well as during single-phase processes.

As a result of various heat transfer correlations analysis, one of them for every heat transfer regime (single-phase heat transfer, evaporation and condensation). In order to maintain the cascade heat exchanger calculation integrity, the heat transfer correlations for both evaporation and condensation were selected from the same group of authors – Han, Lee and Kim. The single-phase correlations were selected with a regard to the range of their possible use (Reynolds number). Pressure drop correlations were neglected as the verification of calculated data in given case would be complicated.

The heat transfer coefficient evolution also showed certain imperfections regarding its calculation using empirical heat transfer correlations. Its evolution along a fluid path is most likely continuous without sudden high drops and local differences. However, the use of correlations for this purpose provides unsatisfactory results in this regard – the observed heat transfer coefficient development is not continuous at all.

As a result of this, the cascade heat exchanger wall temperature evolution is also discontinuous, which cannot happen in the real world. This issue could be partially overcome if the influence of longitudinal conduction inside the wall was considered. This task, however, exceeds the scope of the current thesis and is left for future work, as well as potential future improvement of the heat transfer and pressure drop correlations.

The SEWTLE cascade heat exchanger calculation methodology turned out to be suitable for given task, providing satisfactory accuracy and excellent calculation convergence speed. On the top of that, its potential is not limited only to plate heat exchangers, but can be used for basically every heat exchanger

type and configuration if defined properly. Another advantage is the fact that it can work with heat transfer as well as pressure drop correlations, providing very thorough and elaborate heat exchanger analysis if necessary.

However, whether the SEWTLE procedure would find a final solution can strongly depend on desired accuracy. The iteration process can fall into a never-ending loop under certain unfavorable circumstances (inappropriately chosen input values, too narrow accuracy range etc.). To conclude, the SEWTLE procedure offers a convenient method of heat exchanger analysis under condition, that the input parameters and procedure accuracy settings are reasonable. It proved itself useful for the purpose of this thesis, was successfully verified and can be recommended for further work.

References

Books

[3] BROŽ, Jiří, Zdeněk ČEJKA, Zdeněk FENCL et al. Chladicí a klimatizační technika. Prague: Svaz chladicí a klimatizační techniky, 2014.

[6] PETRÁK, Jiří and Miroslav PETRÁK. Tepelná čerpadla. Prague: CTU, 2004. ISBN 80-010-3126-8.

[15] LIŠKA, Antonín and Pavel NOVÁK. Kompresory. Prague: CTU, 1994. ISBN 80-010-1145-3.

[24] LIŠKA, Antonín and Pavel NOVÁK. Technika stlačeného vzduchu. Prague: CTU, 1996. ISBN 80-010-1430-4.

[35] ACHRER, Jakub. Ochrana ozonové vrstvy v České republice: 20 let od podepsání Montrealského protokolu. Prague: The Ministry of the Environment of the Czech Republic, 2007. ISBN 978-80-7212-471-8.

[50] BERGMAN, T. L. and Frank P. INCROPERA. Fundamentals of heat and mass transfer. 7th ed. /. Hoboken, NJ: Wiley, c2011. ISBN 978-0470-50197-9.

[51] NOŽIČKA, Jiří. Základy termomechaniky. 2nd ed. Prague: CTU, 2008. ISBN 978 800 1040-225.

[59] DVOŘÁK, Zdeněk. Výměníky tepla pro obor chladicí technika a tepelná čerpadla. 1st ed. Prague: CTU, 2001. ISBN 80-010-2468-7.

[68] KUPPAN, T. Heat exchanger design handbook. Second edition. ISBN 978-1-4398-4212-6.

[69] SHAH, R. K. and Dušan P. SEKULIĆ. Fundamentals of heat exchanger design. Hoboken, NJ: John Wiley, 2003. ISBN 04-713-2171-0.

[75] MOUKALLED, F., L. MANGANI and M. DARWISH. The Finite Volume Method in Computational Fluid Dynamics: An Advanced Introduction with OpenFOAM® and Matlab®. Springer, 2016. ISBN 978-3-319-16873-9.

[80] ROHSENOW, Warren M., J. P. HARTNETT and Young I. CHO. Handbook of heat transfer. 3rd ed. New York: McGraw-Hill, c1998. ISBN 978-007-0535-558.

[83] P. KESSELRING and C.S. SELVAGE. The IEA/SSPS solar thermal power plants -- facts and figures final report of the International Test and Evaluation Team (ITET). Berlin: Springer-Verlag, 1986. ISBN 978-364-2826-788.

[95] KAYS, W. M. and A. L. LONDON. Compact heat exchangers. Repr. ed. 1998 with corrections. Malabar, Fla.: Krieger Pub. Co., 1998. ISBN 978-1575240602.

[108] KAKAÇ, S. and A. PRAMUANJAROENKIJ. Heat exchangers: selection, rating, and thermal design. 3rd ed. Boca Raton, FL: CRC Press, c2012. ISBN 978-143-9849-903.

Scientific articles

[10] KILICARSLAN, A. and M. HOSOZ. Energy and irreversibility analysis of a cascade refrigeration system for various refrigerant couples [online]. 2010, **51**(12), 2947-2954 [cit. 2017-05-28]. Available: https://www.researchgate.net/publication/245160161_Energy_and_irreversibility_analysis_of_a_cascade_refrigeration_system_for_various_refrigerant_couples

[23] KOLARČÍK, Kamil, Jaroslav KAMINSKÝ and Mojmír VRTEK. Kompresory [online]. In: . Ostrava: VŠB, 2012 [cit. 2017-05-28]. Available: http://kke.zcu.cz/export/sites/kke/about/projekty/enazp/projekty/01_Stavba-a-provoz-stroju_1-3/1_IUT/002_Kompresory---Kolarcik-a-kol---P3.pdf

[25] DOMANSKI, P.A. and D.A. DIDION. Evaluation of suction-line/liquid-line heat exchange in the refrigeration cycle. International Journal of Refrigeration. 1994, **17**(7), 487-493.

[26] LLOPIS, Rodrigo et al. Experimental evaluation of an internal heat exchanger in a CO2 subcritical refrigeration cycle with gas-cooler. Applied Thermal Engineering. 2015, **80**(5), 31-41.

[27] LLOPIS, Rodrigo et al. Effects caused by the internal heat exchanger at the low temperature cycle in a cascade refrigeration plant. Applied Thermal Engineering. 2016, (103), 1077-1086.

[28] JIANG, P.X., F.Z. ZHANG et al. Efficiencies of subcritical and transcritical CO2 inverse cycles with and without an internal heat exchanger. Applied Thermal Engineering. 2011, **31**(4), 432-438.

[30] KREPINDL, Jiří. Regulace chladivových klimatizačních systémů. Vytápění, větrání, instalace [online]. **2013**(1). [cit. 2017-05-28]. Available: http://users.fs.cvut.cz/~zmrhavla/Publikace/VVI-2013-01_p002.pdf

[33] SEDLÁŘ, Jan. Refrigerants - introduction, definition, history. TZB Info [online]. 2015 [cit. 2017-05-28]. Available: http://vetrani.tzb-info.cz/klimatizace-a-chlazeni/13626-chladiva-uvod-definice-historie

[38] KROEZE, C. Fluorocarbons and SF6: Global Emission Inventory and Options for Control. National Institute for Public Health and the Environment [online]. Netherlands, 1995 [cit. 2017-05-28]. Available: http://rivm.openrepository.com/rivm/bitstream/10029/10522/1/773001007.pdf

[40] BODINUS, William. The Rise and Fall Of Carbon Dioxide Systems. ASHRAE Journal [online]. **1999**(4) [cit. 2017-05-28]. Available: https://www.ashrae.org/File%20Library/docLib/Public/200362710840_326.pdf

[43] HAYES, Niel, Amir JOKAR and Zahid H. AYUB. Study of carbon dioxide condensation in chevron plate exchangers; Pressure drop analysis. International Journal of Heat and Mass Transfer. 2012, **55**(11-12), 2916–2925.

[60] ABU-KHADER, Mazen M. Better Thermal Calculations Using Modified Generalized Leveque Equations for Chevron Plate Heat Exchangers. International Journal of Green Energy. 2007, **4**(4), 351-366.

[61] VLASOGIANNIS, P. et al. Air–water two-phase flow and heat transfer in a plate. International Journal of Multiphase Flow. 2002, **28**(5), 757–772.

[62] SUBBIAH, M. The Characteristics of Brazed Plate Heat Exchangers with Different Chevron Angles. Heat Exchangers - Basics Design Applications. InTech, 2012. DOI: 10.5772/32888. ISBN 978-953-51-0278-6.

[63] ABOU ELMAATY, Talal M. Corrugated plate heat exchanger review. Renewable and Sustainable Energy Reviews. 2017, **70**, 852–860.

[65] GUT, Jorge A. W. and Jose M. PINTO. Modeling of plate heat exchangers with generalized configurations. International Journal of Heat and Mass Transfer. 2003, **46**(14), 2571–2585.

[71] CORBERAN, J.M. et al. Modelling of compact evaporators and condensers [online]. Spain, , 10 [cit. 2017-05-28]. Available: http://lms.i-know.com/pluginfile.php/28867/mod_resource/content/112/Modeliing%20of%20Compact%20Evaporators%20%20Compressors.pdf

[72] CORBERAN, J.M., FERNÁNDEZ, P. Semiexplicit Method For Wall Temperature Linked Equations (SEWTLE): A General Finite-Volume Technique For The Calculation Of Complex Heat Exchangers. Numerical Heat Transfer, Part B: Fundamentals. 2001, **40**(1), 37-59. DOI: 10.1080/104077901300233596. ISSN 1040-7790.

[73] Corberan, J. M.; Gonzalvez, J.; Montes, P.; and Blasco, R., 'ART' A Computer Code To Assist The Design Of Refrigeration and A/C Equipment (2002). International Refrigeration and Air Conditioning Conference. Paper 570. http://docs.lib.purdue.edu/iracc/570

[77] CORBERAN, J.M. et al. Modelling of Tube And Fins Coil Working as Evaporator or Condenser [online]. Spain, , 7 [cit. 2017-05-28]. Available: http://lms.i-know.com/mod/resource/view.php?id=704

[78] ANDERSON JR., J.D. Governing Equations of Fluid Dynamics. Computational Fluid Dynamics: An Introduction [online]. , 15-51 [cit. 2017-05-28]. Available: https://link.springer.com/chapter/10.1007%2F978-3-662-11350-9_2

[81] GARCIA-CASCALES, J .R., CORBERAN, J.M. et al. Assessment of boiling and condensation heat transfer correlations in the modelling of plate heat exchangers. International Journal of Refrigeration. **2007**(30), 1029-1041.

[84] MORI, Hideo. A Study on Characteristics of Cooling Heat Transfer of Supercritical Pressure Fluids in a Plate Heat Exchanger. Heat Transfer Engineering. 2016, **37**(7-8), 659-667.

[85] HAYES, N. and Amir JOKAR. Dynalene/water correlations to be used for condensation of CO2 in brazed plate heat exchangers. ASHRAE Transactions. 2009, **115**(2), 1-17.

[86] KHAN, T.S. et al. Experimental investigation of single phase convective heat transfer coefficient in a corrugated plate heat exchanger for multiple plate configurations. Applied Thermal Engineering. 2010, **30**(8-9), 1058–1065.

[87] HAYES, Niel, Amir JOKAR and Zahid H. AYUB. Study of carbon dioxide condensation in chevron plate exchangers; Heat transfer analysis. International Journal of Heat and Mass Transfer. 2011, **54**, 1121–1131.

[88] MANCIN, Simone et al. Condensation of superheated vapour of R410A and R407C inside plate heat exchangers: Experimental results and simulation procedure. International Journal of Refrigeration. 2012, **35**(7), 2003–2013.

[89] CAVALLINI, A. et al. Condensation of pure and near-azeotropic refrigerants in microfin tubes: A new computational procedure. International Journal of Refrigeration. 2009, **32**(1), 162–174.

[90] YAN, Y.-Y. and T.-F. LIN. Evaporation Heat Transfer and Pressure Drop of Refrigerant R-134a in a Plate Heat Exchanger. Journal of Heat Transfer. 1999, **121**(1), 118-127.

[96] HAN, Dong-Hyouck. The Characteristics of Condensation in Brazed Plate Heat Exchangers with Different Chevron Angles. Journal of the Korean Physical Society. 2003, **43**(1), 66-73.

[97] HAN, Dong-Hyouck. Experiments on the characteristics of evaporation of R410A in brazed plate heat exchangers with different geometric configurations. Applied Thermal Engineering. 2003, **23**, 1209-1225.

[98] HSIEH, Y. Y. and T. F. LIN. Evaporation Heat Transfer and Pressure Drop of Refrigerant R-410A Flow in a Vertical Plate Heat Exchanger. Journal of Heat Transfer. 2003, **125**(5), 852-. DOI: 10.1115/1.1518498. ISSN 00221481

[99] HSIEH, Y.Y. and T.F. LIN. Saturated flow boiling heat transfer and pressure drop of refrigerant R-410A in a vertical plate heat exchanger. International Journal of Heat and Mass Transfer. 2002, **45**, 1033-1044.

[106] CABRAL, R. A. F. et al. Non-newtonian flow and pressure drop of pineapple juice in a plate heat exchanger. Brazilian Journal of Chemical Engineering. 2010, **27**(4).

Websites

[1] Methods of Refrigeration. ME Mechanical [online]. [cit. 2017-05-28]. Available: https://me-mechanicalengineering.com/methods-of-refrigeration/#liquid_gas_refrigeration

[2] Methods of Refrigeration: Vapor Compression Cycle. Bright Hub Engineering [online]. 2008 [cit. 2017-05-28]. Available: http://www.brighthubengineering.com/hvac/20354-methods-of-refrigeration-vapor-compression-cycle/

[4] Lesson 10 - Vapour Compression Refrigeration Systems. NPTEL [online]. India [cit. 2017-05-28]. Available: http://nptel.ac.in/courses/112105129/pdf/RAC%20Lecture%2010.pdf

[5] Principles of the Vapor Compression Refrigeration System. Bright Hub Engineering [online]. 2011 [cit. 2017-05-28]. Available: http://www.brighthubengineering.com/hvac/35435-principles-of-the-vapor-compression-refrigeration-system/

[7] Low temperature systems. SWEP [online]. 2016 [cit. 2017-05-28]. Available: http://www.swep.net/refrigerant-handbook/10.-systems/asdf2/

[8] Refrigeration Cycles. MechFamilyHU [online]. Jordan [cit. 2017-05-28]. Available: http://mechfamilyhu.net/download/uploads/mech1442851570013.pdf

[11] Cascade refrigeration system. Nissin Refrigeration & Engineering Ltd. [online]. Japan, 2012 [cit. 2017-05-28]. Available: http://www.nissin-ref.co.jp/english/product_blog/1-2.html

[12] Types of compressor. CAREL [online]. [cit. 2017-05-28]. Available: http://www.carel.com/types-of-compressor

[13] The Difference Between A Hermetically Sealed, Open, Or Semi-Hermetic Gas Compressor. KB Delta [online]. USA, 2016 [cit. 2017-05-28]. Available: http://kbdelta.com/blog/difference-hermetically-sealed-open-semi-hermetic-gas-compressor.html

[14] Oleje pro chladicí kompresory. MM Spektrum [online]. Prague, 2004 [cit. 2017-05-28]. Available: http://www.mmspektrum.com/clanek/oleje-pro-chladici-kompresory.html

[16] Screws or recips – the customers' choice. Johnson Controls [online]. USA [cit. 2017-05-28]. Available: http://www.sabroe.com/fileadmin/user_upload/Articles/2011/Recip_or_screw_-_the_customers_choice.pdf

[17] Kompresory Copeland Scroll. Schiessl [online]. Czech Republic [cit. 2017-05-28]. Available: https://www.schiessl.cz/soubor-copeland-scroll-kompresory-26-.pdf

[18] Jak funguje SCROLL kompresor v tepelných čerpadlech ? Vytápění.cz [online]. 2010 [cit. 2017-05-28]. Available: http://www.vytapeni.cz/okenko/scroll-kompresor

[19] Atlas Copco Compressed Air Manual [online]. 8th edition. Belgium, 2015 [cit. 2017-05-28]. Available: https://www.scribd.com/doc/294775527/Atlas-Copco-Compressed-Air-Manual-Tcm44-1249312

[20] Scroll Compressor Review. Engineers Edge [online]. 2017 [cit. 2017-05-28]. Available: http://www.engineersedge.com/pumps/scroll_compressor_review_10130.htm

[21] Aplikace kompresorů scroll s EVI systémem. JDK, spol. s r.o. [online]. Czech Republic [cit. 2017-05-28]. Available: http://www.jdk.cz/system/files/ftp/ar_articles/AR007_CZ_Aplikace%20scroll%20EVI_R1.pdf

[22] Enhanced Vapour Injection (EVI) For Zh*Kve Scroll Compressors. Emerson [online]. 2012 [cit. 2017-05-28]. Available: http://www.emersonclimate.com/europe/ProductDocuments/CopelandLiterature/C070403_1107_0512_E_TI_Vapour%20injected%20Scroll%20COMPRESSORS_0.pdf

[29] Expansion Valve. Southwest Tech [online]. USA, 2006 [cit. 2017-05-28]. Available: https://www.swtc.edu/ag_power/air_conditioning/lecture/expansion_valve.htm

[31] Expanzní ventily. JDK spol.s r.o. [online]. Czech Republic, 2012 [cit. 2017-05-28]. Available: http://www.jdk.cz/cs/produkty/expanzni-ventily

[32] Azeotropic/Zeotropic refrigerants. SWEP [online]. 2016 [cit. 2017-05-28]. Available: http://www.swep.net/refrigerant-handbook/5.-refrigerants/sd1/

[34] It seems like we are doing something useful for the future of our planet!. CAREL [online]. Italy, 2017 [cit. 2017-05-28]. Available: http://carel.it/web/guest/blog/-/blogs/598308;jsessionid=EFB8E5C03FF389880799BC17DE047DC8?p_r_p_564233524_tag=refrigerants

[36] The Montreal Protocol On Substances That Deplete The Ozone Layer. UN Environment [online]. 2017 [cit. 2017-05-28]. Available: http://ozone.unep.org/en/treaties-and-decisions/montreal-protocol-substances-deplete-ozone-layer

[37] Fluorované skleníkové plyny. Ministerstvo životního prostředí ČR [online]. Prague, 2017 [cit. 2017-05-28]. Available: http://www.mzp.cz/cz/fluorovane_sklenikove_plyny

[39] EU legislation to control F-gases. European Commission [online]. 2017 [cit. 2017-05-28]. Available: https://ec.europa.eu/clima/policies/f-gas/legislation_en

[41] R744 (Carbon dioxide). Linde [online]. [cit. 2017-05-28]. Available: http://www.linde-gas.com/en/products_and_supply/refrigerants/natural_refrigerants/r744_carbon_dioxide/index.html

[42] R744 refrigerant grade carbon dioxide. Linde Canada [online]. [cit. 2017-05-28]. Available: http://www.lindecanada.com/internet.lg.lg.can/en/images/R744_refrigerant_grade_CO2_leaflet_58473_12135_86988.pdf?v=2.0

[44] BENSAFI, Ahmed and Bernard THONON. Transcritical R744 (CO2) heat pumps - Technicians's Manual. Cetiat [online]. France [cit. 2017-05-28]. Available: http://www.cetiat.fr/docs/newsdocs/166/doc/R744%20Technicians%20Manual%20CETIAT%20GRETH.pdf

[45] CO2 as a Refrigerant — Five Potential Hazards of R744. Emerson [online]. 2015 [cit. 2017-05-28]. Available: https://emersonclimateconversations.com/2015/07/02/co2-as-a-refrigerant-five-potential-hazards-of-r744/

[46] Thermo King adopts R404A replacement. Cooling Post [online]. 2014 [cit. 2017-05-28]. Available: http://www.coolingpost.com/world-news/thermo-king-adopts-r404a-replacement/

[47] Opteon XP44 (R-452A) - a lower GWP alternative to R-404A for transport refrigeration applications. Climalife [online]. 2015 [cit. 2017-05-28]. Available: http://www.idsrefrigeration.co.uk/news-opteon-xp44-r-452a-a-lower-gwp-alternative-to-r-404a-for-transport-refrigeration-applications

[48] Opteon® XP44. Linde Gas [online]. [cit. 2017-05-28]. Available: http://www.linde-gas.cz/cs/produkty_and_zasobovani/refrigerants/hfo_refrigerants/r452a/index.html

[49] Opteon™ XP44 (R-452A) refrigerant. Chemours [online]. [cit. 2017-05-28]. Available: https://www.chemours.com/Refrigerants/en_US/products/Opteon/Stationary_Refrigeration/products/Opteon_XP44.html

[52] Fourier's Law of Heat Conduction. ME Mechanical [online]. 2016 [cit. 2017-05-28]. Available: https://me-mechanicalengineering.com/fouriers-law/

[53] Natural Convection. Simon Fraser University [online]. Canada [cit. 2017-05-28]. Available: http://www.sfu.ca/~mbahrami/ENSC%20388/Notes/Natural%20Convection.pdf

[54] Forced Convection Heat Transfer. Simon Fraser University [online]. Canada [cit. 2017-05-28]. Available: http://www.sfu.ca/~mbahrami/ENSC%20388/Notes/Forced%20Convection.pdf

[55] Other differential equations. University of British Columbia [online]. Canada [cit. 2017-05-28]. Available: http://www.ugrad.math.ubc.ca/coursedoc/math100/notes/diffeqs/cool.html

[56] Stefan-Boltzmann Law. HyperPhysics [online]. Canada [cit. 2017-05-28]. Available: http://hyperphysics.phy-astr.gsu.edu/hbase/thermo/stefan.htm

[57] Stefan-Boltzmann law. Energy Education [online]. Canada [cit. 2017-05-28]. Available: http://energyeducation.ca/encyclopedia/Stefan-Boltzmann_law

[58] Heat Exchangers in Refrigeration. Gunt Hamburg [online]. Germany [cit. 2017-05-28]. Available: http://gunt.de/images/download/heat-exchangers-in-refrigeration_english.pdf

[64] Jak fungují deskové výměníky tepla (BPHE). Kaori [online]. Czech Republic [cit. 2017-05-28]. Available: http://www.kaori-bphe.com/cz/products/page/How_BPHEs_Work

[66] BPHE construction and denomination. SWEP [online]. [cit. 2017-05-28]. Available: http://www.swep.net/refrigerant-handbook/8.-practical-advice/qw7/

[67] Design of heat exchangers. Department of Energetics, CTU [online]. [cit. 2017-05-28]. Available: http://energetika.cvut.cz/files/HEB%20l2.pdf

[70] Difference Between the Effectiveness-NTU and LMTD Methods. Engineered Software, Inc. [online]. 2017 [cit. 2017-05-28]. Available: http://kb.eng-software.com/display/ESKB/Difference+Between+the+Effectiveness-NTU+and+LMTD+Methods

[74] Finite Volume Methods. Department of Mathematics, University of California Irvine [online]. USA [cit. 2017-05-28]. Available: https://www.math.uci.edu/~chenlong/226/FVM.pdf

[76] On the Finite Volume Element Method. Department of Mathematics, Purdue [online]. [cit. 2017-05-28]. Available: http://www.math.purdue.edu/~zcai/pdf-paper/91onfve.pd

[79] Heat Exchangers. NC State University [online]. USA [cit. 2017-05-28]. Available: http://www4.ncsu.edu/~doster/NE400/Text/HeatExchangers/HeatExchangers.PDF

[82] Hydraulic diameter. The Engineering Toolbox [online]. [cit. 2017-05-28]. Available: http://www.engineeringtoolbox.com/hydraulic-equivalent-diameter-d_458.html

[91] The Bisection Method. S.O.S. MATHematics [online]. [cit. 2017-05-28]. Available: http://www.sosmath.com/calculus/limcon/limcon07/limcon07.html

[92] The Bisection Method. Emory College [online]. USA [cit. 2017-05-28]. Available: http://www.mathcs.emory.edu/~cheung/Courses/170/Syllabus/07/bisection.html

[93] The compressor operating envelope. R744.com [online]. 2013 [cit. 2017-05-28]. Available: http://www.r744.com/files/the-compressor-operating-envelope.pdf

[100] REFRIGERATION. Thermopedia [online]. [cit. 2017-05-28]. Available: http://www.thermopedia.com/content/1086/

[101] Schematic diagram of a 4-pass, shell-and-tube cascade heat exchanger. ResearchGate [online]. [cit. 2017-05-28]. Available: https://www.researchgate.net/figure/256967543_fig1_Fig-3-e-Schematic-diagram-of-a-4-pass-shell-and-tube-cascade-heat-exchanger

[102] Hermetically Sealed Refrigeration Compressors. Bright Hub Engineering [online]. [cit. 2017-05-28]. Available: http://www.brighthubengineering.com/hvac/52198-hermetically-sealed-refrigeration-compressors/

[103] GEA Grasso – Screw compressors. HVAC Arena [online]. [cit. 2017-05-28]. Available: https://www.hvacarena.co.uk/companies/southern-sales-and-services/products/gea-grasso-screw-compressors

[104] Refrigerant Expansion & Control Devices. Bangladesh University of Engineering and Technology [online]. [cit. 2017-05-28]. Available: http://teacher.buet.ac.bd/zahurul/ME415/ME415_expansion.pdf

[105] APV Heat Exchangers. Nibley [online]. [cit. 2017-05-29]. Available: http://www.nibleyco.com/apv-heat-exchangers/

[107] Geometry of chevron type plate heat exchanger. ResearchGate [online]. [cit. 2017-05-29]. Available: https://www.researchgate.net/figure/272200283_fig3_Fig-3-Geometry-of-chevron-type-plate-heat-exchanger

[109] Basic constitutive equations. RheoHeat [online]. [cit. 2017-05-29]. Available: http://www.rheoheat.se/b4_heat.html

[110] Lecture 8 Internal Flow. Emaze [online]. [cit. 2017-05-29]. Available: https://www.emaze.com/@AOWTRQIF/Lecture-8-Internal-Flow.pptx

Other

[9] Mechanical Engineering Thermodynamics - Lec 24, pt 2 of 4. YouTube [online]. 2013 [cit. 2017-05-28]. Available: www.youtube.com/watch?v=ZVsMi2IzKBs

[94] ZFD18KVE-TFD EVI Compressor data sheet - software Select 7.13 by Emerson [online]. [cit. 2017-05-28]. Available: http://www.emersonclimate.com/europe/en-eu/Resources/Software_Tools/Pages/Download_Full_Instructions.aspx

[111] B17 Plate Heat Exchanger data sheet – software SSP G7 by SWEP [online]. [cit. 2017-05-28]. Available: http://swep.net/support/ssp-calculation-software/ssp-g7/